National Aerospace University "Kharkiv Aviation Institute"
Ministry of Education and Science of Ukraine

On the rights of the manuscript

SUN YIFANG

UDC 629.735.33.025.1.015.4

DISSERTATION

SCIENTIFIC GROUNDS TO PROVIDE LIFETIME OF REGIONAL PASSENGER AIRPLANE WING STRUCTURAL MEMBERS

Scientific specialty – 134 Aviation and aerospace technology
Field of science – 13 Mechanical engineering

Applied for the Doctor of Philosophy degree

The dissertation contains the results of my own research. The use of other authors' ideas, results and texts have references to the relevant source

Sun Yifang ____________ Sun Yifang

Scientific adviser – Oleksandr Hryhorovych Grebenikov, Doctor of technical sciences, Professor

Kharkiv – 2025

ABSTRACT

Sun Yifang. Scientific grounds to provide lifetime of regional passenger airplane wing structural members – qualifying scientific work on the rights of the manuscript.

Dissertation for obtaining the scientific degree of Doctor of Philosophy in the field of knowledge 13 – Mechanical engineeringon, scientific specialty 134 – Aviation and aerospace technology. National Aerospace University "Kharkiv Aviation Institute", Kharkiv, 2025.

The dissertation is devoted to the decision of a scientific and technical problem of manufacturing new competitive aviation equipment by studying the method for strength design and fatigue life extension of the fitting joint between the center wing section and the outer wing section of a regional aircraft. With the rapid development and application of regional aircraft, this technical problem needs to be solved urgently. The choice of goal is due to the need of aircraft manufacturers to implement wing strength design and fatigue resistance design at all stages of the aircraft life cycle and update existing design methods taking into account the current level of science and technology to increase the competitiveness and safety of their developments.

The wing root connection area of a regional aircraft is the key part of the load exchange balance between the wing and the fuselage. The design requirements of structural strength and durability, structural load transfer efficiency, assembly coordination requirements, and detail processing are very high. Different docking methods have different force transmission methods, which will have a significant impact on the service life and assembly process of the aircraft. Therefore, the fitting joint design between the center wing section and the outer wing section has always been one of the important links in aircraft design.

The development trend of the fitting joint between the center wing section and the outer wing section of a regional aircraft in the world is reviewed and analyzed, and the design of the fitting joint is summarized and classified, and the advantages and disadvantages are compared and analyzed, which provided a reference for the

selection and design of the fitting joint of different regional aircraft. After summary and analysis, the design method of the fitting joint at the root of the wing is proposed. According to this method, the form of frame fitting joint with comb-shaped profile is selected to create the fitting joint model by CATIA.

In order to judge the rationality of the strength design of the fitting joint, an effective solution for the design, quality and static strength calculation method of the fitting joint in the modelling stage is proposed for the first time. This method is based on the calculation of stress caused by the discreteness of force transmission between units. This calculation method obtains a simplified hyperstatic joint model based on the geometric characteristics and force transmission characteristics of the cross section at each node in the flange connection design. During the calculation process, it is determined that the curves of bending moment and axial force obtained by the force method, and the force load distribution of each part of the model to further analyze the static strength. The calculation results obtained are compared with the requirements of the airworthiness standards to determine whether the design requirements are met. At the same time, the finite element ANSYS software is used to propose an indirect method for calculating the stress and strain state of the fitting joint for the first time. The stress and strain results calculated by the indirect method are compared with those calculated by the direct method, and the results are basically consistent. The indirect method has the advantages of small calculation amount and fast calculation speed.

In order to further improve the fatigue life of the fitting joint, the influence of the depth and angle of the extruded arc groove on the fatigue life of the wing panel is further studied through experiments and finite element simulation methods on the basis of existing research. The study shows that for wing panel with functional holes, the extruded arc groove can extend their fatigue life. This is because the residual stress generated after the extrusion process offsets the effect of part of the load to reduce the characteristic stress. The fatigue life of the wing panel with functional holes is affected by the depth of the extruded arc groove. When the depth is

0~0.15 mm, the fatigue life is not extended much; when the depth is 0.15~0.3 mm, the fatigue life is greatly extended; when the depth is greater than 0.3mm, the fatigue life is extended slowly. The fatigue life of the wing panel with functional holes is also affected by the angle of the extruded arc groove. The fatigue life increases with the increase of the angle until the optimal angle is 120°. The use of the optimal extended arc groove can extend the fatigue life of the studied wing panel by more than 2.34 times.

In order to further improve the fatigue life of the fitting joint, the effect of extruded annular groove on the fatigue life of the wing panel with functional holes is studied by experimental methods. The study shows that for aircraft wing panel with functional holes, the extruded annular grooves around the functional holes can improve the fatigue life of the wing panels. The depth of the extruded annular groove has an effect on the fatigue life of the aircraft wing panels with functional holes. With the increase of the depth of the extruded annular groove, the fatigue life of the wing panels changes in an inverted "V" shape. When the groove depth is 0.26 mm, the fatigue life of the aircraft wing panel with functional holes is the longest, which can be increased by 2.35~32.9 times.

The effect of extruded annular groove on the fatigue life of double shear joints of wing panels is studied by experimental methods. The results show that the extruded annular groove can improve the fatigue life of double shear joint. The fatigue life of double shear joint with the extruded annular grooves is about 2.28 times that of double shear joint without the extruded annular grooves. Anti-fretting paste can also improve the fatigue life of double shear joints. The fatigue life of double shear joint coated with anti-fretting paste is about 1.28 times that of double shear joint without anti-fretting paste.

Keywords: regional aircraft, wing, fitting joint, double shear joint, strength, stress-strain characteristics, finite element analysis, experiment, the extruded arc groove, the extruded annular groove, anti-fretting paste, fatigue life.

АНОТАЦІЯ

Сунь Іфан. Наукові основи забезпечення ресурсу конструктивних елементів крила регіонального пасажирського літака. – Кваліфікаційна наукова робота на правах рукопису.

Дисертація на здобуття ступеня доктора філософії в галузі знань 13 – Механічна інженерія, за спеціальністю 134 – Авіаційна та ракетно-космічна техніка. Національний аерокосмічний університет «Харківський авіаційний інститут», Харків, 2025.

Дисертація присвячена вирішенню науково-технічної проблеми виготовлення нової конкурентоспроможної авіаційної техніки шляхом дослідження методу розрахунку на міцність і подовження втомної довговічності фітингового з'єднання між центропланом і від'ємною частиною крила регіонального літака. З бурхливим розвитком і застосуванням регіональної авіації ця технічна проблема потребує термінового вирішення. Вибір мети зумовлений необхідністю авіабудівників впроваджувати проектування міцності крила та опору втоми на всіх етапах життєвого циклу літака та оновлювати існуючі методи проектування з урахуванням сучасного рівня науки і техніки для підвищення конкурентоспроможності своїх розробок.

Зона з'єднання кореневої частини крила регіонального літака є ключовою частиною розподілу навантаження між крилом і фюзеляжем. Вимоги до конструктивної міцності та довговічності, ефективності передачі структурного навантаження, вимоги до ув'язки складання та обробки деталей дуже високі. Різні методи стикування мають різні методи передачі зусилля, що матиме значний вплив на термін служби та процес складання літака. Тому конструкція з'єднання центроплана і від'ємної частини крила завжди була однією з важливих ланок у проектуванні літаків.

Розглянуто та проаналізовано тенденцію розробок фітингових з'єднань між центропланом і від'ємною частиною крила регіонального літака у світі,

узагальнено та класифіковано конструкцію фітингового з'єднання, а також порівняно та проаналізовано переваги та недоліки, надано рекомендації щодо вибору та проектування з'єднання центроплана і від'ємної частини крила різних регіональних літаків. Після підсумків та аналізу пропонується метод проектування фітингового з'єднання в кореневій частині крила. Відповідно до цього методу вибирається форма з'єднання рами з гребінчастим профілем для створення моделі фітингового стику між центропланом і від'ємною частиною крила.

Для судження про раціональність розрахунку на міцність фітингового з'єднання вперше запропоновано ефективне рішення розрахунку конструкції, якості та статичної міцності з'єднання на етапі моделювання. Цей метод заснований на розрахунку напруги, викликаної дискретністю передачі зусилля між вузлами. Цей метод розрахунку дозволяє отримати спрощену модель гіперстатичного з'єднання на основі геометричних характеристик і характеристик передачі зусиль кожної вузлової секції в конструкції фланцевого з'єднання. У процесі розрахунку визначено криві згинального моменту та повздовжньої сили, отримані методом сил, і розподіл силового навантаження кожної частини моделі для подальшого аналізу статичної міцності. Отримані результати розрахунків порівнюються з вимогами стандартів льотної придатності для визначення відповідності вимогам конструкції. У той же час програмне забезпечення кінцевих елементів ANSYS використовується для того, щоб вперше запропонувати непрямий метод розрахунку напружено-деформованого стану фітингового з'єднання. Результати напруги та деформації, розраховані непрямим методом, порівнюються з результатами, розрахованими прямим методом, і результати в основному відповідають. Перевагами непрямого методу є невеликий об'єм обчислення та висока швидкість обчислення.

З метою подальшого підвищення втомної довговічності фітингового з’єднання, вплив глибини та кута екструдованої дугової канавки на довговічність панелі крила додатково вивчається за допомогою експериментів і методів моделювання кінцевих елементів на основі існуючих досліджень. Дослідження показує, що для крилових панелей із функціональними отворами екструдована дугова канавка може подовжити термін їх служби. Це пояснюється тим, що залишкова напруга, що утворюється після процесу екструзії, компенсує дію частини навантаження для зменшення характеристичного напруження. На довговічність панелі крила з функціональними отворами впливає глибина екструдованої дугової канавки. Якщо глибина становить 0 ~ 0,15 мм, втомна довговічність не збільшується; якщо глибина становить 0,15 ~ 0,3 мм, втомна довговічність значно подовжується; коли глибина перевищує 0,3 мм, втомна довговічність продовжується повільно. На довговічність панелі крила з функціональними отворами також впливає кут екструдованої дугової канавки. Зі збільшенням кута довговічність збільшується до оптимального кута 120°. Використання оптимально подовженої дугової канавки може збільшити втомний ресурс досліджуваної панелі крила більш ніж у 2,34 рази.

Для подальшого покращення втомної довговічності фітингового з’єднання досліджено експериментальними методами вплив екструдованої кільцевої канавки на втомну довговічність панелі крила з функціональними отворами. Дослідження показує, що для панелей крила літака з функціональними отворами екструдовані кільцеві канавки навколо функціональних отворів можуть покращити втомну довговічність панелей крила. Глибина екструдованої кільцевої канавки впливає на довговічність панелей крила літака з функціональними отворами. Зі збільшенням глибини екструдованої кільцевої канавки довговічність панелей крила змінюється у вигляді перевернутої букви «V». Коли глибина канавки становить 0,26 мм, довговічність панелі крила літака з функціональними отворами є найдовшою, яку можна збільшити в 2,35–32,9 рази.

Експериментальними методами досліджено вплив екструдованої кільцевої канавки на довговічність двозрізних з’єднань панелей крила. Результати показують, що екструдовані кільцеві канавки можуть покращити довговічність двозрізних з’єднань. Довговічність двозрізних з’єднань із екструдованими кільцевими канавками приблизно в 2,28 рази перевищує довговічність двозрізних з’єднань без екструдованих кільцевих канавок. Антифретингова паста може покращити термін служби двозрізних з’єднань. Довговічність двозрізних з’єднань, покритих антифретинговою пастою, приблизно в 1,28 рази перевищує довговічність двозрізних з’єднань без цієї пасти.

Ключові слова: регіональний літак, крило, фітингове з’єднання, двозрізне з’єднання, міцність, напружено-деформаційні характеристики, аналіз методом кінцевих елементів, експеримент, екструдована дугова канавка, екструдована кільцева канавка, антифретингова паста, втомна довговічність.

LIST OF PUBLICATIONS OF THE APPLICANT BY DISSERTATION TOPIC

Scientific works in which the main scientific results of the dissertation are published:

1. А. Г. Гребеніков, А. М. Гуменний, С. В. Трубаєв, В. А. Гребеніков, Сунь Іфан. Методы обеспечения ресурсных характеристик типовых конструктивных элементов самолетных конструкций // Проблеми створення та забезпечення життєвого циклу авіаційної техніки : матеріали Міжнар. наук.-техн. конф., Харків, 28–29 квіт. 2020 р. Харків, 2020. С. 11. **The collection is included in the international bibliometric and scientometric databases Index Copernicus, WorldCat, Ulrich's Periodicals Directory and Google Scholar.** Personal contribution of the acquirer: collect relevant information on aircraft life performance assurance methods.

2. Yifan Sun. ANALYSIS OF THE STRESS-STRAIN STATE OF COMPONENTS IN THE FITTING JOINT OF OUTER WING SECTION AND CENTER SECTION OF REGIONAL AIRCRAFT / Yifan Sun. A. A. Vendin // Open Information and Computer Integrated Technologies : National Aerospace University «Kharkiv Aviation Institute» , – Kharkiv, 2021 – Vol. 91. – P. 97 – 112. DOI: https://doi.org/10.32620/oikit.2021.91.07. **The collection is included in the international bibliometric and scientometric databases Index Copernicus, WorldCat, Ulrich's Periodicals Directory and Google Scholar.** Personal contribution of the acquirer: build a 3D model and finite element analysis model of the fitting joint.

3. Sun, Y. Analysis of Force Distribution of Four Rows of Bolts in Aircraft Fitting Joint / Sun Yifang, O. G. Grebenikov, Chenghu Li // International Journal of Aerospace Engineering. – 2021. – Vol. 2011, – P. 11. https://doi.org/10.1155/2021/9962645. **The collection is included in the international bibliometric and scientometric databases Scopus (Q3) and Google**

Scholar. Personal contribution of the acquirer: analyze the stress-strain state of the fitting joint by using the finite element software ANSYS.

4. Yifang Sun, O. G. Grebenikov, Chenghu Li. The effect of extrusion arc groove on the fatigue life of wing panel with functional holes: experiment and simulation // Engineering Failure Analysis. 2022 Nov 1; 141:106643. **The collection is included in the international bibliometric and scientometric databases Scopus (Q1) and Google Scholar.** Personal contribution of the acquirer: analyze the optimal depth and angle of the extruded arc groove by finite element software ANSYS.

5. Sun, Y. Method of design calculating of the strength of the transverse joint of the panels of outer wing section and the center wing section of the regional aircraft / Sun Yifang, V. E. Vasilevskiy, O. O. Vendin, O. G Grebenikov // Open Information and Computer Integrated Technologies – Kharkiv: Nat. Aerospace Univ. “KhAI”. – 2023. – Vol. 97. – P. 142 – 157. https://doi.org/10.32620/oikit.2023.97.09. **The collection is included in the international bibliometric and scientometric databases Index Copernicus, WorldCat, Ulrich's Periodicals Directory and Google Scholar.** Personal contribution of the acquirer: analyze the optimal depth and angle of the extruded arc groove by finite element software ANSYS.

6. Yifang Sun. Influence of radial tension of bolts on the characteristics of vat of models of connections of elements of aircraft structures / Yifang Sun // Open Information and Computer Integrated Technologies – Kharkiv: Nat. Aerospace Univ. “KhAI”. – 2023. – Vol. 98. – P. 36 – 45. DOI: https://doi.org/10.32620/oikit.2023.98.03. **The collection is included in the international bibliometric and scientometric databases Index Copernicus, WorldCat, Ulrich's Periodicals Directory and Google Scholar.** Personal contribution of the acquirer: propose an effective solution to the design, quality and static strength calculation of the joint in the modeling stage. The method and its application are introduced by taking the preliminary analysis and design calculation of the flange connection design of the mid-wing of a regional aircraft as an example.

7. Sun Yifang. The effect of cold extruded annular grooves on the fatigue life of wing panels with functional holes / Sun Yifang, O. G. Grebenikov, O. O. Vendin // Open Information and Computer Integrated Technologies – Kharkiv: Nat. Aerospace Univ. "KhAI". – 2023. – Vol. 99. – P. 22 – 31. DOI: https://doi.org/10.32620/oikit.2023.99.02. **The collection is included in the international bibliometric and scientometric databases Index Copernicus, WorldCat, Ulrich's Periodicals Directory and Google Scholar.** Personal contribution of the acquirer: conducted experiments to confirm that extruded annular grooves can extend the fatigue life of perforated wing panels.

8. Li Chenghu, Sun Yifang, Duan Chunxu, Li Renfu. Study on Properties of Z-pin-reinforced and Rivet-reinforced Composite T-joint: Experiment and Simulation// Applied Composite Materials, 2021, 28: 395-408. **The collection is included in the international bibliometric and scientometric databases Scopus (Q2) and Google Scholar.** Personal contribution of the acquirer: carried out model building and simulation, and participated in validation experiments.

CONTENTS

LIST OF CONDITIONAL DESIGNATIONS

CAD\CAM\CAE – computer-aided design, computer-aided manufacturing, computer-aided engineering.

3D – three-dimensional.

FCWS – fitting of center wing section.

IP – intermediate panel.

FOWS – fitting of outer wing section.

SOWS – stringer of outer wing section.

LPOWS – lower panel of outer wing section.

BJRES – butt-jointed rib edge strip

INTRODUCTION

Reasons for choosing the research subject. The global air transport market shows a steady growth trend, which leads to an increase in the demand for regional aircraft. Ukraine is one of the few countries in the world that has industrial and scientific and technological potential and a complete production cycle for the creation and manufacture of modern aviation equipment. In the aviation industry, the introduction of advanced technologies is very intense. The requirements for aviation and environmental safety, efficiency and reliability are constantly growing. This requires the development of new methods of design, production and testing to create new samples of aviation equipment that are better than existing similar equipment.

The fitting joint design of the center wing section and the outer wing section is one of the important links in aircraft design. Different docking methods have different force transmission methods, which will have a significant impact on the service life and assembly process of the aircraft. Foreign countries have accumulated a lot of experience in aircraft design. By analyzing the docking forms and structural characteristics between the center wing section and the outer wing section of foreign aircraft, it has important reference significance for my country's aircraft design research. In addition, the wing root connection area of regional aircraft is a key part of the load exchange balance between the wing and the fuselage. The structural strength and durability, structural load transmission efficiency, assembly coordination requirements, and detail processing are very high. Therefore, it is urgent to develop a calculation and analysis method for the fitting joint between the center wing section and the outer wing section of a regional aircraft. In the early stage of regional aircraft design, it is of great practical significance to carry out detailed fatigue strength design and certain life extension design of the fitting joint between the center wing section and the outer wing section to ensure flight safety and the competitiveness of the domestic aviation industry.

Goal and tasks of the study. The goal of this research subject is to develop a method for strength design and fatigue life extension of the fitting joint between the center wing section and the outer wing section of a regional aircraft to increase the service life of new domestic regional aircraft. In order to achieve the set this goal, the following tasks must be solved:

- Summarize the types of fitting joint between the center wing section and the outer wing section of existing regional aircraft and analyze the design features and design methods of fitting joint;
- Develop new methods for strength calculation and analysis of the fitting joint between the center wing section and the outer wing section of a regional aircraft by means of existing scientific knowledge and simulation technologies;
- Work out new methods for increasing the fatigue life of the fitting joint between the center wing section and the outer wing section of a regional aircraft;
- Implement the methods for designing the fitting joint between the center wing section and the outer wing section and methods for extending the fatigue life in the design and production of promising regional aircraft in the process of production and education at the National Aerospace University "Kharkov Aviation Institute" and in the process of design and production of Chinese aircraft.

Research object – The fitting joint between the center wing section and the outer wing section of a regional aircraft.

Research subject – Scientific grounds to provide lifetime of regional passenger airplane wing structural members. It includes strength design and analysis method of the fitting joint and the method for extending the fatigue life of the fitting joint.

Research method. Theoretical analysis, finite element simulation and experiment were adopted as research methods to solve the above tasks. The design type, method and principle of the fitting joint between the center wing section and the outer wing section of the international regional aircraft are investigated. An effective solution is proposed for the design, quality and static strength calculation method of the fitting joint in the modeling stage and an indirect method for calculating the stress-strain state of the fitting joint. The influence of the depth and angle of the extruded arc groove on the fatigue life of the wing panel is studied by experimental and finite element simulation methods. The extruded annular groove and the application of anti-fretting paste have been confirmed as effective methods for extending the fatigue life of the wing double shear joint.

Scientific novelty of the results

1. For the first time, an effective solution for the design and static strength calculation of the fitting joint in the modeling stage is proposed. The method and its application are introduced by taking the preliminary analysis and design calculation of the flange connection design of the center wing section of a regional aircraft as an example.

2. For the first time, an indirect method for calculating the stress-strain state of the fitting joint between the center wing section and the outer wing section of a regional aircraft is proposed. The indirect method obtains the stress-strain state of the fitting joint through two finite element calculations. The results are consistent with those calculated by direct method.

3. The influence of the depth and angle of the extruded arc groove on the fatigue life of the wing panel is studied in detail by experimental and new finite element simulation methods. The results show that the extruded arc groove can improve the fatigue life of the wing panel and the optimal extruded arc groove depth and angle are obtained.

4. For the first time, the extruded annular groove is proposed to extend the fatigue life of the wing panel with functional holes, and it is verified by experiments.

5. For the first time, a method of the extruded annular grooves in combination with anti-fretting paste to extend the fatigue life of the double shear joint of the wing panel is proposed. The study shows that the combination of the extruded annular grooves and anti-fretting paste can improve the fatigue life of the double shear joint

of the wing panel.

Publications. The main results of the thesis work were published in 8 scientific works, including 4 articles in ukrainian scientific specialized publications, 3 articles in the collection of scientific works included in SCOPUS, 1 report was published in the Scientific and Technical Conference.

Personal contribution of the acquirer. All the main results that constitute the essence of the dissertation work were obtained by the author himself. Together with the scientific supervisor, the tasks were formulated, the main results were analyzed and interpreted, and the scientific conclusions were formulated. In the co-authored report [1], the applicant proposed to develop a new method to ensure the specific resource characteristics of structural elements and study its effectiveness, considering the consideration of fretting coatings on the contact surface to reduce or eliminate the influence of fretting corrosion. In the co-authored articles [2-3], the applicant used the CAD/CAM/CAE system to create an assembly joint model and used the ANSYS system to analyze the characteristics of its stress-strain state using the finite element method. The author's personal contribution was to create a three-dimensional model of the fitting joint and perform finite element analysis. According to the results of the stress-strain state analysis, the force distribution of the four rows of bolts was obtained by calculating the average stress of the cross section between the bolts. In the co-authored article [4], the applicant studied in detail the effect of the extruded arc groove on the fatigue life of the wing wall panel with functional holes. The author's personal contribution was to calculate the optimal depth and angle of the extruded arc groove through finite element simulation. In the co-authored article [5], the applicant proposed an effective method to solve the design, quality and static strength calculation of the joint in the modelling stage. The author's personal contribution is to simplify the connection joint by segments. In the personal article [6], the influence of interference on the mechanical properties of the bolted connection structure was studied. The appropriate interference fit for the aircraft wing bolt connection structure can significantly improve the stress distribution of the hole edge structure and reduce stress concentration. In the co-authored article [7], the applicant verified the effect of extruded annular groove on the fatigue life of the perforated wing panel through experiments. The author's personal contribution is to develop the test plan and implement the test. In the co-authored article [8], the applicant studied the performance of z-pin and rivet reinforced composite T-joints through experiments and finite element simulations, and compared the reinforcement effects of z-pin and rivets.

Approbation of dissertation materials. The main contents and results of the thesis work are carried out at the seminar of the Department of Aircraft and Helicopter Design of the Aerospace University "Kharkov Aviation Institute" (2019 – 2025).

Connection of work with scientific programs, plans, subjects. The subject of the dissertation work is directly related to the implementation of the state budget subject No. DR 0113U001047 “Methods of creating advanced aircraft designs for 20 local airlines using information technologies” and No. DR 0118U004041 “Methods of integrated design, construction and modeling of efficient aviation equipment using modern CAD\CAM\CAE systems”, which are agreed upon in accordance with the Order of the Cabinet of Ministers of Ukraine of December 27, 2008 No. 1656-p “On approval of the development strategy” and implementation of the strategy for the development of the domestic aviation industry until 2024. This dissertation work is supported by the National Scholarship Council of China (No. 201908360296).

Practical significance of the obtained results. The practical value of the dissertation work is mainly as follows:

1. The design type, method and principle of the fitting joint between the center wing section and the outer wing section of international regional aircraft are investigated, the difficulty analysis of the root connection design of the regional

aircraft wing, the load transfer characteristics analysis, the root rib arrangement method and its characteristics analysis, and the comparative analysis of different root fitting joint design schemes are given, and a flexible compensation design method for alleviating structural assembly stress is proposed, and the feasibility of the relevant flexible compensation design method is verified by experimental results.

2. For the first time, an effective solution for joint design, quality and static strength calculation method in the modelling stage are proposed. The method and its application are introduced by taking the preliminary analysis and design calculation of the flange connection design of the center wing section of a regional aircraft as an example. The method is based on the calculation of stress caused by the discreteness of force transmission between units. The calculation method obtains a simplified hyperstatic joint model based on the geometric characteristics and force transmission characteristics of the cross section at each node in the flange connection design. During the calculation process, the following are determined: the curves of bending moment and axial force obtained by the force method, and the force load distribution of each part of the model, in order to further analyze the static strength reserve. The calculation results obtained are compared with the requirements of the airworthiness standards to determine whether they meet the design requirements. For components with large static strength or that do not meet the requirements, it is recommended to change the design parameters additionally to ensure the effective design of the connection between the center plane and the aircraft wing and subsequent recalculation. The calculation method has practical value as a preliminary engineering analysis.

3. For the first time, an indirect method for calculating the stress-strain state of the fitting joint between the center wing section and the outer wing section is proposed. This indirect method obtains the stress-strain state of the fitting joint through two finite element calculations. In order to prove the validity of the calculation results, the stress-strain state results calculated by the indirect method

are compared with those calculated by the direct method. The results show that the calculation results of the indirect method are consistent with those of the direct method. Therefore, the indirect method is a very feasible method for obtaining the stress-strain state of the fitting joint. Compared with the direct method, the indirect method has the advantages of small calculation amount and fast calculation speed.

4. The influence of the depth and angle of the extruded arc groove on the fatigue life of the wing panel with functional holes is studied by experimental and finite element simulation methods. The study shows that for wing panel with functional holes, the extruded arc groove can extend their fatigue life. This is because the residual stress generated after the extrusion process offsets the effect of part of the load to reduce the characteristic stress. The fatigue life of the wing panel with functional holes is affected by the depth of the extruded arc groove. When the depth is 0~0.15 mm, the fatigue life is not extended much; when the depth is 0.15~0.3 mm, the fatigue life is greatly extended; when the depth is greater than 0.3 mm, the fatigue life is extended slowly. The fatigue life of the wing panel with functional holes is also affected by the angle of the extruded arc groove. The fatigue life increases with the increase of the angle until the optimal angle is 120 °. The use of the optimal extended arc groove can extend the fatigue life of the studied wing panel by more than 2.34 times.

5. The effect of extruded annular groove on the fatigue life of the wing panel with functional holes is studied by experimental methods. The study shows that for aircraft wing panels with functional holes, the extruded annular grooves around the functional holes can extend the fatigue life of the wing panels with functional holes. The depth of the extruded annular groove has an effect on the fatigue life of the aircraft wing panel with functional holes. With the increase of the depth of the extruded annular groove, the fatigue life of the wing panel changes in an inverted "V" shape. When the groove depth is 0.26 mm, the fatigue life of the aircraft wing panel with functional holes is the longest, which can be increased by 2.35~32.9 times.

6. The effect of extruded annular groove and anti-fretting paste on the fatigue life of the double shear joint of the wing panel is studied by experimental methods. The study shows that the extruded annular groove can increase the fatigue life of the double shear joint. The fatigue life of the double shear joint with the extruded annular groove is about 2.28 times that of the double shear joint without the extruded annular groove. Anti-fretting paste can increase the fatigue life of the double shear joint. The fatigue life of the double shear joint coated with anti-fretting paste is about 1.28 times that of the double shear joint without anti-fretting paste.

The extruded arc grooves, the extruded annular grooves, application of anti-fretting paste, these methods of extending fatigue life of the wing have been applied in actual engineering with good results. The results obtained in the thesis work have been applied in the educational process of the National Aerospace University "Kharkov Aviation Institute" and in the process of design and production of Chinese aircraft.

The structure and scope of the dissertation. The paper consists of an abstract, introduction, five chapters, a general conclusion, a list of resources used, and an appendix. The full paper is 175 pages long, including 137 pages of text, 14 tables, 106 figures, 71 references, and 3 appendices.

CHAPTER 1

STRUCTURAL ANALYSIS OF FITTING JOINT BETWEEN THE CENTER WING SECTION AND THE OUTER WING SECTION OF A REGIONAL AIRCRAFT

Regional aircraft typically operate aircraft, such as regional jets and turboprops, with a seating capacity ranging from 19 to 130 seats, on short to medium-haul routes. Regional aviation demonstrated its strongest traffic growth over the last three decades. At the beginning of 2020, the regional aviation world fleet was performing scheduled connections of roughly 9300 units representing more than 30% of the worldwide commercial fleet. Over the next 20 years, regional air traffic is expected to increase at an average yearly rate of over 4.5% (compared to a 4% rate expected in total commercial aviation), generating a market demand of over 8200 new regional aircraft (including the large regional aircraft) with a market value of about €390 billion (averaging €19.5 billion per year). For such a huge market demand, regional aircraft require higher technical guarantees. The wing root connection area of a regional aircraft is the key part of the load exchange balance between the wing and the fuselage. The design requirements of structural strength and durability, structural load transfer efficiency, assembly coordination requirements, and detail processing are very high. Different docking methods have different force transmission methods, which will have a significant impact on the service life and assembly process of the aircraft. Therefore, the fitting joint design between the center wing section and the outer wing section has always been one of the important links in aircraft design.

According to the requirements of design, manufacturing and use, wings often need to be arranged with a certain number of detachable and non-detachable separation surfaces. The detachable separation surface is called the design separation surface, and the non-detachable separation surface is called the process separation surface. The design separation surface is used to meet the requirements of transportation, fuel tank testing, storage space, etc., the process separation surface is used to meet the requirements of blank supply, parts manufacturing, assembly, etc. In order to meet the design requirements of different aircraft, the wing separation surface connection forms of different aircraft are different. Most transport aircraft, such as aircraft B747, L-1011, B787, A320, etc., set the separation surface at the junction between the outer wing section root and the center wing section on the side of the fuselage [1], as shown in Fig. 1.1.

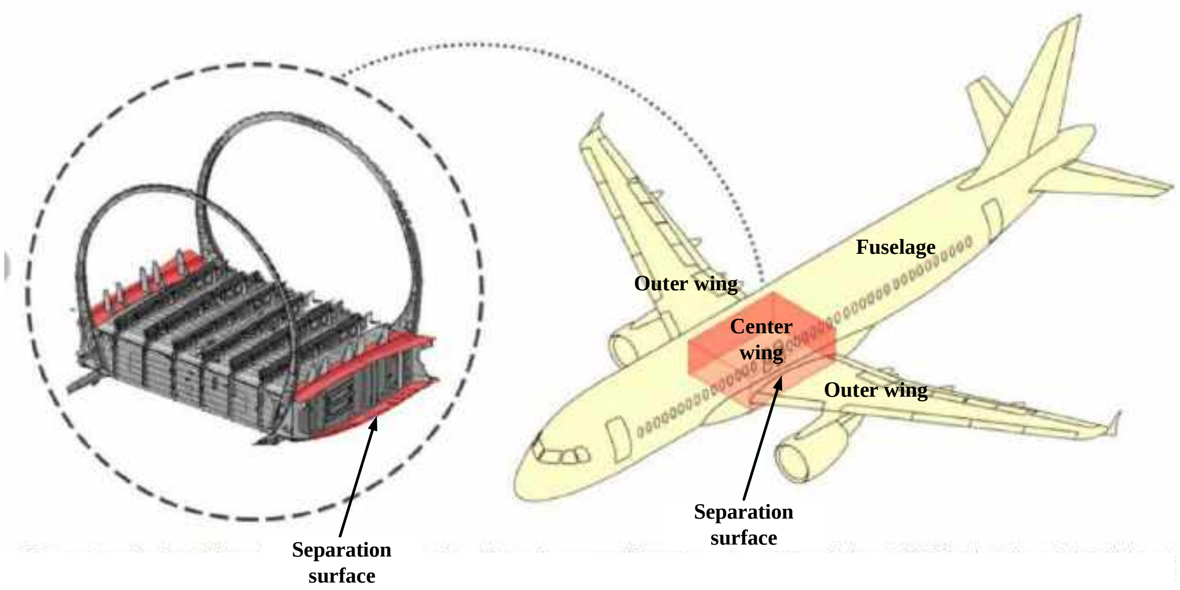

Fig. 1.1 The separation surface between the center wing section and the outer wing section

Considering the requirements of aerodynamic efficiency, handling stability and maintainability, the basic layout of the current international advanced regional aircraft adopts a layout with a large sweep angle, a certain dihedral angle and a lower wing. The longitudinal parts such as the wall panels and beams of the wing box pass through the fuselage. The wing box structure is designed with a separation surface according to the design, manufacturing and assembly requirements. It is generally divided into the center wing section and the left and right outer wing sections with the root docking rib (also often called the first rib, hereinafter referred to as the root rib) as the interface [2]. Usually, the center wing section is first connected to the middle fuselage structure (including the wing floor longitudinal beam, keel beam and the front and rear beam frame of the middle fuselage and the wing frame structure) at the component assembly stage to complete the wing-fuselage interface connection, and then the outer wing box and the center wing middle fuselage combined section are connected to the wing root at the final assembly stage, and finally the fitting joint between the center wing section and the outer wing section is formed. The design feature of this fitting joint is that the assembly process mainly considers the coordination complexity of the balanced treatment of the wing-fuselage connection and the wing root docking, the convenience of reference positioning and attitude adjustment, and the efficiency of component assembly and final assembly. The typical fitting joint between the center wing section and the outer wing section is shown in Fig. 1.2. The fitting joint mainly connects the center wing section box and the outer wing section box, as shown in the wing root connection area in Fig. 1.2. It can be seen that the load on the wing is transferred to the fuselage by this fitting joint, which is one of the most important components on the aircraft.

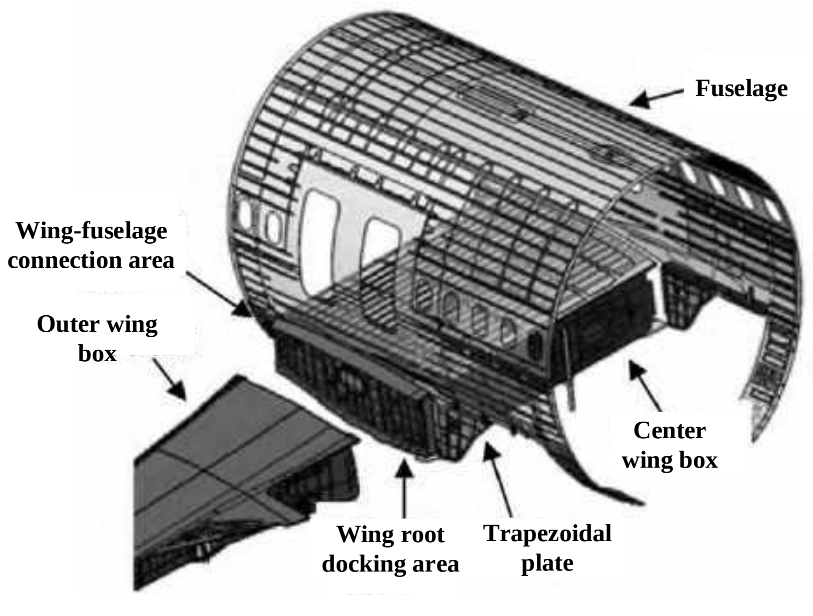

Fig. 1.2 Typical wing-fuselage structural connection interface

The fitting joint is related to the design and use requirements of the aircraft, the structural form and size of the wing and other factors. The fitting joint between the center wing section and the outer wing section is the key area for the exchange and balance of wing-fuselage loads. From the perspective of structural strength, the components in this area are subjected to a high level of complex state loads, and the components are large in size, highly complex, and have complex deformation coordination relationships. The design requirements for static strength, fatigue, damage tolerance, etc. are very high. As far as assembly connection is concerned, constraint contradictions are formed due to the complex connection assembly interface, limited spatial accessibility, and the complex interface and wing attitude adjustment movement freedom. At the same time, when the large-size wing is horizontally measured and adjusted in complex three-dimensional space, it is difficult to control the tolerance of the docking area, the interface matching is difficult, the probability of exceeding the tolerance is high, the local gap detection is difficult, and forced assembly stress is easy to generate, and the compensation requirements are high. There are also difficulties in making holes and installing large-size fasteners with large thickness and complex laminations.

In general, the fitting joint at the root of the wing of regional aircraft shows the characteristics of many constraints, high requirements, and complex interfaces, so the wing root connection design is the focus and difficulty of regional aircraft structural design. The design of the fitting joint between the center wing section and the outer wing section is one of the important links in aircraft design. Different connection methods have different ways of transmitting force, which will have a significant impact on the service life and assembly process of the aircraft. The engineering field has also conducted analysis and experimental research on the local detailed structure of the root connection [3-8].

1.1 Introduction to typical fitting joint between the center wing section and outer wing section of a regional aircraft

The docking forms of the wing-fuselage joints of a regional aircraft can be roughly divided into two categories: one is the centralized docking form, and the other is the decentralized docking form. The centralized docking form is mainly used for beam-type wings and multi-web-type wings of mid-wings. The wing beam joint is docked with the fuselage frame joint. The docking point is the separation surface of the wing and fuselage. Its docking form is the same as the docking form between the beam wing and the fuselage. This structure is rarely used now.

The decentralized docking forms mainly include frame fitting joint with multiple single joints, frame fitting joint with comb-shaped profiles, fitting joint with a butt-jointed rib edge strip integral profile, fitting joint with a T-shaped integral profile and fitting joint without profile. The decentralized docking structure layout can make the internal space utilization rate of the fuselage high, the structure weight light, and the economy good. It is widely used in modern aircraft [9].

1.1.1 Frame fitting joint with multiple single joints

Frame fitting joint with multiple single joints includes multiple dispersed joints. These dispersed single joints are connected to single joints set along the wing-fuselage connection section.

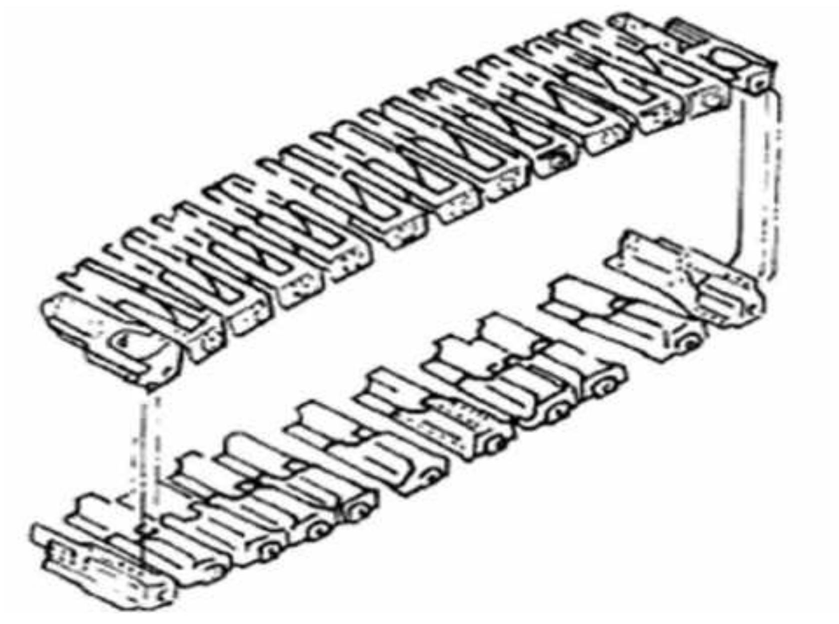

Fig. 1.3 Frame fitting joint with multiple single joints

The single joint is connected to the skin and long stringer of the wing wall panel through shear bolts, and the corresponding joints of the two wing sections are connected through tension bolts. This fitting joint form has been applied on aircraft such as P2V-7, YS-11, DC-6 and DC-7. The fitting joint form is shown in Fig. 1.3.

1.1.2 Frame fitting joint with comb-shaped profiles

The wing panel is connected to the comb-shaped profile joint through multiple shear bolts, and the beam flange is also connected to the beam flange joint through shear bolts. The comb-shaped profile joint and the beam flange joint overlap to form a frame fitting joint with comb-shaped profiles. The profile joint and the beam flange joint have tension bolt grooves, and the two sections of the wing panel and the beam flange are connected as a whole through tension bolts. The web ends of the two sections of the beam are provided with strengthening columns, and the columns and the webs are connected as a whole through bolts, as shown in Fig. 1.4. This form of fitting joint is applied to the docking of the upper wing, lower wing and each section of the mid-wing aircraft that penetrates the fuselage.

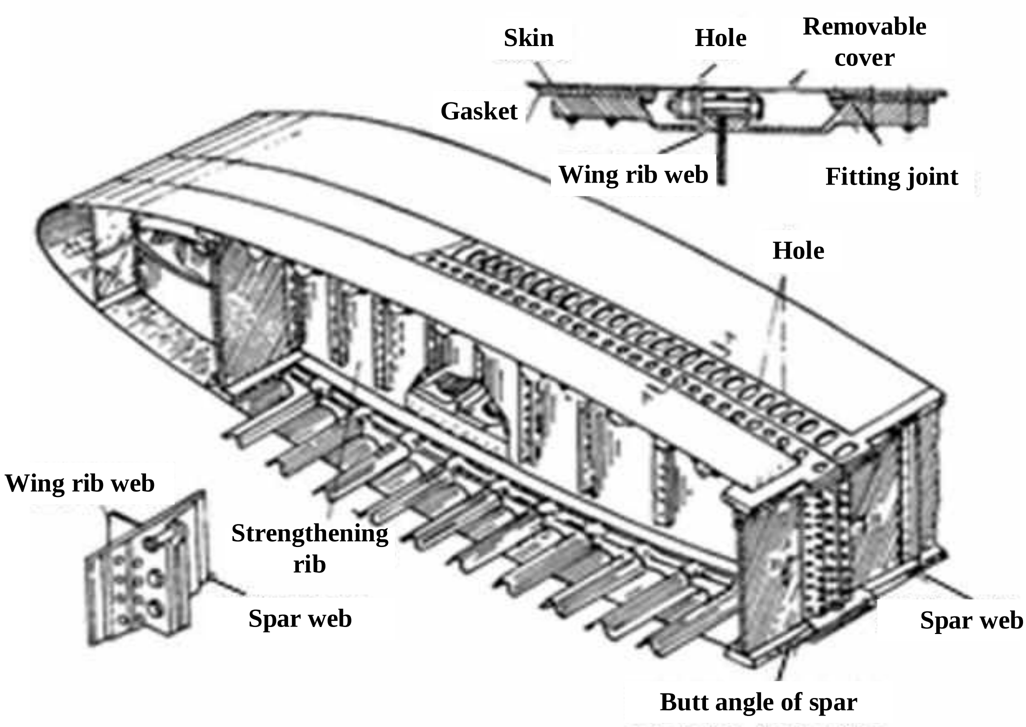

Fig. 1.4 Frame fitting joint with comb-shaped profiles

1.1.3 Fitting joint with a butt-jointed rib edge strip integral profile

The BJRES integral profile is a butt-jointed rib edge strip. The lower edge strip of the BJRES integral profile is connected to the wing panels and strengthening strips (there are even fuselage frame reinforcements) of each section through shear bolts. The upper edge strip of the BJRES profile is directly connected to the upper edge strip of the wing wall panel long stringer or connected in shear by bolts using a transition joint, as shown in Fig. 1.5. This form has been used in aircraft such as L-1011, B707, B727 and B737.

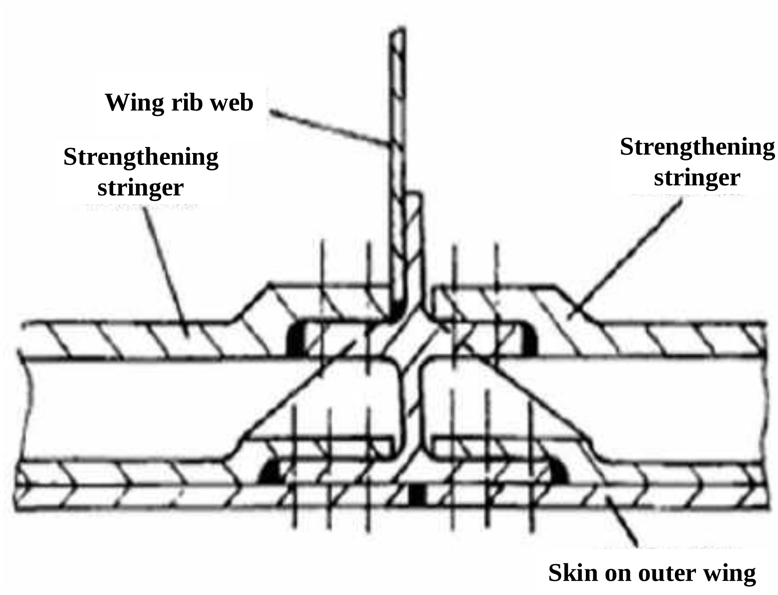

(a) Fitting joint with single BJRES integral profile

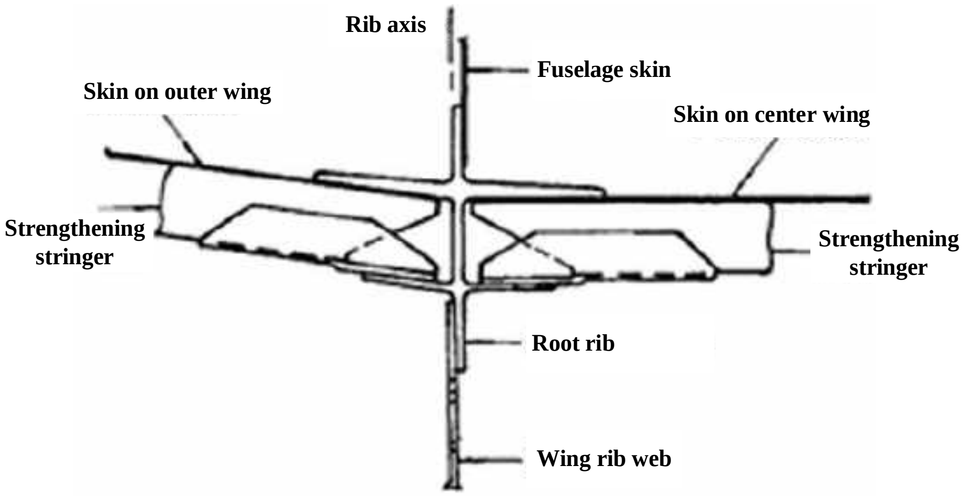

(b) Fitting joint with double BJRES integral profile

Fig. 1.5 Fitting joint with a BJRES integral profile

1.1.4 Fitting joint with a T-shaped integral profile

Fitting joint with a T-shaped integral profile is to butt the lower edge strip with the skin and the lower edge strip of the long stringer through the T-shaped profile. Generally, this fitting joint form is more common on the lower wing surface. This structure is simple, the force transmission path is clear, and the reliability and fatigue resistance are relatively good, as shown in Fig. 1.6.

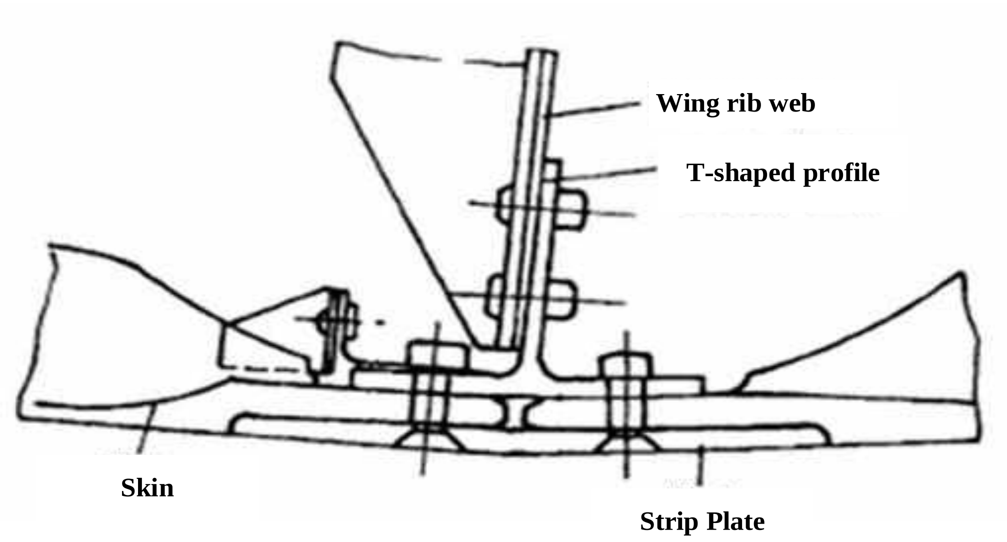

(a) Typical fitting joint of Lockheed's wing root

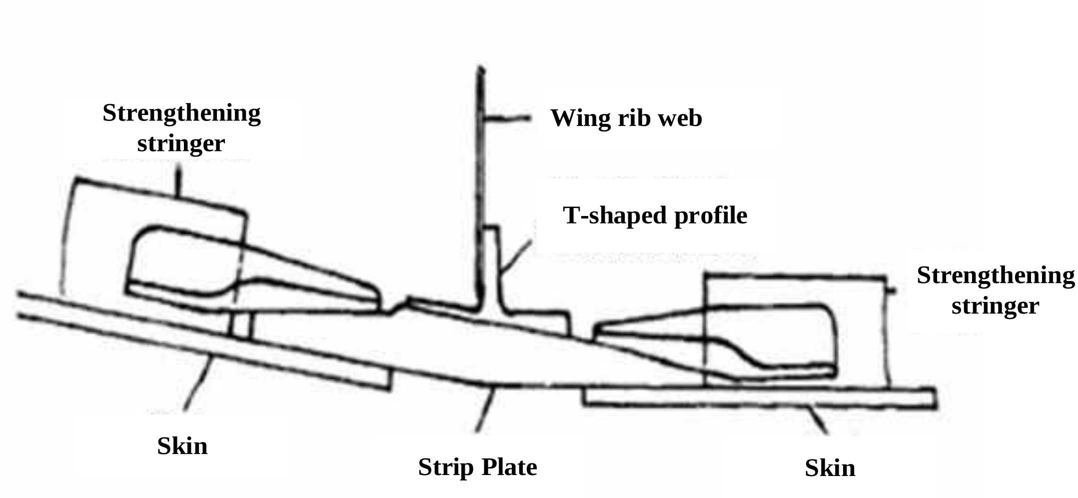

(b) Typical fitting joint of Boeing's wing root

Fig. 1.6 Fitting joint with a T-shaped integral profile

1.2 Analysis of the fitting joint between the center wing section and outer wing section of a typical aircraft

With the increasing use of composite materials in modern aircraft, the requirements for wing docking structures are also getting higher and higher. Complex docking forms will affect the fatigue life of composite wings, because if composite structures are connected by conventional bolts, the stress concentration at the edge of the holes is more serious than that of metal structures, which has a greater impact on the safety of the structure. In order to minimize bolting and riveting connections, and avoid drilling and cutting fibers, advanced aircraft have derived structural forms that meet the requirements of composite wing docking based on the above-mentioned docking structures, and their advantages are outstanding. The following analysis of the wing docking structures of B777, B787 and A320 provides technical support for the design of regional passenger aircraft in my country.

1.2.1 Analysis of the fitting joint between the center wing section and the outer wing section of B777

The upper wing surface of B777 uses BJRES profiles to connect the outer wing section and the middle wing wall panels, the upper web of the upper edge strip is connected to the fuselage side wall panel, the lower web is connected to the wing rib web, the upper edge strip is connected to the skin on both sides, and the lower edge strip is connected to the long stringers on both sides. The outer wing section and the upper wall panel of the central wing are docked through the upper edge strip and the upper long stringer.

The lower wing surface uses T-shaped profiles, the lower edge strip is a ⊥-shaped extruded profile, the vertical edge plate is connected to the wing rib web, and the horizontal edge strip is connected to the wall panels on both sides. The outer wing section and the lower wall panel of the center wing section are docked through the lower edge strip and the lower long stringer joint, as shown in Fig. 1.7.

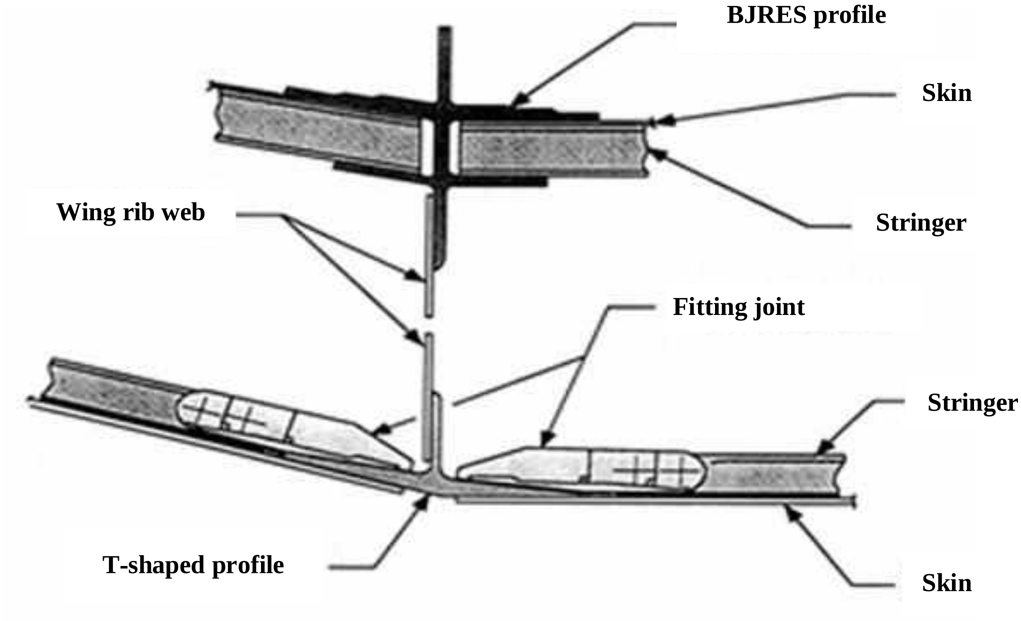

Fig. 1.7 The fitting joint between the center wing section and the outer wing section of B777

This type of fitting joint has the following advantages.

1) The structure is simple and clear, the reliability and fatigue resistance are relatively good, and it has inherent damage safety.

2) Both the tensile and compressive forces are converted into shear forces of the butt bolts, and the shear forces are transmitted by the BJRES profile edge strips.

3) The force transmission route is direct and short, the bolts are mainly subjected to shear force, and the fitting joint area structure basically transmits loads by extrusion, so the fitting joint area structure has a relatively long service life.

This type of fitting joint has the following disadvantages.

1) The processability is relatively complex, and mechanical processing and forming are relatively difficult, and the assembly accuracy requirements are relatively high.

2) The thickness of the siding skin at the joint is relatively large.

1.2.2 Analysis of the fitting joint between the center wing section and the outer wing section of A320

The fitting joint of the A320 series aircraft is more complex than that of Boeing aircraft. It uses 5 independent cross-shaped fitting joints to dock the fuselage, outer wing section, and center section. The outer wing section upper wing surface uses a cross-shaped profile to dock with the long stringer of the center wing section upper wall panel, and uses a butt profile to connect with the long stringer. The lower wing surface uses a T-shaped profile to dock the lower wall panel, and uses a long stringer joint to overlap the lower edge strip, as shown in Fig. 1.8.

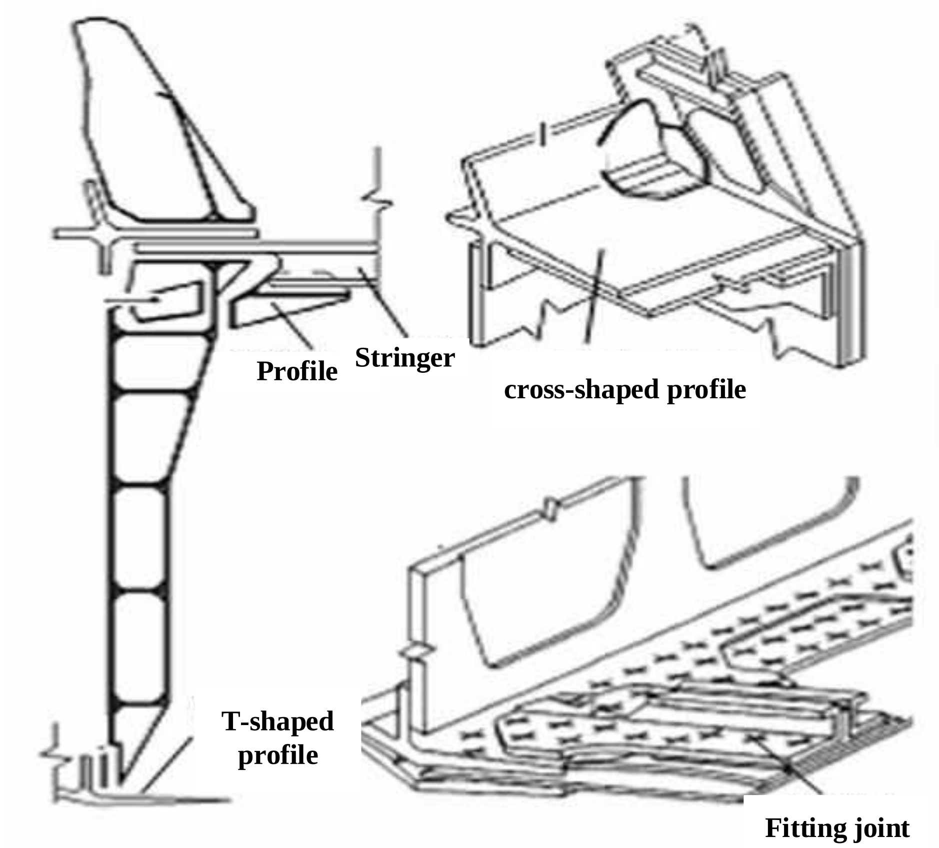

Fig. 1.8 The fitting joint between the center wing section and the outer wing section of A320

Compared with the fitting joint of Boeing aircraft, the upper wing docking structure is simple to assemble, but the force transmission route is complex and the structure is heavy. The docking method adopted by the lower wing is simple and practical, but under the long-term action of the wing load, cracks are prone to occur in the docking area, affecting the service life of the aircraft.

1.2.3 Analysis of the fitting joint between the center wing section and the outer wing section of B787

The B787 Dreamliner is a new generation of main passenger aircraft developed by Boeing in the United States. It adopts a large number of advanced technologies, and the use rate of composite materials has exceeded 50 %. Most of the structural parts of the outer wing section and central wing of the B787 aircraft are made of carbon fiber composite materials. Compared with the metal wing, the weight is greatly reduced, thereby effectively improving the economy of the aircraft.

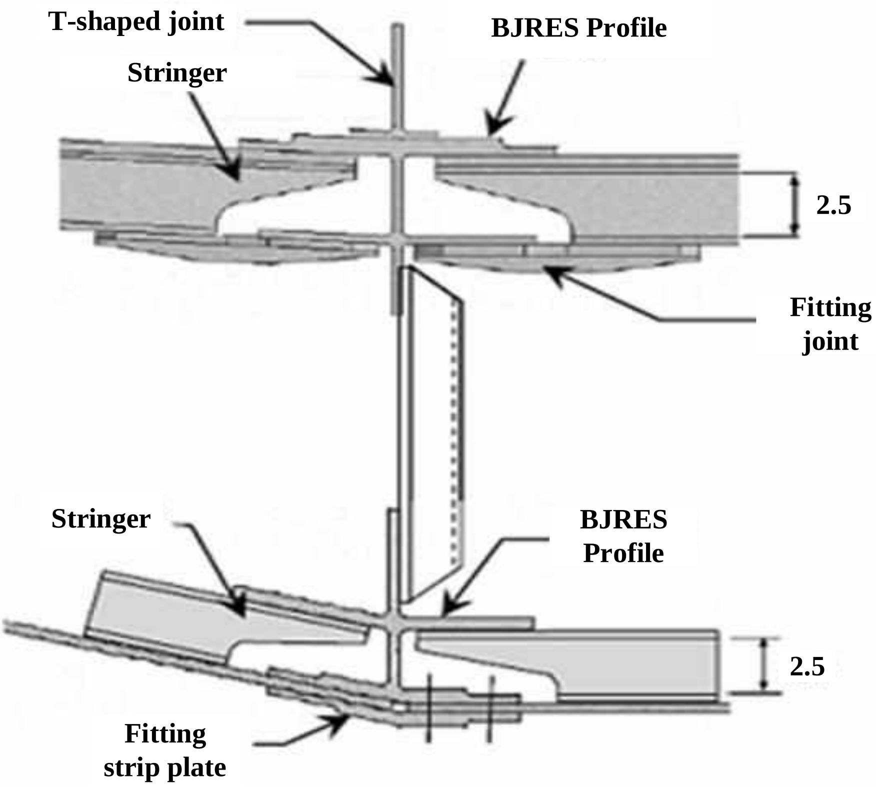

Fig. 1.9 The fitting joint between the center wing section and the outer wing section of B787

The fitting joint between the center wing section and outer wing section of the

B787 aircraft is shown in Fig. 1.9. It not only inherits the BJRES profile docking structure of traditional Boeing aircraft, but also improves some docking details. The use of BJRES profiles on its lower wing surface has the following advantages.

In order to avoid the brittleness of the composite material causing uneven load bearing on each nail hole and resulting in greater stress concentration, mechanical connections and multiple nail connections are reduced. The lower wing surface connection bolts bear double shear force, which is more reliable than the single shear force of the bolts of the T-shaped profile. At the same time, the fitting joint is installed at the lower part of the upper wall panel butt girders, which enhances the force transmission characteristics of the upper BJRES profile, weakens the rigidity of the wall panel butt girders, increases the flexibility of the butt area, and improves fatigue life of the fitting joint structure.

The double BJRES fitting joint structure of B787 has more outstanding advantages. However, the BJRES profile fitting joint structure of the lower wall plate has higher assembly accuracy requirements than the T-shaped profile structure, and the processability is more complicated.

1.3 Design method of fitting joint between the center wing section and the outer wing section of a regional aircraft

1.3.1 Load transfer characteristics and structural design principles of fitting joint

The aerodynamic load and inertial load acting on the wing surface are accumulated along the span direction. The resultant force on any section can be characterized by three components: shear force, bending moment, and torque. Finally, the load balance is achieved in the root rib section through the center wing section structure or the interface between the root rib and the fuselage structure, where the upper and lower bending moments are self-balanced on the center wing symmetry plane, and the torque is balanced with the fuselage load through the root rib and fuselage side wall connection structure and the central wing and floor longitudinal beam and keel beam connection structure, and the wing shear load is balanced with the fuselage inertial load. Considering aerodynamic efficiency, in order to improve the lift-drag ratio characteristics and critical speed of aircraft, the current aircraft wing aerodynamic design adopts a larger aspect ratio and a larger sweep angle, which will result in larger bending moment and torque in the wing root area. Under the most critical vertical 2.5g overload condition, for the wing root, because the accumulated head torque of the wing surface is in a positive superposition relationship with the shear force of the rear beam web, the shear force of the rear beam web at the wing root is very large. In order to better diffuse the concentrated load, advanced regional aircraft structures usually arrange a "trapezoidal plate" on the rear side of the rear beam. The front end of the trapezoidal plate is connected to the center wing rear beam, usually coplanar with the root rib, and connected to several fuselage frames (2 to 3) on the upper side, which can achieve load diffusion and balance between the wing and the fuselage in a larger area. It will significantly reduce the load concentration in the rear beam connection area and the structural weight of the rear beam frame, which is more beneficial to the structural durability. At the same time, the trapezoidal plate is coplanar with the root rib plane and can be regarded as a backward extension of the root rib structure. The torque on the root rib web surface can be balanced with the inertial load from the rear fuselage through the trapezoidal plate shear force, achieving torque diffusion in a larger range, reducing the torque transmitted to the central wing box and the floor longitudinal beam and keel beam interface, making the overall structure more efficient and reducing the structural weight.

1.3.2 Method for defining the root rib position

When optimizing the wing-fuselage connection structure, a key design point is to consider the layout of the root ribs that coordinate with the surrounding interface. The layout of the root ribs needs to consider the separation surface position between the center wing section and the outer wing section, the structural coordination relationship and load transfer efficiency between the root ribs and the fuselage sidewalls, the direction of the root ribs, and the load and weight they carry in the wing-fuselage connection structure. The general principles for determining the orientation of the root ribs are as follows.

1) Fully consider the intersection relationship between the wing and fuselage surfaces, and try to make the structure of the wing-fuselage connection area more compact and efficient.

2) The smaller the angle between the root rib and the tangent of the fuselage side wall, the better, so as to reduce the out-of-plane load component and secondary bending moment at the interface.

3) Reduce the demand for fairing size by the root rib slat structure, reduce the size and weight of the fairing structure, minimize lift surface loss, and reduce drag.

4) Fully consider the space requirements for wing root docking holes and fastener installation to ensure necessary accessibility and work efficiency. For thick and complex interlayers, the space requirements for automated tools need to be fully considered.

According to the above principles, there can be many arrangements and parameter definitions of the root ribs. However, the definition of the root rib arrangement of advanced regional aircraft has evolved through history, and there are currently two main types as follows.

1) The first rib is perpendicular to the ground and parallel to the fuselage symmetry plane. At a certain position, the fuselage side wall transitions from the original arc shape to a plane shape parallel to the fuselage symmetry plane. At this time, the plane projection shape of the central wing is a rectangle. Traditionally, this turning point is usually the intersection of the floor beam reference and the fuselage curved surface, which can better balance loads at nodes, as shown in the second definition method in Fig. 1.10. For new composite fuselage structures, which are

more sensitive to out-of-plane loads and consider the sensitivity of automated manufacturing to excessive local curvature, this turning point may be the maximum width of the fuselage, as shown in the first definition method in Fig. 1.10.

2) The fuselage as a whole maintains a cylindrical structure, and the root rib is perpendicular or not perpendicular to the ground and not parallel to the fuselage symmetry plane. Its position is determined based on the three-dimensional space curve formed by the intersection of the wing and the fuselage aerodynamic shape surface. Considering the spatial characteristics of the wing installation angle, the root rib is slightly away from the fuselage symmetry plane in the front beam direction and slightly close to the fuselage symmetry plane in the rear beam direction. At this time, the plane projection shape of the center wing section is a trapezoid with a wide front beam and a narrow rear beam. The fuselage can maintain the arc of the barrel section, or consider the local structural step difference to perform local small-scale modification, as shown in the third definition method in Fig. 1.10. A variant of this scheme is to deflect the lower side of the root rib inward in the direction of the fuselage symmetry plane, which will further reduce the tangent angle between the root rib web and the fuselage barrel section, reduce the local bending moment at the fuselage connection interface, and the envelope size of the middle fuselage section is small, which is convenient for transportation, as shown in the fourth definition method in Fig. 1.10. The fuselage of the "Beluga" aircraft A350 adopts this scheme.

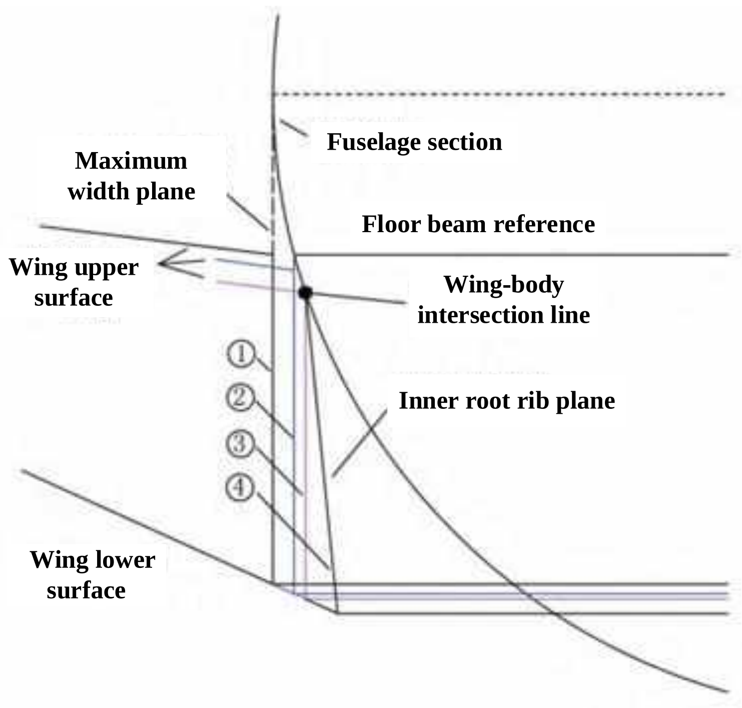

Fig. 1.10 Several typical root rib plane definition methods

1.3.3 The connection interface between the center wing section and the outer wing section

Theoretically, under the premise of ensuring structural safety and processability, the connection between the upper and lower wall panels of the front and rear beams can be in various forms. However, after long-term practical optimization, the main connection methods of the root of the transport wing can be divided into two categories, namely, the sleeve-type connection and the butt-type connection.

1.3.3.1 The sleeve-type connection

The sleeve-type connection is connected by overlapping. The root rib connection structure is assembled in place on the central wing section or the outer wing section. The outer wing section box structure moves to the side of the center wing section during attitude adjustment and is sleeved on the root rib docking structure [2]. In order to ensure the horizontal measurement and attitude adjustment of the wing, this connection method must leave freedom for the movement of the outer wing section box, so a certain nominal gap needs to be left between the fixed structure and the movable structure. After the structure is adjusted in place, padding is added for compensation. The advantages of the sleeve-type connection are compact structure, small width of the connection area connection structure, light weight, and direct force transmission, but its disadvantage is that the limited nominal gap constrains the approach path of the wing attitude adjustment. In particular, considering the wing's dihedral angle, installation angle and swept attitude, according to the specific root rib assembly plan, the wing movement path under specific conditions needs to be specially set, thereby affecting the docking assembly efficiency. Another disadvantage is that under the in-place condition, the measurement of the padding gap of the fitted structure in the front and rear beam areas is more complicated than that of the beam fitting joint type. The internal nominal gap padding amount is large [10]. The large padding amount around the root rib affects the assembly efficiency. At the same time, when the padding thickness is large, it also affects the structural strength and durability [11-12].

1.3.3.2 The beam butt-type connection

This scheme is to connect the root of the front and rear beams with the root rib connection structure, as shown in Fig. 1.11. The upper and lower wall panels are overlapped with the upper and lower edge strips of the root rib. When overlapping, considering reducing the restrictions on attitude adjustment, the upper and lower wall panel mating surfaces are both on the lower side of the edge strip, and the wing box can achieve attitude adjustment approach through the path of inward-forward-upward (according to the design characteristics, if the front and rear directions are not constrained, the forward step can be omitted). Considering the flat structural characteristics of the wing, when overlapping on the upper and lower edge strips of larger size, the efficiency advantage of the overlap structure should be utilized, thereby reducing the structural weight, and also reducing the requirements for the size of the fairing and the impact on aerodynamic performance. Fitting joint is used in the front and rear beam areas to reduce attitude adjustment restrictions, and at the same time, better compensation characteristics are achieved in this area at a lower weight cost, that is, the corresponding mating surfaces can be accurately measured under open conditions, and the connecting strips can be matched and processed, and the assembly quality is easy to ensure.

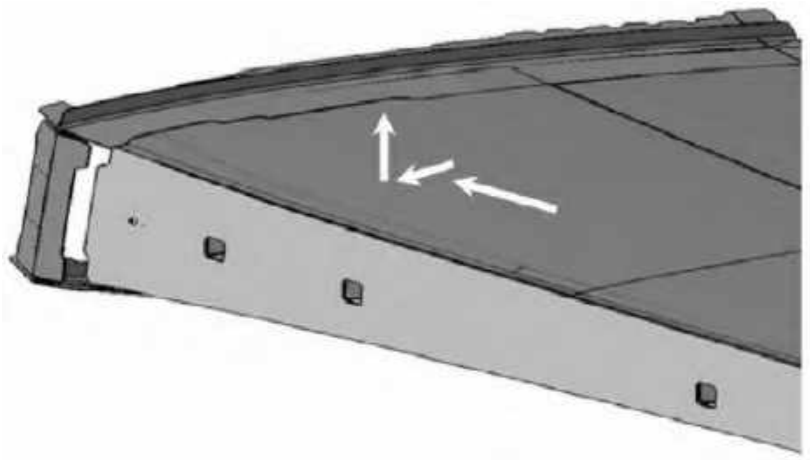

Fig. 1.11 Schematic diagram of a typical wing assembly attitude adjustment approach path

1.3.4 Design method of outer wing section root connection

The wing root connection can be divided into beam connection and panel connection.

1.3.4.1 Beam connection

The goal of beam connection design requirements is to ensure that the shear force of the beam web and the axial force of the beam flange can be effectively transmitted to the connected structure. At the same time, it is considered that in the actual structure, the web shear load level is low and the flange axial load is large. And for axial loads, especially tensile loads and local secondary bending moments, they will have a significant impact on the durability of the structure. Therefore, it is recommended to use double shear connection in areas where axial load exists. It is beneficial in improving the extrusion strength of nail holes, the allowable stress of the connection structure, and reducing the local secondary bending moment and structural durability. In summary, beam connections are generally divided into three areas.

1) A prefile is arranged inside the upper edge strip to form a double shear connection structure with the connecting strip plates on the upper wall plate and the web.

2) The connection method between the lower edge strip, the lower wall panel and the prefile is the same as the upper edge strip.

3) The main shear load transfer area of the beam web is a single shear connection, except for the local area close to the edge strip that forms a double shear connection due to the presence of the prefile.

1.3.4.2 Panel connection

The connection of the wall panels takes into account two aspects: the tensile and compressive normal stress load of the wall panel skin and the torsional shear flow load along the wing section. The connection method is similar to the beam structure, that is, the relatively low shear load component has no special requirements for the structural connection, and the main consideration is the influence of the higher tensile and compressive normal stress load and the local secondary bending moment on the structural strength and durability. In traditional metal models, the wall panels often adopt Z-type long girders, I-type long girders, J-type long girders and other structural forms. In this way, the structure adopts an integral double shear connection structure at the wall panel connection, that is, the structure on one side of the skin adopts a single shear connection, the independent edge strip of the long girders adopts a single shear connection, but the overall connection of the wall panel constitutes a double shear, as shown in Fig. 1.12 (a). The local stiffness of the structure is large, and the adverse effects of the secondary bending moment can be effectively controlled as a whole. For the upper wall panel structure controlled by stability, the end support coefficient is also increased, thereby increasing the critical stress of structural instability. However, this type of structure has many coordinated interfaces for connection, and assembly coordination is not easy. If the traditional BJRES structure is adopted, the parts processing is difficult, the assembly coordination and padding workload is large, and it is easy to generate assembly stress under improper processing conditions [6], or generate high additional internal stress under deformation coordination conditions.

Another double shear structure is that the wall plate and the edge strip are matched on one side. The long stringer gradually bevels to the root of the wing to transition to a T shape, and then connects through a connecting profile. Therefore, in the structure involved in the root docking, whether it is the skin side or the long stringer web docking area, it is a double shear structure, as shown in Fig. 1.12 (b). For the lower wall of the wing, because it mainly bears tensile loads, the design concept is to try to smoothly transition the load to the two-dimensional plane docking structure configuration, which will simplify the optimization of structural stiffness, better achieve the coordination of the rigid center, reduce the local secondary bending moment, and optimize the distribution ratio of the nail load, so as to better ensure the strength and fatigue characteristics of the structure. The typical structural details are shown in Fig. 1.13. Reference [5] also conducted finite element analysis and experimental research on different detail design configurations, and gave a better detail design principle considering the distribution of nail loads.

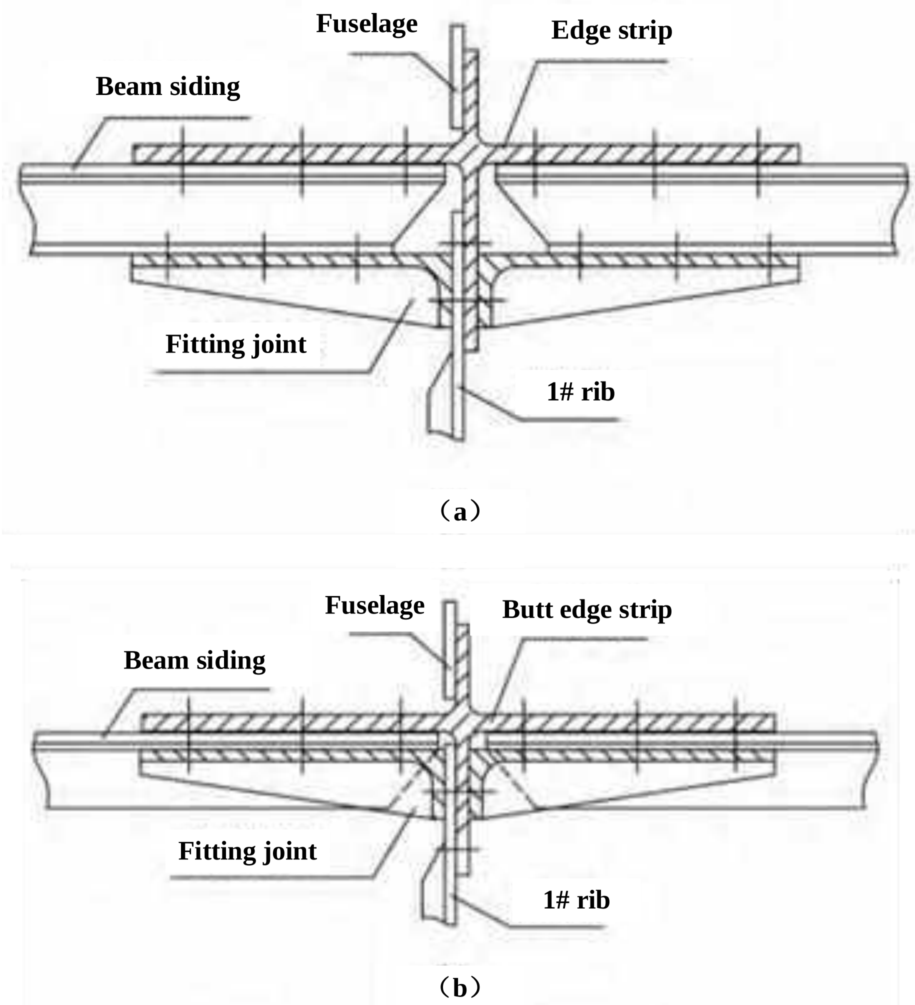

Fig. 1.12 Typical connection form of the upper wing panel

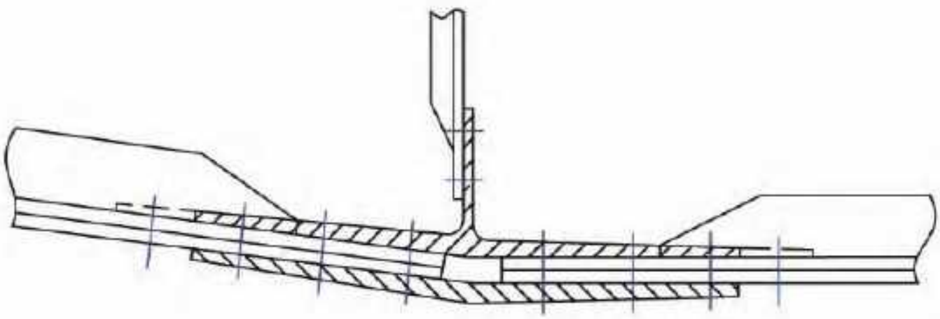

Fig. 1.13 Typical connection form of the lower wing panel

In the process of panel docking design, the hole making, fastener installation and fastener replacement in the root connection area under maintenance conditions have relatively high requirements for accessibility and space, which will affect the assembly efficiency of aircraft, structural safety and subsequent maintenance characteristics. Therefore, the current development trend of the root docking of international advanced civil aircraft panels is to simplify the hole making and fastener installation methods as much as possible in structural design (especially for the upper panel connection area), including:

1) The top edge strip is eliminated from the connection area purlin to make the hole making path on the skin-side wall panel structure or web structure unobstructed.

2) For some new composite wing aircraft, integral connection is adopted, and even fasteners are not installed on the web of the long stringer. Under the premise of meeting the structural connection requirements, the coordination efficiency and assembly efficiency of the mating surface are further simplified, the tolerance and lightning protection gap control requirements are met, and the hole making and fastener installation costs are reduced (as shown in Fig. 1.12 (b)).

In summary, for the root connection structure of large regional aircraft, the design idea is double shear connection, end beveling, rigid center alignment, and margin control. The design of double shear connection mainly considers improving the extrusion strength of nail holes in key areas, reducing secondary bending moments, improving structural durability, and having failure safety characteristics. The main consideration of end beveling is to optimize local stiffness, slow down interface mutation, reduce secondary bending moment, and optimize structural weight. Margin control is very critical for the root connection area. Considering the high structural safety requirements of the root connection area, the difficulty of structural crack/defect inspection and repair, and the high difficulty of structural maintenance operation, the structural design of the wing root connection area should have sufficient margin in both static strength and fatigue strength. For regional aircraft structures, the minimum fatigue strength margin of the metal structure corresponding to the controlled stress level under the specified fatigue life conditions is recommended to be no less than 0.1. An appropriate weight penalty is used to ensure structural safety and durability, while reducing subsequent maintenance costs and safety risks.

1.3.5 Flexible compensation design method

For the wing root fitting joint, the forced assembly stress caused by the incomplete matching between the complex coordinated interfaces is always difficult to avoid, and the structural detail design must strive to minimize these stresses and their effects.

To achieve this goal, the following 4 measures can be taken in design and process.

1) Precise control of the mating interface and related benchmarks for parts manufacturing and assembly: when manufacturing parts, the processing and treatment processes must be optimized so that the shape accuracy of the manufactured parts is controlled within the allowable tolerance range. At the same time, when assembling, the complexity and efficiency of the outer wing section docking interface are fully considered to ensure the contour requirements of the components at the docking interface as much as possible.

2) The local stiffness characteristics of the wing root docking structure are fully considered to fully ensure the connection stiffness along the main load direction, which is beneficial to the load transfer efficiency and durability of the structure. At the same time, a good stiffness transition is carried out to optimize the nail load distribution in the connection area.

3) Fully release the structural stiffness perpendicular to the main load direction. For the wing root connection, it means fully releasing the structural stiffness along the height direction. This is also the fundamental reason for the two-dimensional connection recommended in the previous article. As shown in Figs 1.12 and 1.13,

the root ribs of the upper and lower wing panels are two-dimensional plate structures in the docking area. Under the condition of maximizing the accuracy of parts and assembly, if there is an internal gap, under the preload of the fastener, due to the low out-of-plane stiffness of the plate structure, flexible compensation can be provided to comply with the structure with larger stiffness. The assembly stress caused at this time will be significantly reduced, which fully guarantees the stress corrosion characteristics and durability of the structure. References [6] and [7] confirmed the load-bearing superiority of this design through test results and simulation analysis respectively.

4) This flexible compensation will be more meaningful when the front and rear beam structures are connected in the same way. At present, the wing structure of advanced regional aircraft adopts a C section beam structure. When the wing root is docked, the mismatch of the beam root is inevitable due to the combined influence of various reasons such as manufacturing accuracy, assembly accuracy, attitude change, temperature change, etc. the mismatch of the root of the beam is inevitable. When tightening the connection, if there is a gap inside, the beam web provides a higher stiffness in the height direction, and a high transfer stress is generated in the R zone where the beam flange and the web transition. Under the action of complex external loads, stress corrosion and fatigue problems are prone to occur [13-14]. For composite beam structures, delamination of the R zone will occur. The recommended solution is to cut off part of the web and flange in the root connection area or cut a seam between the flange and the web of the beam. By separating the flange and the web in the structure, flexible release is achieved, solving the problem of high assembly stress caused by the difficulty of interface matching of large-size beam structures. Then, the structure is reconnected using a profile with a precisely prepared mating surface, and the integrity of the structure is restored without increasing the assembly stress.

Reference [15] also confirmed this conclusion through finite element analysis and experimental research on the local connection area of the root of the wing upper wall panel.

When the wing roots of a domestically-made regional aircraft using the above-mentioned design were docked, there was a local gap error in the connection of the lower wall panel during the first assembly. After applying external force to fit the lower wall panel of the outer wing section with the connecting edge strip, the assembly stress caused on the wall panel was measured to be approximately 10 MPa, which did not exceed 3% of the allowable stress. The impact on the static strength and fatigue strength was evaluated to be acceptable, confirming the effectiveness of the relevant design method, as shown in Fig. 1.14.

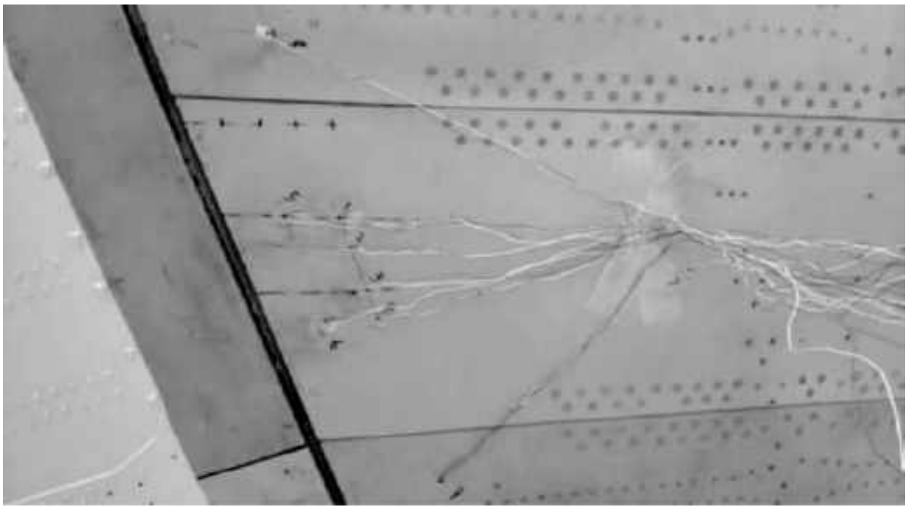

Fig. 1.14 Strain measurements of the wing root during the forced assembly attempt

1.4 Analysis and discussion

For the wing structure that is developing rapidly internationally, the wing root scheme is generally similar to the requirements of the traditional structure, but there are typical characteristics of the composite structure under load.

Try to avoid the composite structure from bearing out-of-plane loads and complex stress states, including out-of-plane loads and interlayer additional loads caused by forced assembly [16]. Due to the structural characteristics of layered composite materials and the weak interlayer interface, the ability of composite materials to withstand out-of-plane loads is very low. Therefore, in the connection area at the root of the wing, the additional bending moment and the additional load state that may be caused by deformation coordination should be controlled as much as possible, and a connection structure with a reasonable slope transition and a simple force transmission route should be adopted. This is also the main reason why the wall panel connection scheme has developed from a three-dimensional spatial connection structure to a two-dimensional one in the current new composite civil aircraft structure connection.

The thickness tolerance of the composite structure formed based on the curing of the layers is large, and the size variation range of the thicker structure is large, which may constrain the wing assembly attitude adjustment and have an adverse effect on the assembly. The commonly used treatment method is to design a machineable layer (sacrificial layer) on the inner surface of the wing lower wall panel, and accurately control the mating surface through machining based on the assembly reference to ensure the assembly requirements.

Reverse preparation technology for mating surfaces. Consider the connection profile at the flange of the front and rear beams, which needs to be matched with the three interfaces of the beam flange, beam web, and root rib web. The traditional matching grinding assembly method is inefficient and has poor precision. The more advanced manufacturing method is to reconstruct the mating surface of the connected structure by three-dimensional space scanning under the condition that the components are in place. The data is transferred to the finishing platform in a digital way. The matching surface of the profile with appropriate margin is matched. The matching surface of the profile structure has high precision, high processing efficiency, and is completed in one time. It has been verified in practice that after adopting this method, the matching accuracy can be improved to within 0.1 mm, which is beneficial to the safety and durability of the structure. The assembly process of the wing wall panel and the frame of the A350 also adopts this technology [17].

High reliability fastening connection design for complex connection areas. For the root connection area, even the traditional all-metal structure has the problem of difficulty in installing large diameter interference fit fasteners. The solution adopted by an advanced manufacturer is to use conical fasteners to match the conical holes on the structure when the fastener diameter is large. After the fastener is tightened, the interference fit is formed by extrusion through the conical surface. However, this method is difficult to make holes, the cost is high, and the interference is limited. At present, for pure metal sandwiches, the better solution to this problem is to use high interference pull-in fasteners. With the extensive application of composite materials on the center wing section and outer wing section boxes, the root connection area of the wing has become a large thickness (total thickness can reach more than 80 mm), complex sandwich (3 to 4 layers, including composite materials, titanium, aluminum and other sandwiches), and large diameter fastener connection area. Traditionally, this area uses clearance fit fasteners to avoid composite delamination. In this way, it will lead to a series of problems such as reduced nail hole extrusion strength, increased uneven load of nail groups, and reduced fatigue life of metal structures due to clearance fit. Considering that a reasonable amount of interference will improve the strength, fatigue characteristics and stiffness of the structural connection [18-19]. The use of bushing bolts that expand circumferentially during installation, do not cause composite material delamination, and are also applicable to metal structures, will be a better solution to this problem.

1.5 Conclusion of this chapter

This chapter completes the dissertation work task: summarize the types of fitting joint between the center wing section and the outer wing section of existing regional aircraft and analyze the design features and design methods of fitting joint. The complexity, main constraints and requirements of the wing-fuselage connection and root docking area of aircraft, as well as the characteristics and advantages and disadvantages of different mainstream root connection schemes are analyzed. It gives different definition methods and features analysis of root ribs as design and assembly benchmarks, and gives a comparative analysis of the sleeve-type scheme and beam-type scheme of the root docking scheme between the wing and the central wing, as well as the typical design method of the wing root connection and its main considerations. From the perspective of structural efficiency and relieving assembly stress, a design method for stiffness optimization and flexibility compensation of the wing root rib fitting joint is proposed. The main conclusions are as follows:

The arrangement of the root rib has an important influence on the determination of the separation surface between the wing and the fuselage, the structural load transfer efficiency and the structural assembly efficiency. It should be considered comprehensively based on the overall design of the aircraft structure, the wing-fuselage structure, the material and its load-bearing characteristics, the coordination relationship of the wing-fuselage connection area interface, and the weight. The docking area should be compact and efficient, meet the requirements of relevant structural load balance, manufacturing and assembly processability, reduce lift surface loss, and reduce drag.

The connection design of the wing root should be considered from the perspective of load transmission efficiency. The structural connection stiffness and structural integrity in the main load direction should be guaranteed as much as possible, and the connection stiffness perpendicular to the main load direction should be fully released. For the front and rear beam profiles, it is recommended to design reasonable features to release the local stiffness constraints of the beam and the web, use the assembled profiles to restore the structural integrity, and control the assembly stress through flexible compensation.

The wing root connection requires the establishment of a design concept of double shear connection, end beveling, rigid center alignment, and margin control to optimize local stiffness transition, simplify the force transmission route in the connection area, limit additional bending moment, optimize nail load distribution, ensure structural safety and durability in key connection areas, and reduce potential structural maintenance costs.

As the key process of final assembly, the processability, assembly efficiency and cost impact of the wing connection area must be considered together during the structural design. The root connection design should achieve a coordinated balance in terms of structural efficiency, processability and weight. For regional aircraft structures, the impact of cost needs to be specially considered. For the connection of thick and complex laminated wing root structures, efficient, high-quality and automated hole making has become a trend, and the equipment accessibility requirements need to be specially considered during the design.

CHAPTER 2

METHOD OF FITTING JOINT STRUCTURE DESIGNING ACCOUNTING FOR STRENGTH AND FATIGUE LIFE REQUIREMENTS

An aircraft is composed of tens of millions of structural components, and the service life of these structural components directly determines the service life of the aircraft. For regional aircraft, structural components are usually connected by bolts or rivets. Fig. 2.1 shows a typical bolted connection between the wing and center wing box panels of a regional aircraft. Studies have shown that most of the damage in aircraft structures occurs at these connection locations, and the main causes of damage are stress concentration and fretting corrosion [20]. In the aircraft design process, in order to avoid the occurrence of stress concentration, it is crucial to analyze the force changes and safety factor of the components in the joints on the aircraft to ensure the safe flight of the aircraft. In order to meet the strength and fatigue life requirements of aircraft, structure designing must be performed during the design stage of the fitting joint.

Safety factor is a factor used in engineering structure design methods to reflect the safety level of a structure. It represents the ratio between the bearing capacity of a structure or component and the load under consideration. The significance of the safety factor is to ensure that the structure can withstand the possible loads during the design period and to prevent structural damage due to material defects, changes in working conditions, or calculation errors. Choosing an appropriate safety factor requires finding a balance between safety and economy, taking into account material consumption and cost while ensuring structural safety. Today, the Federal Airworthiness Regulation Part 25.303 – Factor of Safety states: "Unless otherwise specified, a factor of 1.5 must be applied to the prescribed limit loads which are considered external loads on the structure." [21,22]

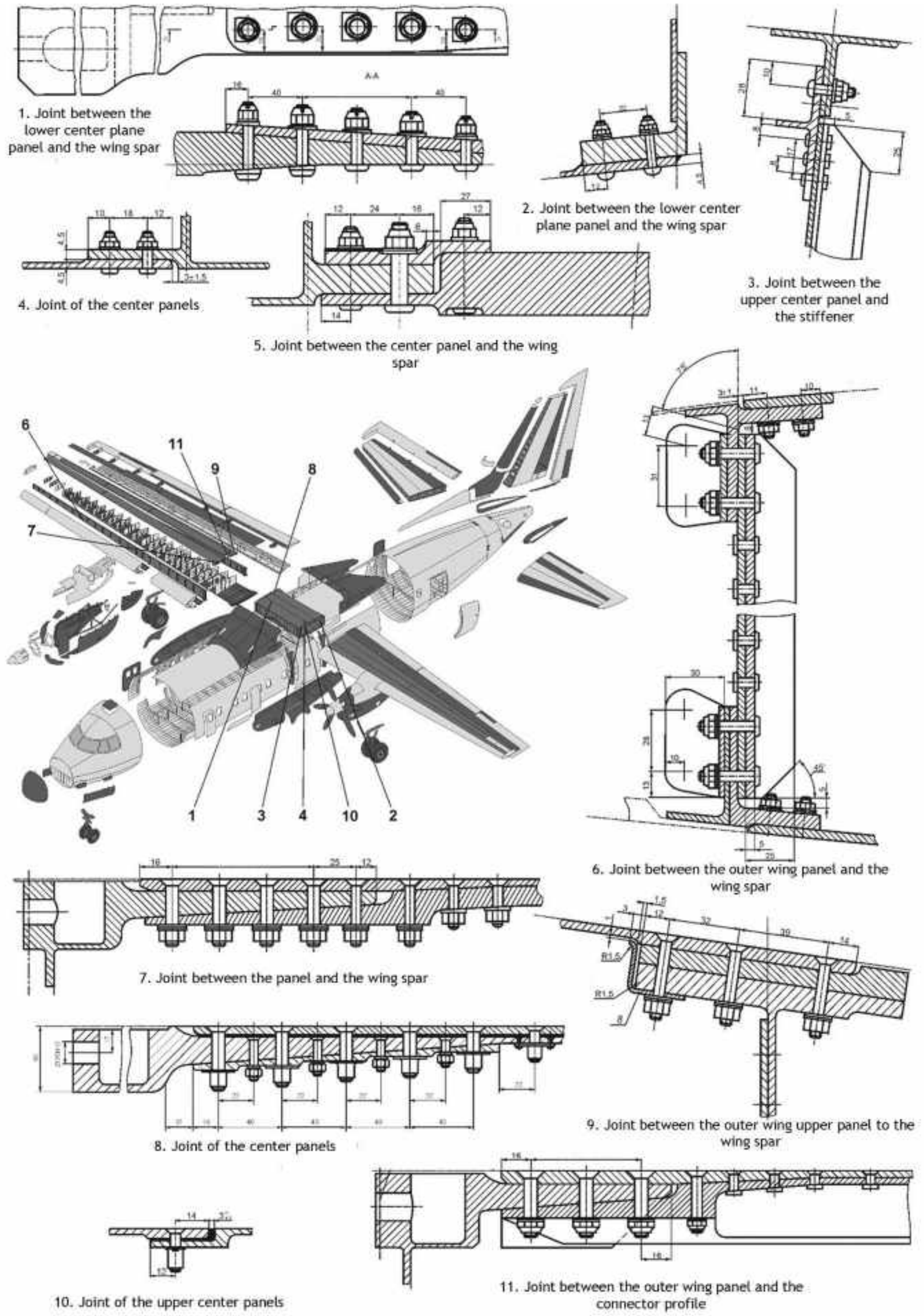

Fig. 2.1 Typical bolted connections of wing panels and center wing section of a regional aircraft

Currently, there are two types of connection methods for connecting the wing panels between the center wing section and the outer wing section of a regional aircraft: flange connection and shear connection [23]. In the case of flange connection, the wing panel is connected to the flange joint through a set of bolts. The middle joint at the other end of the flange joint is connected to the wing central section joint through a large diameter tension bolt. The middle joint and the flange joint form the wing outer section joint. The three-dimensional structure of the flange connection is shown in Figs 2.2~2.3. Due to the change in the stiffness of the material of the joint component and the point-like nature of force transmission, stress concentration occurs in the joint. In order to ensure that the joint is not damaged by stress concentration, the cross-sectional area of the load-bearing unit must be increased. However, the limitation of the load-bearing unit size of the theoretical wing profile means that the cross section can only be increased from the inside of the wing panel, which causes eccentricity in the force transmission, resulting in local bending of the wing panel. Therefore, the strength calculation of the wing panel joint is simplified to the calculation of the structural area with a non-linear stiffness axis, accompanied by changes in stiffness and boundary conditions. It can be seen that the forces on each component in the structure connected by the joint are very complex. In order to avoid stress concentration in each component and ensure the safe flight of the aircraft, it is necessary to analyze the force and safety margin of each component.

2.1 Fitting joint design

According to the design method proposed in Chapter 1, this chapter uses frame fitting joint with comb-shaped profiles to design the fitting joint between center wing section and outer wing section of a regional aircraft, as shown in Fig. 2.2. It can be seen that the structure of the fitting joint is very complex, so the model of the fitting joint must be simplified for analysis.

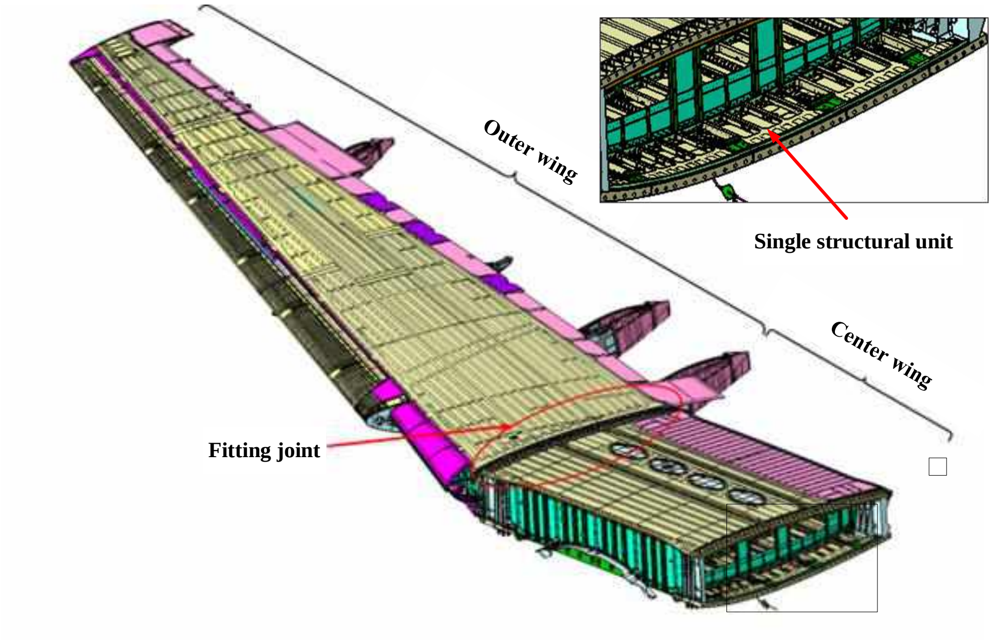

Fig. 2.2 The fitting joint between the center wing section and the outer wing section

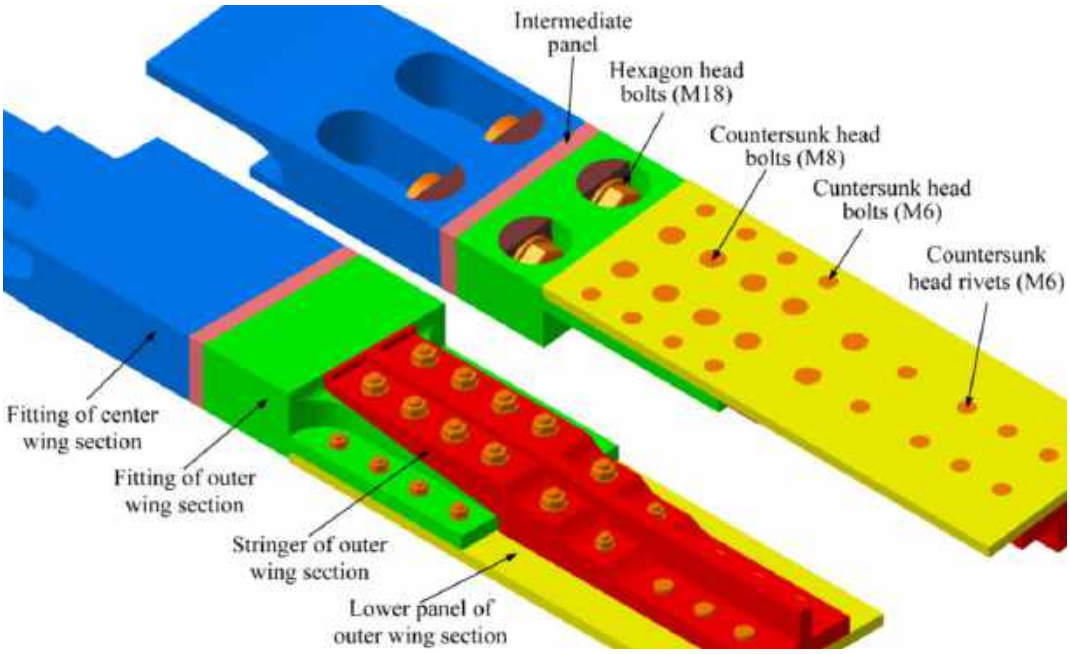

Fig. 2.3 The three-dimensional structure of flange connection (single structural unit)

The connection between the center wing section and outer wing section can be seen as a combination of many similar structural units. For these similar structural units, the same method can be used to calculate their stress-strain state. In this chapter, the single connecting unit in the middle below between the center wing section and outer wing section is taken as the research object for analysis. The fitting joint structure of a single connection unit in the middle below is shown in Fig. 2.2. This fitting joint structure includes fitting of center wing section (FCWS), intermediate panel (IP), fitting of outer wing section (FOWS), stringer of outer wing section (SOWS), lower panel of outer wing section (LPOWS), hexagon head bolts (M18), countersunk head bolts (M8 and M6) and countersunk head rivets (M6), as shown in Fig. 2.3.

2.2 Initial data

In the design of flange connection structure, the dimensional parameters of each component, the mechanical properties of the materials used and the boundary conditions of the components will affect its service life. In order to accurately calculate the force and safety factor of the flange connection structure, these initial data must be clearly known before calculation. The dimensional parameters of the flange connection structure are shown in Fig. 2.4.

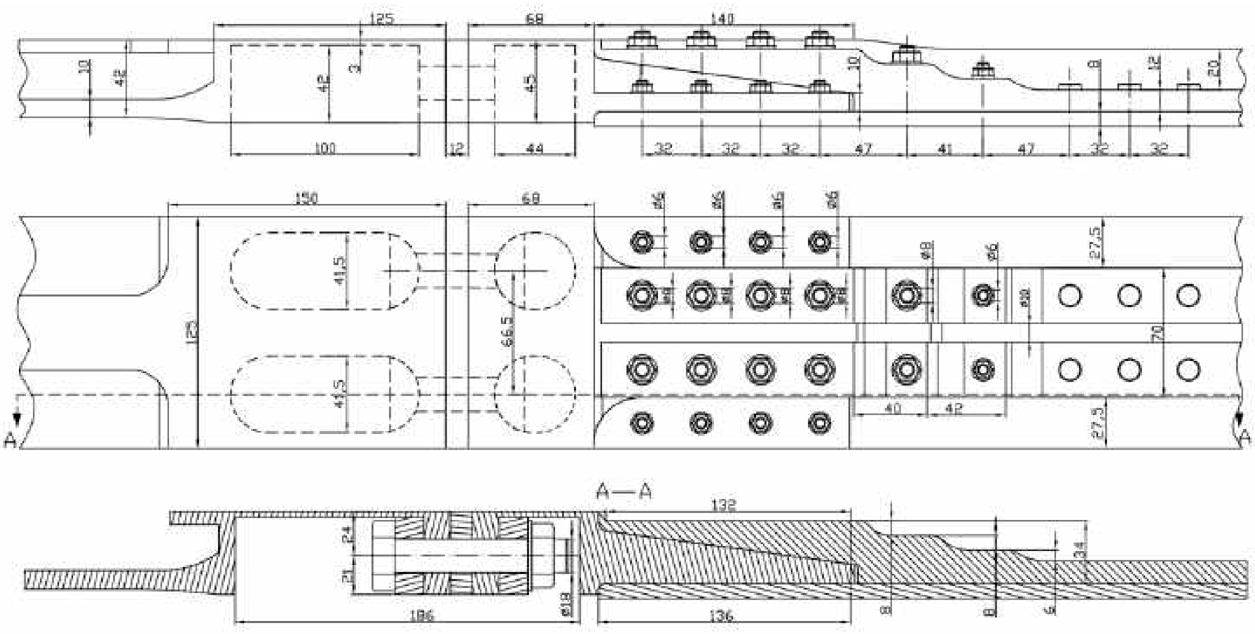

Fig. 2.4 The dimensional parameters of flange connection structure

The forces acting on the wing include lift, gravity and drag. Lift is generated according to Bernoulli's theorem, formed by the pressure difference between the upper and lower surfaces of the wing; gravity is the downward force that attracts all objects vertically toward the center of the earth; drag includes friction drag, pressure difference drag, induced drag and interference drag, etc. Among the forces acting on the wing, lift is the main type of force, usually accounting for the vast majority of the total force, followed by drag and other forces. Therefore, only lift is considered when calculating flange joints. The equivalent stress of the gross load at the end section is $\sigma_{eq} = 150MPa$ [24].

The FCWS, IP, FOWS, SOWS, LPOWS are all made of aluminum alloy D16T. The mechanical properties of the aluminum alloy D16T are shown in Table 2.1. The hexagon head bolts (M18), countersunk head bolts (M8 and M6) and countersunk head rivets (M6) are all made of titanium alloy VT22. The mechanical properties of the titanium alloy VT6 are shown in Table 2.2.

Table 2.1 The mechanical properties of aluminum alloy D16T [25]

Density	Young's Modulus	Ultimate Strength	Yield Strength	Poisson's Ratio
2780 (kg/m^3)	72 (GPa)	564 (MPa)	447 (MPa)	0.3

Table 2.2 The mechanical properties of titanium alloy VT22[26]

Density	Young's Modulus	Ultimate Strength	Yield Strength	Poisson's Ratio
4450(kg/m^3)	115 (GPa)	1455 (MPa)	1380 (MPa)	0.35

2.3 Calculation method and steps

2.3.1 Calculation method

A large number of literatures show that there are many different calculation methods for flange connection structures, which are mainly manifested in the complexity of the calculation and the accuracy of the settlement results. Combining the calculation method of flange connection in references [23,27], the simplified method of force system in reference [28] and the application method of force method in reference [29], this chapter proposes a calculation method for flange connection structure, as shown in Fig. 2.5 below.

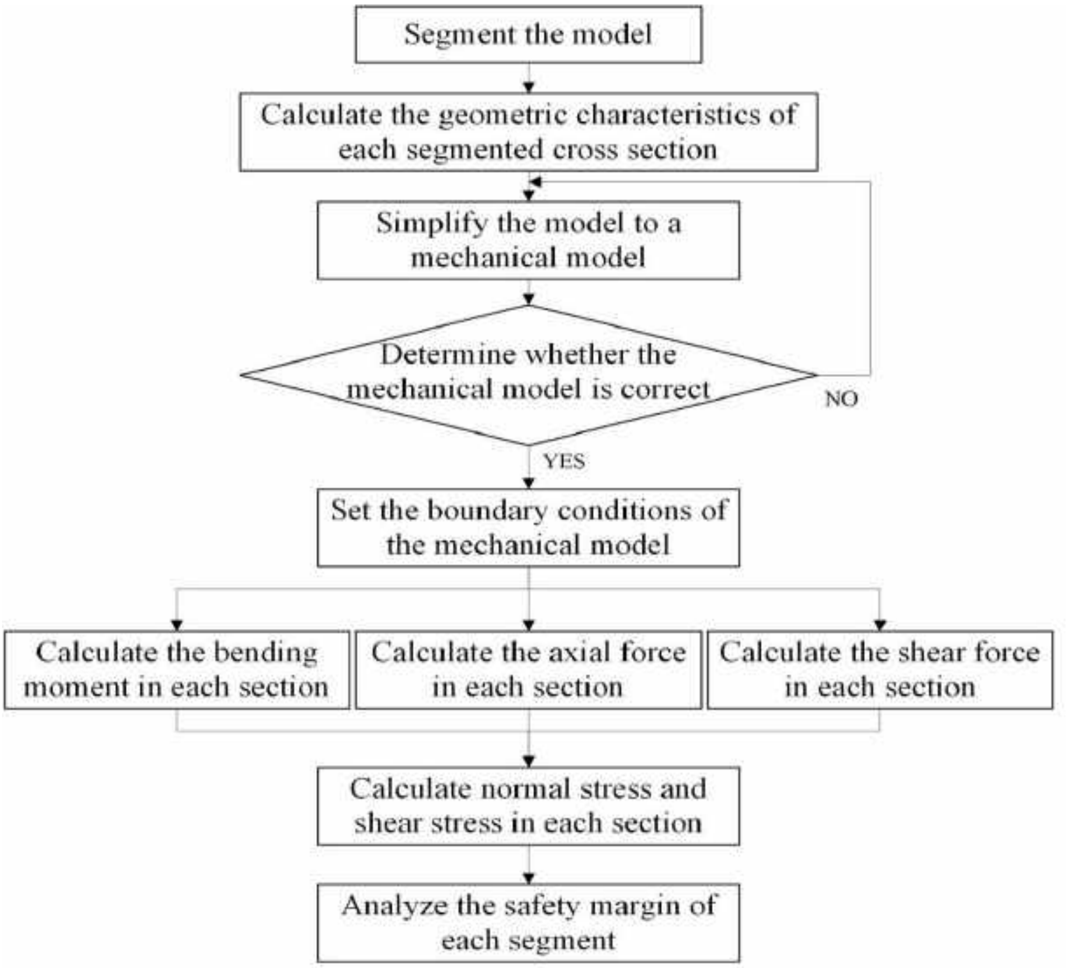

Fig. 2.5 Calculation method

2.3.2 Calculation steps

According to the above calculation method, the following calculation steps are proposed.

Step 1: Transversely cut the flange connection joint and segment the flange connection joint according to the changes in cross-sectional area and center of gravity height. In order to simplify the calculation, the segmentation of the wing panel is the same as that of the flange joint.

Step 2: Calculate the geometric characteristics (area, height of center of gravity, and moment of inertia) of each segmented cross section.

If the cross section is a single cross section or a multi-unit cross section and the unit material is the same, the geometric characteristics of any cross section can be directly calculated by computer. In the 3D modeling software CATIA, create a new section that is the same as the cross section, and then directly read the geometric characteristics of the new section to obtain the corresponding geometric characteristics. It should be noted that when creating a new section that is the same as the cross section, the coordinate system corresponding to the section must be kept the same as the coordinate system corresponding to the original cross section. Fig. 2.6 below shows the new section created in CATIA corresponding to a certain cross section, and Fig. 2.7 shows the interface for reading the geometric characteristics of the new section.

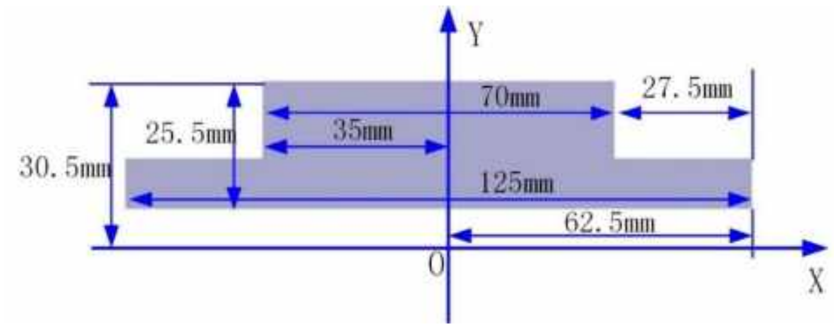

Fig. 2.6 Section created in CATIA

Fig. 2.7 Creating and reading section data in CATIA

In the figure, F is the area of the cross section, M_s is the surface mass corresponding to the cross section, Y_{sec} is the height of the center of gravity of the cross section relative to the theoretical airfoil coordinates, and J is the rotational torque of the cross section. The moment of inertia of the cross section is calculated as follows:

$$I = \frac{J}{M_s} \tag{2.1}$$

If the cross section is composed of multiple unit cross sections and the unit materials are different, the unit cross section area is increased or decreased according to the selected base material. The area of the cross section, the height of the center of gravity and the moment of inertia are calculated as follows:

$$F_{\sec} = \sum_{i=1}^{n} \left(b_i \times \delta_i \times \varphi_i \right) \tag{2.2}$$

$$Y_{\sec} = \frac{\sum_{i=1}^{n} \left(b_i \times \delta_i \times \varphi_i \times Y_i \right)}{F_{\sec}} \tag{2.3}$$

$$Y_{\Delta i} = Y_{\sec} - Y_{end} \tag{2.4}$$

$$I_{\sec} = \sum_{i=1}^{n} \left(b_i \times \delta_i \times \varphi_i \times Y_{\Delta i}^2 + \frac{b_i \times \delta_i^3 \times \varphi_i}{12} \right) \tag{2.5}$$

$$\varphi_i = \frac{E_i}{E_0} \tag{2.6}$$

Where $F_{\sec}$ - The total area of the cross section; b_i - The width of the i-th element of the cross section; δ_i - The thickness of the i-th element of the cross section; φ_i - Reduction factor for the i-th element; Y_i - The height of the center of gravity of the i-th element is relative to the theoretical wing profile coordinates; $Y_{\sec}$ - The height of the center of gravity of the entire cross section is relative to the theoretical wing profile coordinates; Y_{end} - The height of the line of action of the load force P is relative to the theoretical wing profile coordinates; $Y_{\Delta i}$ - The height of the center of gravity of the entire cross section is relative to the height of the line of action of the load force P; $I_{\sec}$ - The total moment of inertia of entire cross section; E_i - Young's modulus of the i-th element of the cross section; E_0 - Young's modulus of the element taken as basic during reduction.

Step 3: Based on the area of each cross section F and the normal stress σ, the longitudinal load maximum force P acting on each cross section and along the center of gravity of the cross section can be determined. The calculation formula is as follows:

$$P = F \cdot \sigma \tag{2.7}$$

The connection structure between flange joint and wing panel is shown in Fig. 2.8. In bolted joints, the joint is a structural area of stress concentration, since the force transmission from one component to another does not occur over the entire panel cross section, but only at individual points (along the fasteners). The locality of the force transmission leads to a reduced efficiency in the use of panel materials, which requires an increase in the cross section of the joint components. Changing the cross section of the panel leads to a change in the coordinates of the center of gravity of the panel part in the joint area, which in turn leads to local bending in the joint. In addition, in flanged panel joints, the axis of the butt bolts usually does not coincide with the line of action of the load force P acting in the joint, which leads to the appearance of local bending.

Due to the misalignment of the axis of the butt bolts and the line of action of the load force, the joint opens around point A under gravity. It should be noted that the joint opens around point B under longitudinal load force. Point A or B is the point farthest from the bolt axis and is located in the plane of the flange type (when there is a chamfer, points A and B are at the beginning of the radius of curvature).

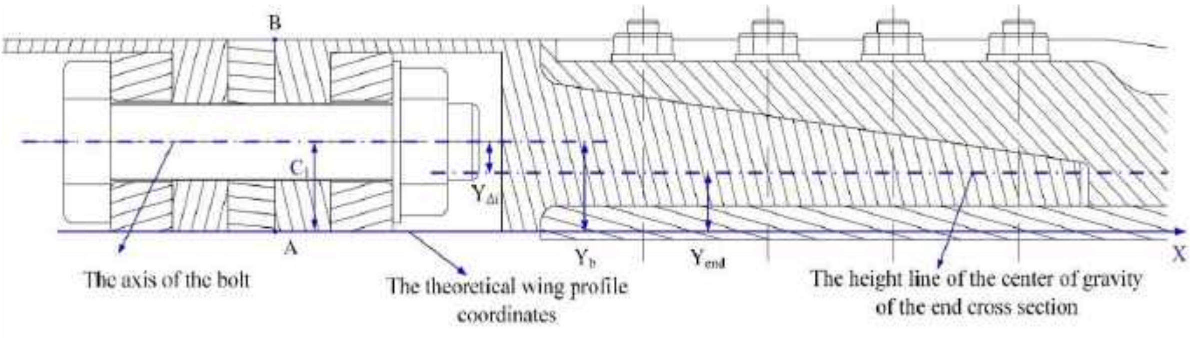

Fig. 2.8 Connection structure between flange joint and wing panel

Step 4: Simplify the model and calculate the bending moment diagram of the simplified structure. According to the force transmission path and the position of the support in the model structure, the model is simplified to the structure shown in Fig. 2.9. The straight line is the force transmission path, the solid circle is the fixed support, the hollow circle is the hinge support, and the solid circles 2 and 3 are rigid connection points.

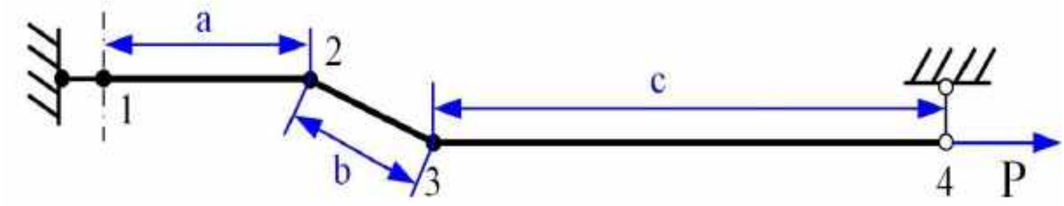

Fig. 2.9 Simplified structure of the model

From the simplified structure of the model, it can be seen that the structural system is statically indeterminate (a hyperstatic structure), so the force method can be used for calculation. The constraints at 4 locations are released to obtain the basic structure of the original simplified model structure, and then the unknown constraint force X_1 (which cannot be calculated by the static equilibrium equation) is used to replace the released constraint effect, and the original load force P is added to obtain the equivalent structure of the original simplified model structure.

According to the force method solution (superposition principle), Δ_1 is regarded as the superposition of the displacement Δ_{1p} caused by the load force P alone and the displacement $\Delta_{1X_1} = \delta_{11} \times x_1$ caused by X_1 alone, that is, the force method canonical equation of the above-mentioned super statically indeterminate structure is as follows.

$$\delta_{11} \times x_1 + \Delta_{1p} = 0 \tag{2.8}$$

The bending moment diagram M_P under the load force is shown in Fig. 2.10.

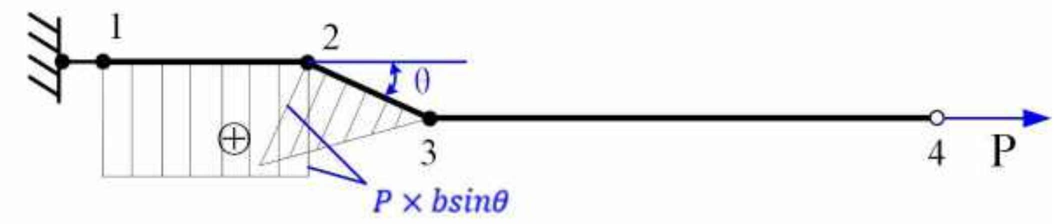

Fig. 2.10 Bending moment diagram under load

The bending moment diagram M_1 under unit force is shown in Fig. 2.11.

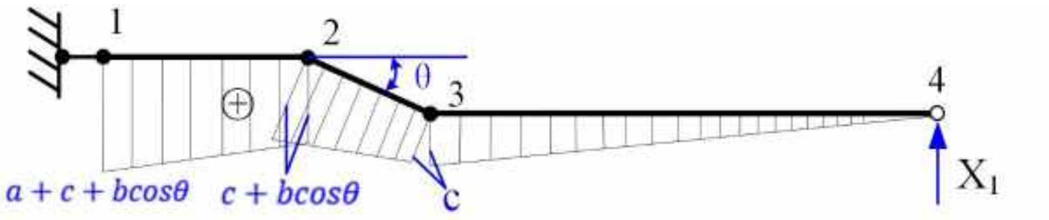

Fig. 2.11 Bending moment diagram under unit force

Considering the case when the simplified structure of the model is made of a material with the same Young's modulus for all elements, the relevant parameters are calculated as follows.

$$\delta_{11} = \frac{1}{E} \times \left(\begin{array}{l} \dfrac{a\left[(a+c+b\cos\theta)^2 + (c+b\cos\theta)^2 + (a+c+b\cos\theta)\times(c+b\cos\theta)\right]}{3I_{1-2}} \\ + \dfrac{b\left[(c+b\cos\theta)^2 + c^2 + c(c+b\cos\theta)\right]}{3I_{2-3}} + \dfrac{c^3}{3\times I_{3-4}} \end{array} \right) \tag{2.9}$$

$$\Delta_{1p} = \frac{P \times \mathrm{b} \times \sin\theta}{E} \times \left(\frac{a(a+2b\cos\theta+2c)}{2I_{1-2}} + \frac{b(\frac{2}{3}b\cos\theta + c)}{2I_{2-3}} \right) \tag{2.10}$$

$$X_1 = \text{-}P \times \mathrm{b}\sin\theta \times \frac{\dfrac{a(a+2b\cos\theta+2c)}{2I_{1-2}} + \dfrac{b(\frac{2}{3}b\cos\theta+c)}{2I_{2-3}}}{\left(\begin{array}{l}\dfrac{a\left[(a+c+b\cos\theta)^2+(c+b\cos\theta)^2+(a+c+b\cos\theta)\times(c+b\cos\theta)\right]}{3I_{1-2}} \\ +\dfrac{b\left[(c+b\cos\theta)^2+c^2+c(c+b\cos\theta)\right]}{3I_{2-3}}+\dfrac{c^3}{3\times I_{3-4}}\end{array}\right)} \quad (2.11)$$

Where I_{1-2} - The Moment of inertia of rod 1-2; $I_{2\text{-}3}$ - The Moment of inertia of rod 2-3; $I_{3\text{-}4}$ - The Moment of inertia of rod 3-4.

The bending moment diagram M of the simplified structure of the original model is calculated as follows.

$$M = M_1 X_1 + M_P \quad (2.12)$$

The bending moment diagram M of the simplified structure of the model is drawn as shown in Fig. 2.12.

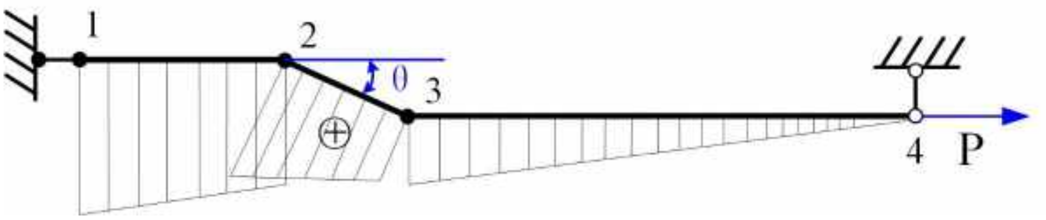

Fig. 2.12 Bending moment diagram under unit force

Step 5: Calculate the axial force in each section of the model, and then calculate the stress at the maximum load point of any cross section based on the axial force and bending moment diagram.

$$\sigma_{\sec} = \frac{N}{F_{\sec}} \pm \frac{M}{I_{\sec}} \cdot \left(Y_{\Delta i} + 0.5 \times \delta_i\right) \quad (2.13)$$

For the transition zone of the rigid shaft, the shear force Q and the axial force N are defined as follows.

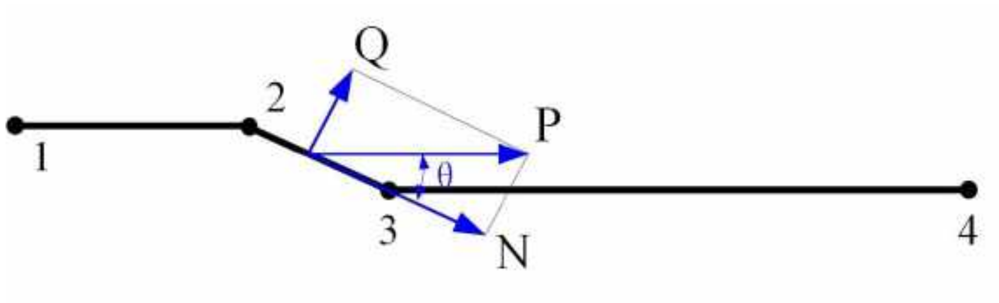

Fig. 2.13 Axial force and shear force

Shear force Q:

$$Q = P \times \sin\theta \tag{2.14}$$

Axial force N:

$$N = P \times \cos\theta \tag{2.15}$$

Step 6: The additional load (when there is bending tension at the joint), total load and safety factor of the butt bolts are calculated by the magnitude of the bending moment in the joint plane.

Additional load of the butt bolts:

$$P_M = \frac{M}{C_1} \tag{2.16}$$

Where C_1 is the distance from the bolt axis to the stop point of the connector profile when opening the joint (see Fig. 2.8).

Therefore, the total load acting on the butt bolt:

$$P_{\mathrm{b}} = P + P_M \tag{2.17}$$

According to the number of bolts n and the breaking force value of the bolts P_{m}, the safety factor of the butt bolts is calculated according to the “bolt joint calculation” methodology [27] as follows.

$$\eta_{\mathrm{b}} = \frac{n \times P_{\mathrm{m}}}{P_b} \tag{2.18}$$

Step 7: Calculate the safety factor of the intermediate joint under the butt bolt washer under shear force.

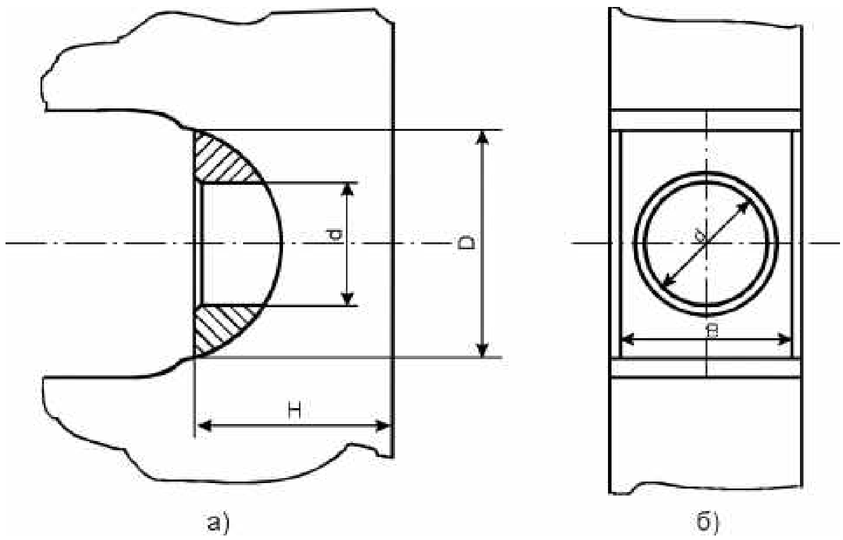

Fig. 2.14 Connection structure between gasket and intermediate joint

Calculation of the shear area of the intermediate joint below the gasket.

In case of square gasket:

$$F_s = 2 \times B \times H \tag{2.19}$$

In case of round washers:

$$F_s = 2.5 \times D \times H \tag{2.20}$$

The maximum shear stress borne by the intermediate joint is:

$$\tau_s = K_n * \frac{P_б}{F_s} \tag{2.21}$$

Where Kn is the distribution inequality coefficient, Kn=1.5 (rectangular section).

Therefore, the safety factor of the intermediate joint under the gasket under shear force is:

$$\eta_s = \frac{0.6 \times \sigma_в}{\tau_s} \tag{2.22}$$

Step 8: Calculation of safety factor of the intermediate joint under pressure under the butt bolt washer.

Area of pressure acting on the intermediate joint under the washer:

In case of square washer:

$$F_{\text{n}} = 0.9 \times B \times D - \frac{\pi \times d^2}{4} \quad (2.23)$$

In case of round washers:

$$F_{\text{n}} = 0.65 \times D^2 - \frac{\pi \times d^2}{4} \quad (2.24)$$

The maximum compressive stress of the intermediate joint is:

$$\sigma_{\text{n}} = \frac{P_{б}}{F_n} \quad (2.25)$$

Therefore, the safety factor of the intermediate joint under the gasket under pressure is:

$$\eta_{\text{n}} = \frac{1.0 \times \sigma_{в}}{\sigma_n} \quad (2.26)$$

Step 9: Based on the shear stiffness of the connecting bolts and wing panels, the forces acting in the joint are redistributed between the fasteners to calculate the safety factor of the connecting flange joint and the connecting bolts.

The total shear stiffness of the fasteners is:

$$Ж_0 = \sum_{i=1}^{n} \left(F_s^i * G_i \right) \quad (2.27)$$

Where F_s^i - Shear area of the ith fastener, G_i - Shear modulus of the ith fastener material.

The shear force transmitted by a single bolt is:

$$P_i = K_{\text{n}} \times \frac{F_s^i \times G_i}{Ж_0} \times P \quad (2.28)$$

Where Kn - Uneven load factor of fasteners in multi-point connections (Kn = 1.25).

Then the shear safety factor of the connection bolts is calculated according to the static strength calculation method and formula (2.18).

Under the action of the load force P and the connection bolts, the flange joint is subjected to the extrusion force of the M6 and M8 connection bolts.

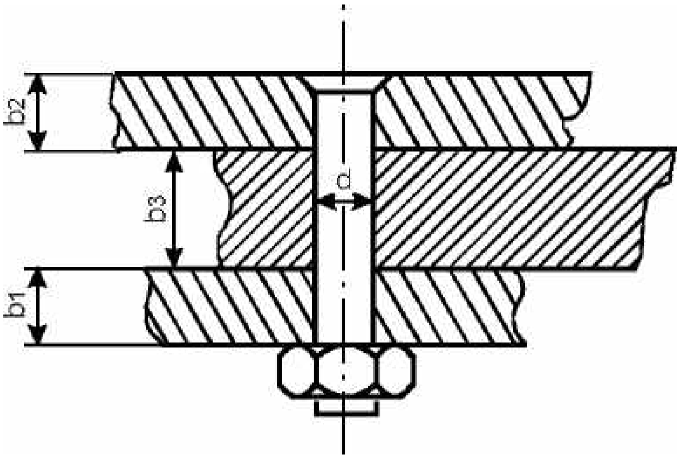

Fig. 2.15 Flange joint and wing panel connection structure

In the case where the thickness of the panel element is close to the diameter of the fastening element, it can be assumed that the contact between the bolt and the panel occurs throughout the thickness of the panel, but if $b_3 \gg d$, it should be assumed that the effective thickness of the contact area does not exceed 2d, that is, $b_v \leq 2d$.

The area of the contact area is:

$$F_{\mathrm{n}} = b_{\mathrm{v}} \times d \tag{2.29}$$

The stress in the contact area is:

$$\sigma_n = \frac{P_i}{F_{\mathrm{n}}} \tag{2.30}$$

Therefore, the safety factor of the flange joint under the extrusion force of the connecting bolts is:

$$\eta_{\mathrm{n}} = \frac{1.0 \times \sigma_b}{\sigma_n} \tag{2.31}$$

2.4 Calculation example

According to the calculation steps in chapter 2.3, the calculation process of the flange connection joint is as follows.

1) The flange connection joint is transversely cut to obtain nine different cross sections, as shown in Fig. 2.16.

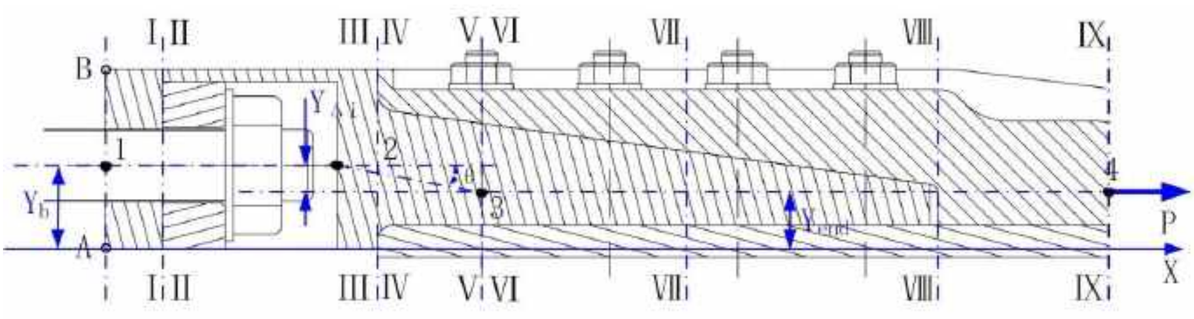

Fig. 2.16 Schematic diagram of each cross section

2) Calculate the geometric characteristics of each cross section (area, center of gravity height and moment of inertia).

For section I-I:

The geometric shape of section I-I is shown in Fig. 2.17, and its geometric characteristics are calculated as follows.

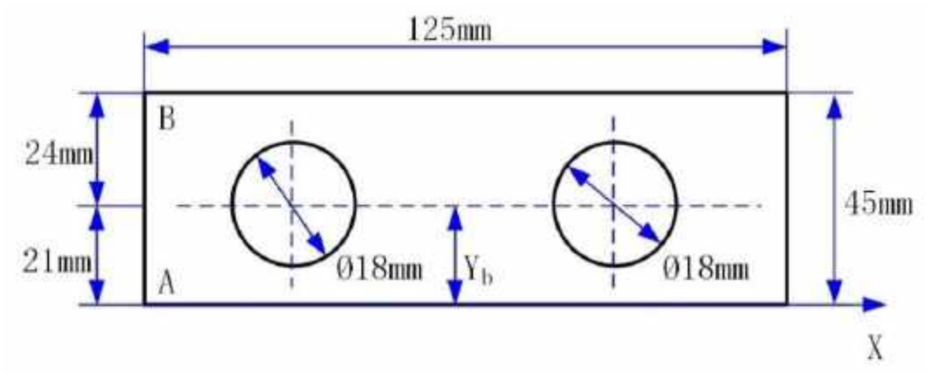

Fig. 2.17 Section I-I

The area of a single bolt hole circle is:

$$F_0 = \pi \cdot \mathrm{r}^2 = 3.14 \times 9^2 = 254.34mm^2$$

The moment of inertia of a single bolt hole circle is:

$$I_0 = \frac{\pi \cdot \mathrm{D}^4}{64} = \frac{3.14 \times 64^4}{64} = 5150.39mm^4$$

The area of the rectangular cross section is:

$$F_1 = \mathrm{b} \cdot \mathrm{h} = 125 \times 45 = 5625.00mm^2$$

The moment of inertia of a rectangular cross section is:

$$I_1 = \frac{b \cdot \mathrm{h}^3}{12} = \frac{125 \times 45^3}{12} = 949218.75mm^4$$

The area of cross-section I-I is:

$$F_{I-I} = 5625.00 - 2 \times 254.34 = 5116.32mm^2$$

The moment of inertia of cross section I-I is:

$$I_{I-I} = 949218.75 - 2 \times 5150.39 = 938917.97mm^4$$

The height of the line of action of the force in the cross section I-I is:

$$Y_{I\text{-}I} = Y_b = 21.00\mathrm{mm}$$

For Section II-II:

The geometry of Section II-II is shown in Fig. 2.18, and its geometric features are calculated as follows:

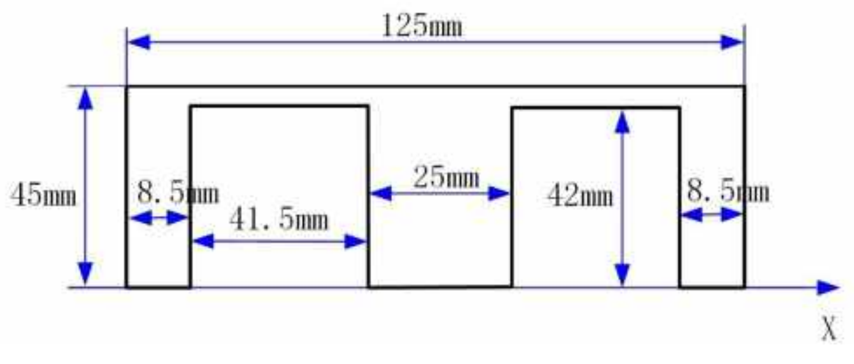

Fig. 2.18 Section II-II

The area of cross-section II-II is:

$$F_{II-II} = 2139.00\mathrm{mm}^2$$

The moment of inertia of cross section II-II is:

$$I_{II-II} = 416200.00\text{mm}^4$$

The height of the line of action of the force in the cross section II-II is:

$$Y_{II-II} = 24.945mm$$

For section III-III:

The geometry of section III-III is shown in Fig. 2.19, and its geometric features are calculated as follows.

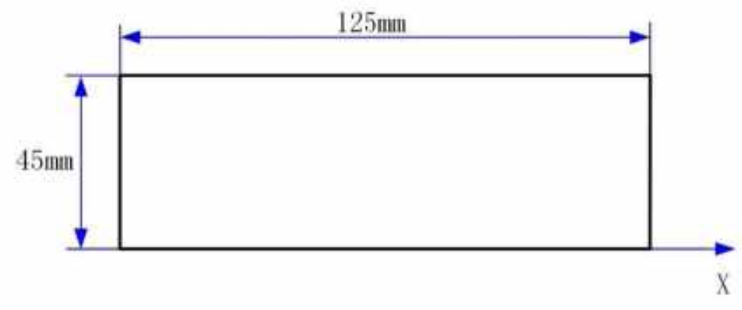

Fig. 2.19 Section III-III

The area of cross-section III-III is:

$$F_{III-III} = 5625.00\text{mm}^2$$

The moment of inertia of cross section III-III is:

$$I_{III-III} = 949200.00mm^4$$

The height of the line of action of the force in the cross section III-III is:

$$Y_{III-III} = 22.50mm$$

For section IV-IV:

The geometry of section IV-IV is shown in Fig. 2.20, and its geometric features are calculated as follows.

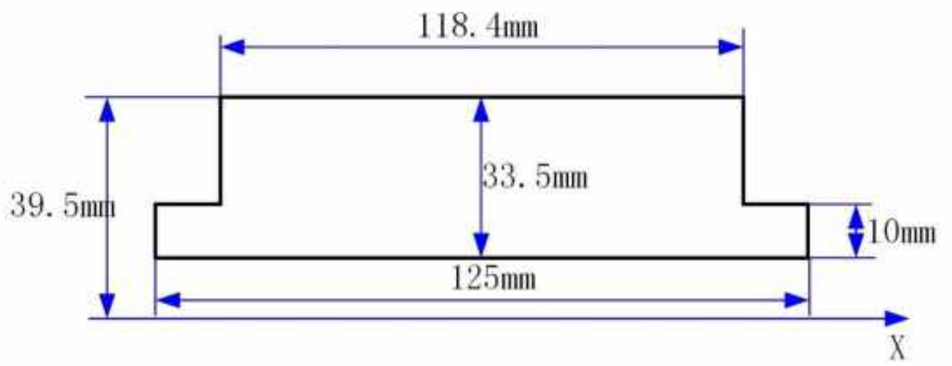

Fig. 2.20 Section IV-IV

The area of cross-section IV-IV is:

$$F_{IV-IV} = 4032.40\text{mm}^2$$

The moment of inertia of cross section IV-IV is:

$$I_{IV-IV} = 403700.00\text{mm}^4$$

The height of the line of action of the force in cross section IV-IV is:

$$Y_{IV-IV} = 20.19\,mm$$

For section V-V:

The geometry of the section V-V is shown in Fig. 2.21, and its geometric features are calculated as follows:

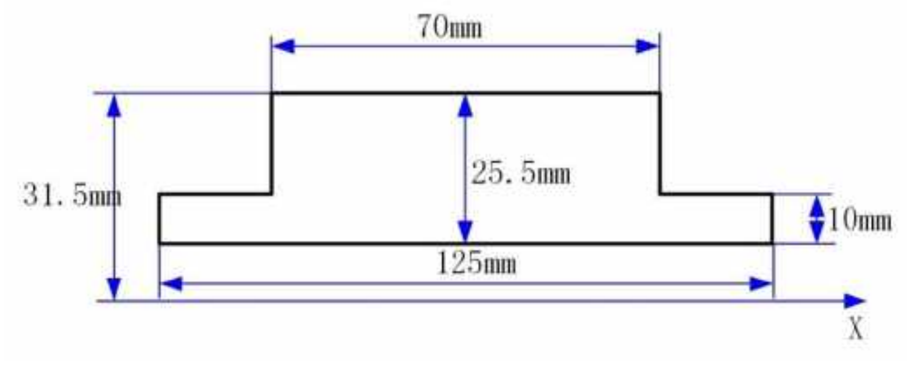

Fig. 2.21 Section V-V

The area of cross-section V-V is:

$$F_{V-V} = 2335.00mm^2$$

The moment of inertia of cross section V-V is:

$$I_{V-V} = 126600.00mm^4$$

The height of the line of action of the force in the cross section V-V is:

$$Y_{V-V} = 15.93\,mm$$

For VI-VI section:

The geometry of the section VI-VI is shown in Fig. 2.22, and its geometric features are calculated as follows:

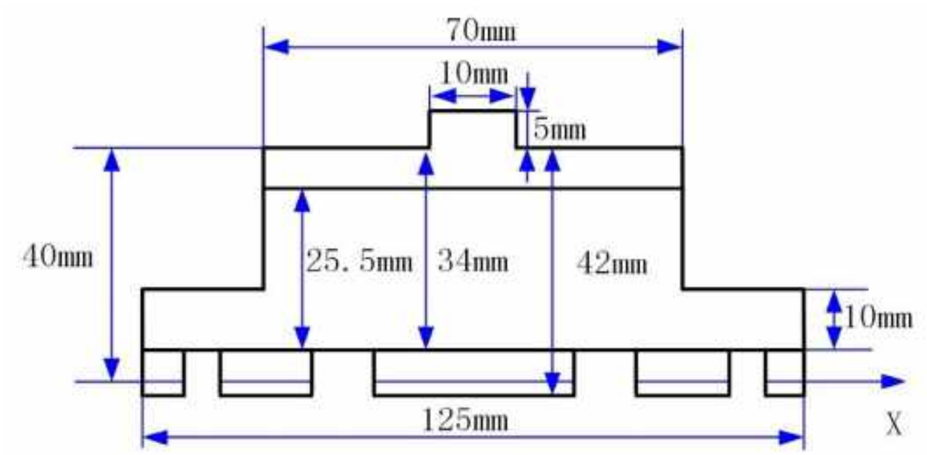

Fig. 2.22 Section VI-VI

The area of cross-sectional VI-VI is:

$$F_{VI-VI} = 3756.00mm^2$$

The moment of inertia of cross section VI-VI is:

$$I_{VI-VI} = 550600.00mm^4$$

The height of the line of action of the force in the cross section VI-VI is:

$$Y_{VI-VI} = 17.164\,mm$$

For section VII-VII:

The geometry of section VII-VII is shown in Fig. 2.23, and its geometric features are calculated as follows.

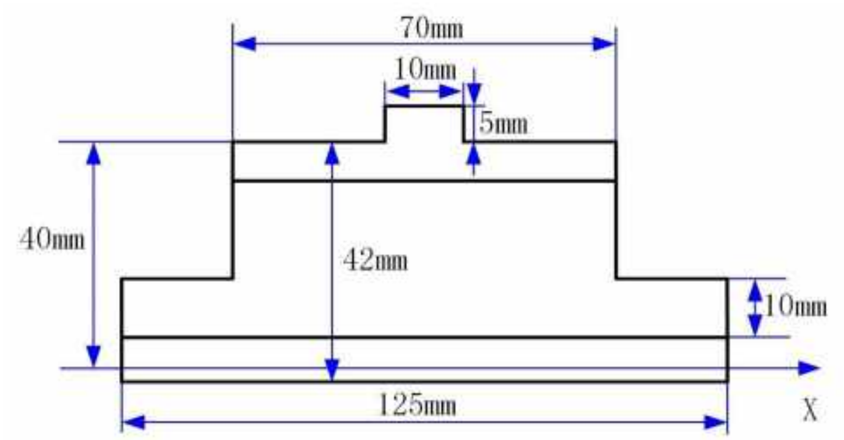

Fig. 2.23 Section VII-VII

The area of cross-sectional VII-VII is:

$$F_{VII-VII} = 3980.00mm^2$$

The moment of inertia of cross section VII-VII is:

$$I_{VII-VII} = 600400.00\text{mm}^4$$

The height of the line of action of the force in cross section VII-VII is:

$$Y_{VII-VII} = 16.31mm$$

For section VIII-VIII:

The geometry of section VIII-VIII is shown in Fig. 2.24, and its geometric features are calculated as follows.

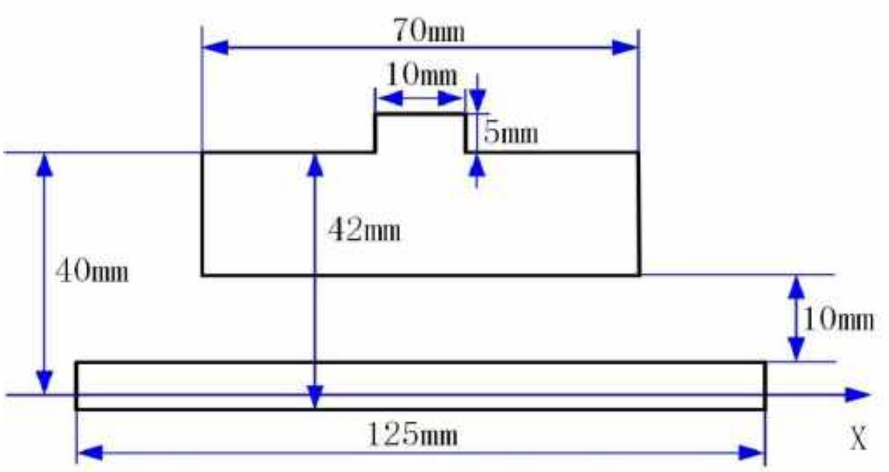

Fig. 2.24 Section VIII-VIII

The area of cross-section VIII-VIII is:

$$F_{VIII-VIII} = 2730.00mm^2$$

The moment of inertia of cross section VIII-VIII is:

$$I_{VIII-VIII} = 538600.00\text{mm}^4$$

The height of the line of action of the force in the cross section VIII-VIII is:

$$Y_{VIII-VIII} = 18.742\, mm$$

For the end section (IX-IX):

The geometry of the end section (IX-IX) is shown in Fig. 2.25, and its geometric features are calculated as follows:

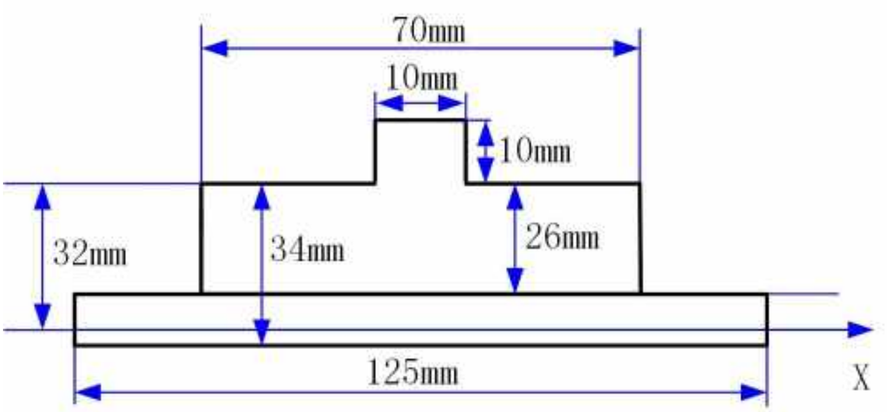

Fig. 2.25 End section (IX-IX)

The area of the end section (IX-IX) is:

$$F_{IX-IX} = 2920.00\text{mm}^2$$

The moment of inertia of the end section (IX-IX) is:

$$I_{IX-IX} = 351\,000.00\text{mm}^4$$

The height of the center of gravity of the end section (IX-IX) is:

$$Y_{IX-IX} = 13.795\text{mm}$$

Therefore, the geometric characteristics of each section are shown in Table 2.3 below.

Table 2.3. The Geometric characteristic parameters of each section

	I-I	II-II	III-III	IV-IV	V-V
F (mm^2)	5116.32	2139.00	5625.00	4032.40	2335.00
I (mm^4)	938917.97	416200.00	949200.00	403700.00	126600.00
Y_{sec} (mm)	21.00	24.945	22.50	20.19	15.93
$Y_{\Delta i}$ (mm)	7.205	11.150	8.705	6.395	2.135
	VI-VI	VII-VII	VIII-VII	IX-IX	end
F (mm^2)	3756.00	3980.00	2730.00	2920.00	2920.00
I (mm^4)	550600.00	600400.00	538600.00	351000.00	351000.00
Y_{sec} (mm)	17.164	16.31	18.742	13.795	13.795
$Y_{\Delta i}$ (mm)	3.369	2.515	4.947	0	0

3) Calculate the loading force on the end section.

$$P = P_{\text{end}} = F_{end} \times \sigma_{end} = 2920 \times 150 = 438000\ N$$

4) Simplify the model and calculate the bending moment diagram of the simplified structure.

The moment of inertia of each segment of the simplified structure of the model is calculated by the average method as follows.

The average moment of inertia on segment 1-2 is:

$$I_{1-2} = \frac{938917.97 \times 14.00 + 416200.00 \times 44.00}{14.00 + 44.00} = 542373.30\text{m m}^4$$

The average moment of inertia on segment 2-3 is:

$$I_{2-3} = \frac{0.5 \times (949200 + 403700) \times 10 + 0.5 \times (403700 + 126600) \times 26}{10 + 26} = 379400\ mm^4$$

The average moment of inertia on segment 3-4 is:

$$I_{3-4} = \frac{0.5 \times (550600 + 600400) \times 114 + 0.5 \times (538600 + 351000) \times 29}{114 + 29} = 548994.41 mm^4$$

Substituting the above numerical calculations, there is:

$$X_1 = -P \times 36.714 \times 0.196 \times \frac{\dfrac{58(58+2\times 36.714\times 0.981+2\times 143)}{2\times 542373.30} + \dfrac{36.714(\frac{2}{3}\times 36.714\times 0.981+143)}{2\times 379400.00}}{\left(\begin{array}{l} \dfrac{58\left[\begin{array}{l}(58+143+36.714\times 0.981)^2+(143+36.714\times 0.981)^2 \\ +(58+143+36.714\times 0.981)\times(143+36.714\times 0.981)\end{array}\right]}{3\times 542373.30} \\ +\dfrac{36.714\left[(143+36.714\times 0.981)^2+143^2+143(143+36.714\times 0.981)\right]}{3\times 379400.00} \\ +\dfrac{143^3}{3\times 548994.41} \end{array}\right)}$$

$$= -0.025445P$$

Therefore, the bending moment magnitude of node 1 is 1.166P, the bending moment magnitude of node 2 is 2.641P, the bending moment magnitude of node 3 is -3.639P, and the bending moment magnitude of node 4 is 0. The bending moment diagram is drawn as follows.

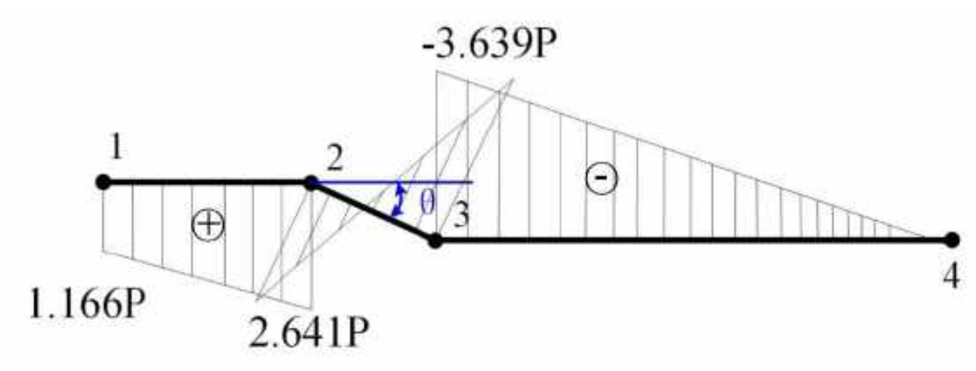

Fig. 2.26 Bending moment diagram under load force P

5) Calculate the axial forces in each part of the simplified model, and then calculate the stress at the maximum load point of any cross section based on the axial force and bending moment diagram.

The axial force on segment 1-2 is:

$$N_{1\text{-}2} = P$$

The axial force on segment 2-3 is:

$$N_{2\text{-}3} = P \times \cos\theta = 0.981P$$

The axial force on segment 3-4 is:

$$N_{3\text{-}4} = P$$

6) The additional load (when there is bending tension at the joint), total load and safety factor of the butt bolts are calculated by the magnitude of the bending moment in the joint plane.

Additional load force of butt bolts:

$$P_M = \frac{M}{C_1} = \frac{1.166P}{21mm} = 0.0555P$$

Therefore, the total load acting on the butt bolt is:

$$P_{\text{b}} = P + P_M = 1.0555\,P$$

The load borne by a single bolt is:

$$P_{1\text{b}} = \frac{P_b}{n} = \frac{1.0555\,P}{2} = 0.528\,P$$

Then the safety factor of the butt bolt is:

$$\eta_{\text{b}} = \frac{P_{\text{m}}}{P_{1b}} = \frac{1455 \times \pi \times 9^2}{0.528P} = 1.6$$

7) Calculation of safety factor of the intermediate joint under the butt bolt washer under shear force.

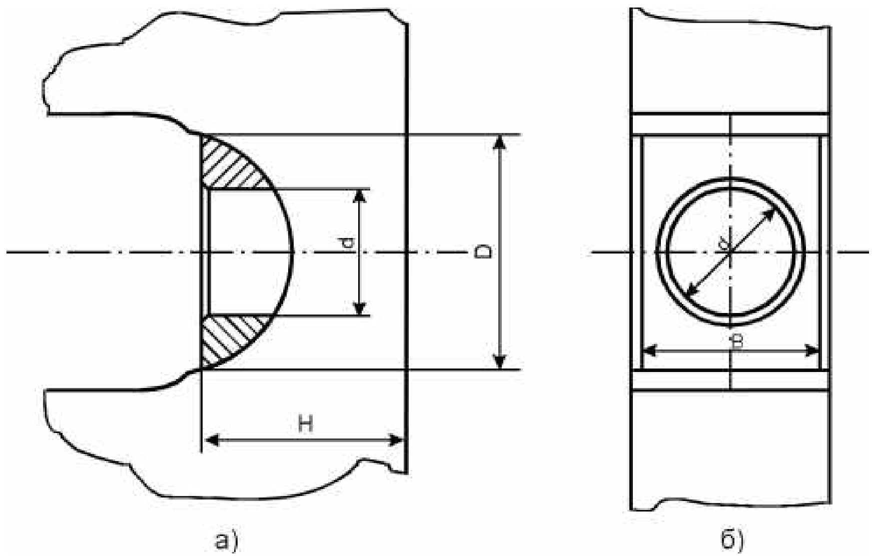

Fig. 2.27 Connection structure between gasket and connector profile

The shear area of the intermediate joint below the gasket is calculated as follows.

In case of square gasket:

$$F_{\mathrm{s}} = 2 \times B \times H = 2520.00\mathrm{mm}^2$$

The maximum shear stress is:

$$\tau_s = K_{\mathrm{n}} \times \frac{P_{1\mathrm{b}}}{F_{\mathrm{s}}} = 137.66MP\mathrm{a}$$

Where Kn is the distribution inequality coefficient, Kn=1.5 (rectangular section).

Therefore, the safety factor of the intermediate joint under the gasket under shear force is:

$$\eta_s = \frac{0.6 \times \sigma_{\mathrm{b}}}{\tau_s} = 2.45$$

8) Calculation of safety factor of the intermediate joint under the butt bolt washer under pressure.

The area of the intermediate joint under the washer under pressure:

In the case of square washers：

$$F_{\mathrm{n}} = 0.9 \times B \times D - \frac{\pi \times d^2}{4} = 1257.66\mathrm{mm}^2$$

The maximum compressive stress is:

$$\sigma_{\mathrm{n}} = \frac{P_{1\mathrm{b}}}{F_n} = 183.88MPa$$

Therefore, the safety factor of the intermediate joint under pressure below the gasket is:

$$\eta_{\mathrm{n}} = \frac{1.0 \times \sigma_{\mathrm{b}}}{\sigma_n} = 3.06$$

9) According to the shear stiffness of the connecting bolts and the wing panel,

the force acting in the joint is redistributed between the fasteners, and the force and safety factor of the connecting bolts connecting the flange joint and the wing panel are calculated. The flange joint and the wing panel are connected by eight M8 bolts and eight M6 bolts, as shown in Fig. 2.4.

The shear model G_i of the material used for the bolts is 42.59GPa, the force area of a single M8 bolt is 50.24mm^2, and the force area of a single M6 bolt is 28.26mm^2, then the total shear stiffness of the fastener is:

$$Ж_0 = \sum_{i=1}^{n}\left(F_s^i * G_i\right) = 8\times 50.24\times \mathrm{G_i} + 8\times 28.26\times \mathrm{G_i} = 628G_i$$

Where F_s^i is shear area of the ith fastener, G_i is shear modulus of the ith fastener material.

The shear force transmitted by a single row of M6 bolts is:

$$P_{M6} = \frac{F_{\mathrm{s}}^i \times G_i}{Ж_0}\times P = \frac{4\times 28.26\times G_i}{628\times G_i}\times P = 0.18P$$

The shear force transmitted by a single M6 bolt is:

$$P_{1M6} = K_{\mathrm{n}} \times \frac{P_{M6}}{\mathrm{n}} = 0.05625\ P$$

The shear force transmitted by a single row of M8 bolts is:

$$P_{M8} = \frac{F_{\mathrm{s}}^i \times G_i}{Ж_0}\times P = \frac{4\times 50.24\times G_i}{628\times G_i}\times P = 0.32P$$

The shear force transmitted by a single M8 bolt is:

$$P_{1M8} = K_{\mathrm{n}} \times \frac{P_{M6}}{\mathrm{n}} = 0.1P$$

Where Kn is factor of uneven load of fasteners in multi-point connections (Kn = 1.25).

Then the safety factor of the connection bolts is:

$$\eta_6 = \frac{2\times \sigma_{\mathrm{b}} \times 28.26}{P_{1M6}} = 3.33$$

$$\eta_8 = \frac{2 \times \sigma_b \times 50.24}{P_{1M8}} = 3.33$$

For the connection between the flange joint and the wing panel, the flange joint is squeezed and deformed under the action of the load force P and the connecting bolts.

The area of the M6 connecting bolt contact area is:

$$F_n = b_v \times d = 2 \times 6 \times 6 = 72\text{mm}^2$$

The stress in the contact area of the M6 connecting bolt is:

$$\sigma_n = \frac{P_{1M6}}{F_n} = 342.18MPa$$

The compressive safety factor of the M6 connecting bolt connecting the panel bolts is:

$$\eta_n = \frac{1.0 \times \sigma_b}{\sigma_n} = 1.64$$

The area of the M8 connection bolt contact area is:

$$F_n = b_v \times d = 2 \times 8 \times 8 = 128\text{mm}^2$$

The stress in the contact area of the M8 connecting bolt is:

$$\sigma_n = \frac{P_{1M8}}{F_n} = 342.19MPa$$

The shrinkage safety factor of the flange joint under the extrusion of the M8 connecting bolt is:

$$\eta_n = \frac{1.0 \times \sigma_b}{\sigma_n} = 1.65$$

2.5 Conclusion of this chapter

Connection joints are generally assembled from multiple parts. It is very difficult to analyze their performance parameters due to their variable structures and complex forces. Most of the damage in aircraft structures occurs at the location of the connection joints, so analyzing the force changes and safety factors of the parts in the joints on the aircraft is crucial to ensure the safe flight of the aircraft.

This chapter takes the connection structure of the flange joint and the wing panel as an example to show in detail the mechanical analysis and calculation methods of the complex model structure of the aircraft. The method is to first obtain the primary hyperstatic structure of the simplified joint model based on the geometric characteristics and force transmission characteristics of the cross section at each node in the flange joint structure, and then solve the bending moment diagram and axial force diagram by using the force method regular equation. In this way, the force conditions at each node of the model can be obtained to further analyze the safety factor of each component, and finally compare the airworthiness standards to determine whether each component meets the design requirements. Among them, the geometric characteristics of the cross section are read in the 3D modeling software CATIA.

The calculation results are as follows: the safety factor of the butt bolt is 1.6; the safety factor of the connecting bolt under pressure and shear force is 3.33; the safety factor of the intermediate joint under shear force is 2.45, and the safety factor under pressure is 3.06; the safety factor of the flange joint under the extrusion of the M6 connecting bolt is 1.64, and the safety factor under the extrusion of the M8 connecting bolt is 1.65. According to the provisions of the airworthiness standard that the safety factor of bolted connection parts shall not be less than 1.5 [21,22,30,31], it can be seen that the safety factor of the flange joint meets the requirements and the basic design is reasonable. However, the structural strength of the flange joint has a certain surplus, especially the connecting bolts. It is recommended to further modify the parameters of the structure to ensure the reasonable structural design of the aircraft. This calculation method can be added to have good practical value in engineering applications.

This chapter completes the dissertation work task: develop new methods for strength calculation and analysis of the fitting joint between the center wing section and the outer wing section of a regional aircraft by means of existing scientific knowledge. For the first time, an effective solution for the design and static strength calculation of the fitting joint in the modeling stage is proposed. The method and its application are introduced by taking the preliminary analysis and design calculation of the flange connection design of the center wing section of a regional aircraft as an example.

CHAPTER 3

FINITE ELEMENT ANALYSIS METHOD FOR STRESS-STRAIN STATE OF FITTING JOINT

In mechanical structure design, many components are often connected by fitting joints. For example, fitting joints are widely used in aircraft structures, and fitting joints are responsible for the interconnection of important components, such as the connection between the center wing section and outer wing section, and the connection between the horizontal and vertical tail and the fuselage. Once these fitting joints are damaged, the aircraft will not be able to fly in the sky and the consequences can be very serious. Therefore, the design and analysis of fitting joints is one of the most important issues in mechanical design. However, the force transmission in the fitting joint is very complicated, which is due to the complicated structure of the fitting joint, so it is difficult to analyze the performance of the fitting joint. With the development of numerical methods and the application of finite element software, it becomes possible to analyze the entire fitting joint and each component. The stress-strain state of the fitting joint is an important indicator for judging whether the fitting joint meets the design requirements. In this chapter, the finite element calculation method of calculating stress-strain state of the fitting joint will be introduced emphatically.

Relevant scholars have done a lot of research to analyze stress-strain state of important components in aircraft structures. For the simple model, it is very convenient to directly calculate its stress-strain state in ANSYS. Andrianov [32] developed an alternative research method. In his research, the stress-strain state of the aircraft fuselage was simulated by studying the stress-strain state of the thin-walled blank during the stretch forming process in ANSYS. Oskouei [33] discussed a finite element modelling of aluminium alloy 7075-T6 bolted plates, which are extensively used in aircraft structures. The ANSYS was used for modelling the joint and estimating the stresses and strains created in the joint due to initial clamping forces and subsequent longitudinal tensile loadings. The reference Z-stringer component of the Prakash's [34] paper is modeled by CATIA and numerical simulation is carried out by ANSYS has been used for splice joint presents in the aircraft fuselage with three combinations of joints such as riveted joint, bonded joint and hybrid joint. Then the stress-strain states of the riveted joint, bonded joint and hybrid joint are compared in his paper.

PATRAN/NASTRAN is a finite element analysis software similar to ANSYS, which is very helpful for direct finite element analysis of simple models. Babu [35] calculated the stress of the joint using the finite element method with the aid of PATRAN/NASTRAN. And the stress analysis of the joint was carried out to predict the stresses at rivet holes due to by-pass load and bearing load. The result showed that a fatigue crack will appear at the location of high tensile stress in an airframe structure. Pavan [36] used CATIA V5 to model the components and imported to MSC PATRAN; MSC NASTRAN was used as a solver. From the obtained maximum tensile stresses, fatigue analysis was carried out to find fatigue life of the spar joint with different fatigue load spectra.

However, for complex models, Grebenikov [37-39] proposed a simplified and segmented method to analyze the general stress-strain state of the fitting joint of center section in ANSYS. Then the local stress-strain state of each component was obtained according to the general stress-strain state of the fitting joint. The advantage of this method is that it can greatly reduce the amount of calculation. Doru [40, 41] proposed a three-dimensional non-linear finite element method. In his paper, the stress analyses in the single-lap joint were performed with a three-dimensional non-linear finite element method by considering the geometrical non-linearity and non-linear material behaviors of both adhesive (DP460) and adherend (AA2024-T3). Vinogradov [42] used a classical mathematical model for the adopted calculation scheme. Based on the mathematical model, the initial problem was analytically solved and an effective algorithm for the multiparameter solution of the corresponding boundary value was constructed. The results of a quantitative analysis of the stress-strain state for the aircraft body were presented.

Some scholars have conducted research through a combination of experiments and finite element methods. Balalayeva [43] uses the finite element method to calculate the stress-strain state in the frame of the open crank press, and compared theoretical calculations with experimental data. It is found that the using of compensators reduces the angular deformation in the frame by 10~24%, and reduces the tensile stress by 6~42%. In Zeng's [44] paper, both numerical and experimental investigations were carried out on the stress/strain characteristics in riveted aircraft lap joints. A special specimen was designed for the test of strain variations on the faying surface of the sheet by microstrain gages. A comparison of the strain variations between the experimental results and FE simulations shows a general good agreement, although there may be some difference for points measured near the hole surface. Zhao [45] presented a method for obtaining the flow curve of sheet metals over a large range of strain through the combination of simple tensile test and finite element analyses. The appropriate finite element model for accurate simulation of the anisotropic plastic deformation during diffuse necking was determined. Different hardening functions were evaluated for their capabilities in approximating the entire flow stress curves up to localized necking. A modified Hockett–Sherby function was proposed and its performance was demonstrated.

It can be seen from the above researches that obtaining stress-strain state of components is an important way to analyze the performance of the components. In this chapter, based on Grebenikov's method [37-39], the stress-strain state of the fitting joint between the center wing section and outer wing section will be emphatically calculated to prepare for the analysis of the performance of the fitting joint， and the effectiveness of this method will be verified.

3.1 Model of the fitting joint

The joint model calculated in this chapter is consistent with the joint model in Chapter 2. As shown in Fig. 2.3, the fitting joint structure includes fitting of center wing section (FCWS), intermediate panel (IP), fitting of outer wing section (FOWS), stringer of outer wing section (SOWS), lower panel of outer wing section (LPOWS), hexagon head bolts (M18), countersunk head bolts (M8 and M6) and countersunk head rivets (M6). The equivalent stress of the gross load at the end of the fitting joint is $\sigma_{eq} = 150MPa$. In the total section of the regular area, the load P on the end section can be obtained by the following formula:

$$P = \sigma_{eq} \cdot S_{sec} \tag{3.1}$$

Where S_{sec} is the area of the cross section.

The fitting of center wing section, intermediate panel, fitting of outer wing section, lower panel of outer wing section, stringer of outer wing section are all made of D16T aluminum alloy. The mechanical properties of the D16T aluminum alloy are shown in Table 3.1. The hexagon head bolts (M18), countersunk head bolts (M8 and M6) and countersunk head rivets (M6) are all made of VT22 titanium alloy. The mechanical properties of the VT6 titanium alloy are shown in Table 3.2.

Table 3.1 The mechanical properties of D16T aluminium alloy

Density	Young's Modulus	Tensile Strength	Yield Stress	Poisson's Ratio
2780 (kg/m^3)	72 (GPa)	564 (MPa)	447(MPa)	0.33

Table 3.2 The mechanical properties of VT22 titanium alloy

Density	Young's Modulus	Tensile Strength	Yield Stress	Poisson's Ratio
4450(kg/m^3)	115 (GPa)	1455 (MPa)	13805 (MPa)	0.32

3.2 Indirect method to calculate stress-strain state of the fitting joint

In order to reduce the amount of calculation and speed up the calculation, the model of the fitting joint can be considered to be segmented and simplified, and then the simplified and segmented models are calculated separately to obtain their stress-strain state. Finally, the integral stress-strain state is obtained according to the local stress-strain state. This calculation method is called the indirect method to calculate the stress-strain state of the fitting joint. Due to the numerous structural components, complex structures, and variable types of such fitting joint, it is very effective and convenient to use the indirect method to calculate the stress-strain state of the fitting joint.

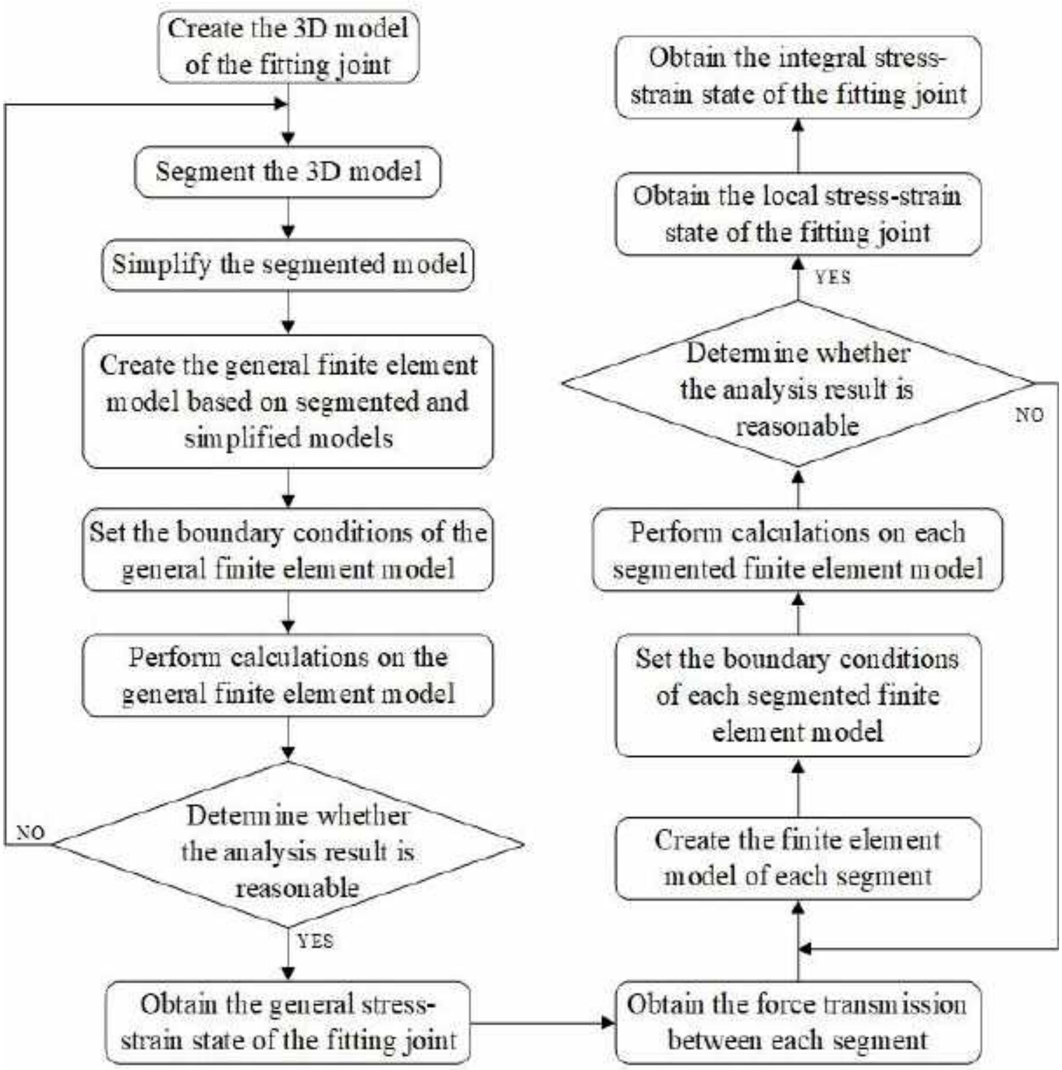

Fig. 3.1 Indirect method to calculate stress-strain state of the fitting joint

3.2.1 Segment and simplify the model of the fitting joint

In the three-dimensional model of fitting joint, the cross-sectional shapes at different positions of the model can be obtained by transverse cutting. According to the different cross-sectional shapes, 15 different cross-sections are determined, which divide the model into 15 segments, as shown in Fig. 3.2. These 15 segments reflect the characteristics of the cross-sectional geometry (changes in cross-sectional shape), and the structure and force characteristics of the design model (moment of inertia and position of the center of gravity). It can be seen that the area S and the height of the center of gravity Hz of each cross section are different. In Fig. 3.2, a) shows a schematic diagram of the longitudinal section of the fitting joint. b) shows a schematic diagram of the position of different cross-sections. c) shows a schematic diagram of segmented the models of the fitting joint. d) shows a schematic diagram of the area of different cross-sections. e) shows a schematic diagram of the height of the center of gravity of different cross-sections.

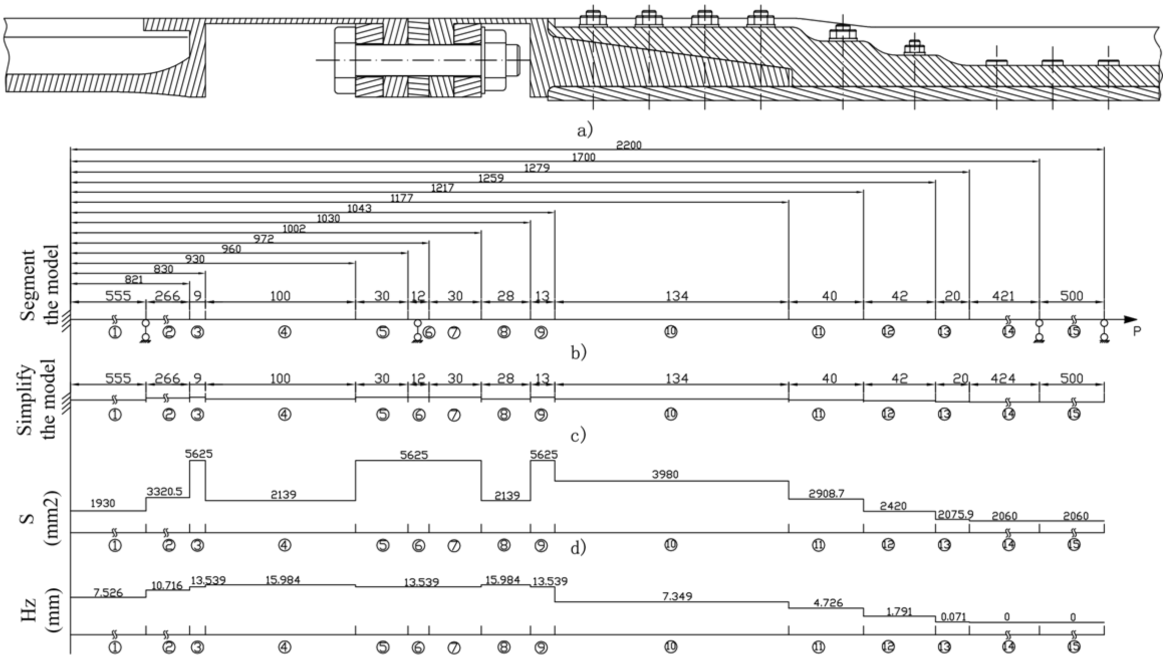

Fig. 3.2 The segmentation and simplification of the model of the fitting joint

a) The longitudinal section of the fitting joint; b) The position of different cross-sections; c) The segmented models of the fitting joint; d) The area of different cross-sections; e) The height of the center of gravity of different cross-sections

3.2.2 Finite element analysis of the general fitting joint

In order to obtain the transmitted force at the two ends of each segment, the segmented and simplified models of the fitting joint is analyzed using the ANSYS Workbench. In the process of establishing the finite element model, each segmented model is regarded as a whole, and replaced with a finite element beam element. The general finite element model of the fitting joint is created as shown in Fig. 3.3. The point L_0 is a fixed constraint, the points L_{555}, L_{966}, L_{1700} and L_{2200} are simply supported constraints, and the point L_{2200} bears a horizontal load P. In the calculation, a cross-sectional shape is assigned to each segment, and the assigned cross-sectional shape is the same as the cross-sectional shape obtained by transverse cutting at different positions of the three-dimensional model. When the gross stress is 150 MPa, the calculation results of shear force, bending moment, displacement and axial stress are shown in Fig. 3.4-3.7.

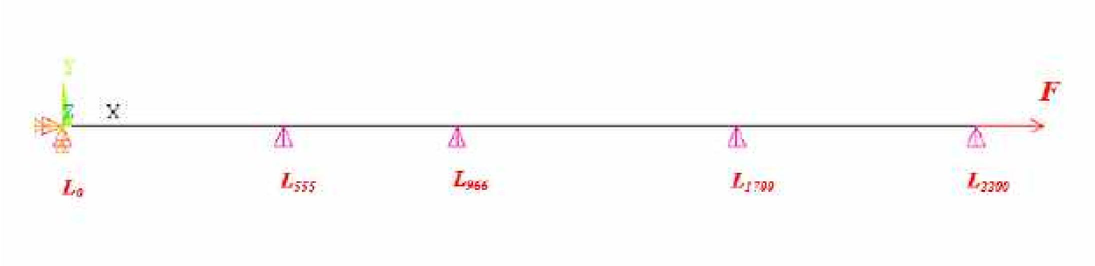

Fig. 3.3 The general finite element model in Workbench

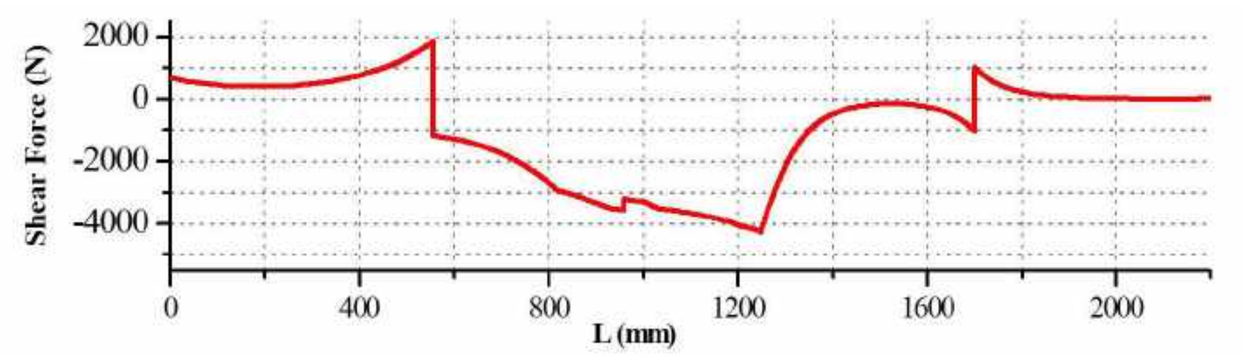

Fig. 3.4 Shear force diagram when the gross stress is 150 MPa

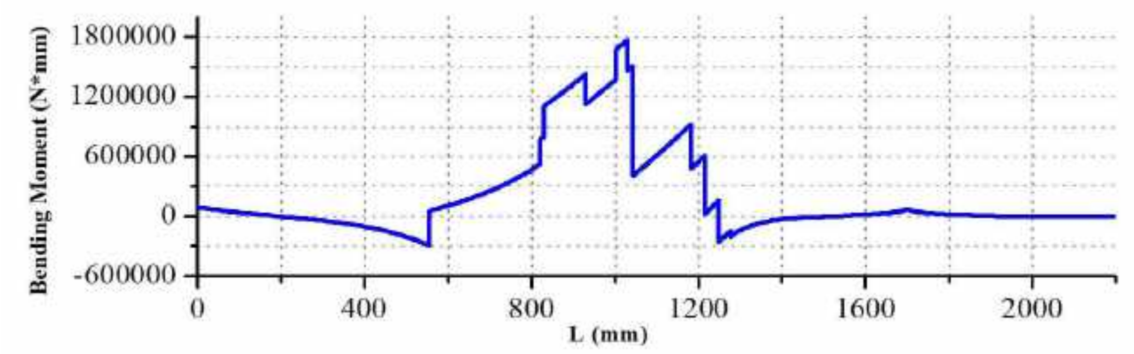

Fig. 3.5 Bending moment diagram when the gross stress is 150 MPa

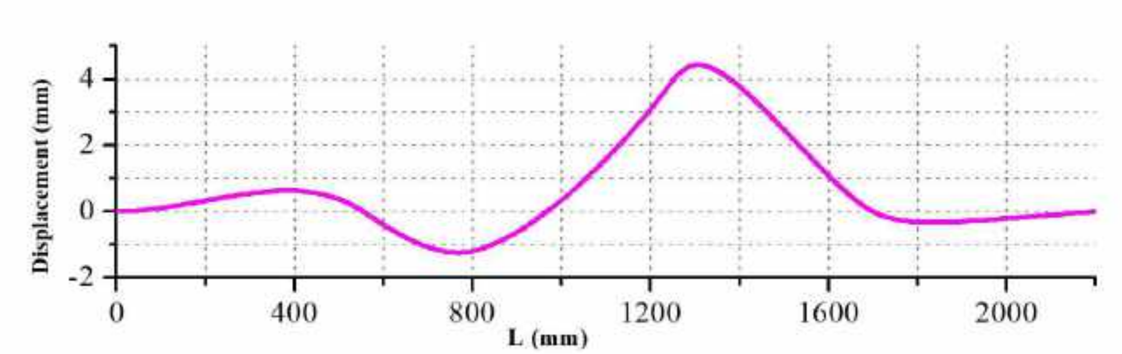

Fig. 3.6 Displacement diagram when the gross stress is 150 MPa

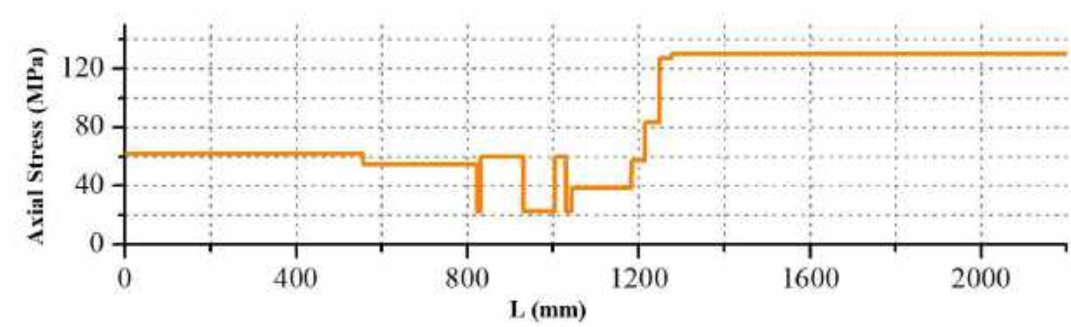

Fig. 3.7 Axial stress diagram when the gross stress is 150 MPa

Therefore, the shear force at each position of the general finite element model can be obtained from the shear force results shown in Fig. 3.4. The bending moment at each position of the general finite element model can be obtained from the bending moment results shown in Fig. 3.5. The displacement of each position of the general finite element model can be obtained from the displacement result shown in Fig. 3.6.

The axial stress at each position of the general finite element model can be obtained from the axial stress result shown in Fig. 3.7. The force transmission in the end face of each segment is shown in Table 3.3.

Table 3.3 The force transmission in the end face of each segment

Segments	①	②	③	④	⑤	⑥	⑦	⑧
Axial stress (MPa)	61.8	54.8	22.6	59.4	22.6	22.6	22.6	59.4
Shear force (N)	1850.8	-2969.6	-2981.4	-3512.6	-3578	-3245.9	-3315.7	-3507
Bending moment (N*mm)	-2.92e5	5.29e5	8.04e5	1.43e6	1.23e6	1.27e6	1.37e6	1.77e6
Displacement (mm)	0	-1.111	-1.065	-0.349	-0.060	0.061	0.374	0.680
Segments	⑨	⑩	⑪	⑫	⑬	⑭	⑮	
Axial stress (MPa)	22.6	38.9	57.0	83.0	130	130	130	
Shear force (N)	-3545.2	-3941.9	-4135.2	-4250.9	-3066	-1023.6	11.694	
Bending moment (N*mm)	1.51e6	9.25e5	6.10e5	1.61e5	-1.52e5	67313	-587.32	
Displacement (mm)	0.842	2.794	3.340	3.923	4.296	0	0	

3.2.3 Finite element analysis of the local fitting joint

It can be seen from Fig. 2.3 that there are two important local fitting joints (I fitting joint and II fitting joint) for the overall fitting joint. Three-dimensional models of I fitting joint and II fitting joint are shown in Fig. 3.8. According to the finite element analysis results of the general fitting joint, the boundary conditions of the finite element models of local fitting joints can be obtained, and then the local stress-strain state of the local fitting joint can be calculated with the help of finite element software ANSYS Workbench. The boundary conditions of the finite element model of the local fitting joint are the axial force, shear force, bending moment and displacement on each segment section. The three-dimensional model is imported into ANSYS Workbench through the intermediate format stp., and the finite element models of I fitting joint and II fitting joint are obtained as shown in Figs 3.9 and 3.10.

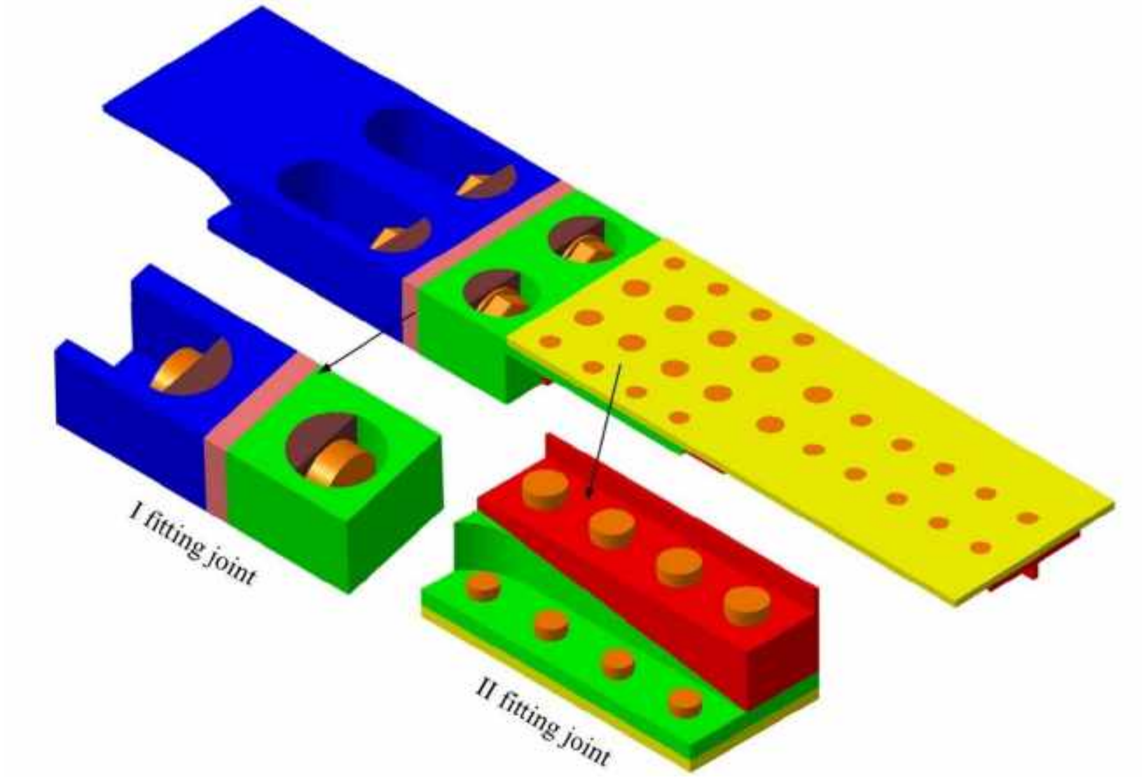

Fig. 3.8 Three-dimensional models of I fitting joint and II fitting joint

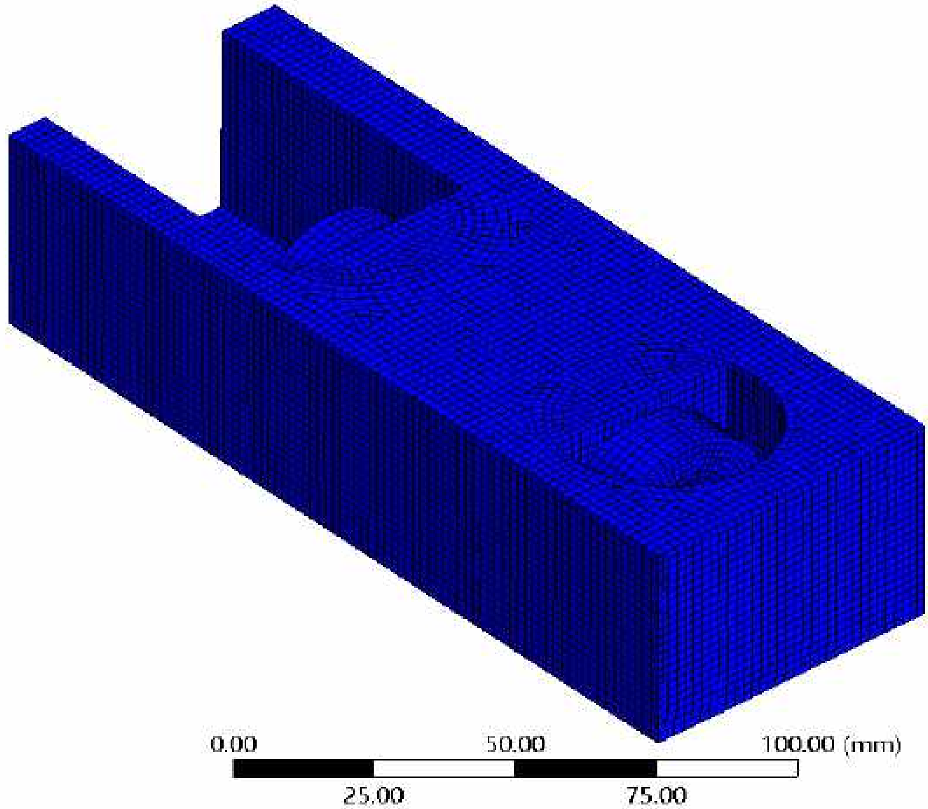

Fig. 3.9 The finite element model of I fitting joint

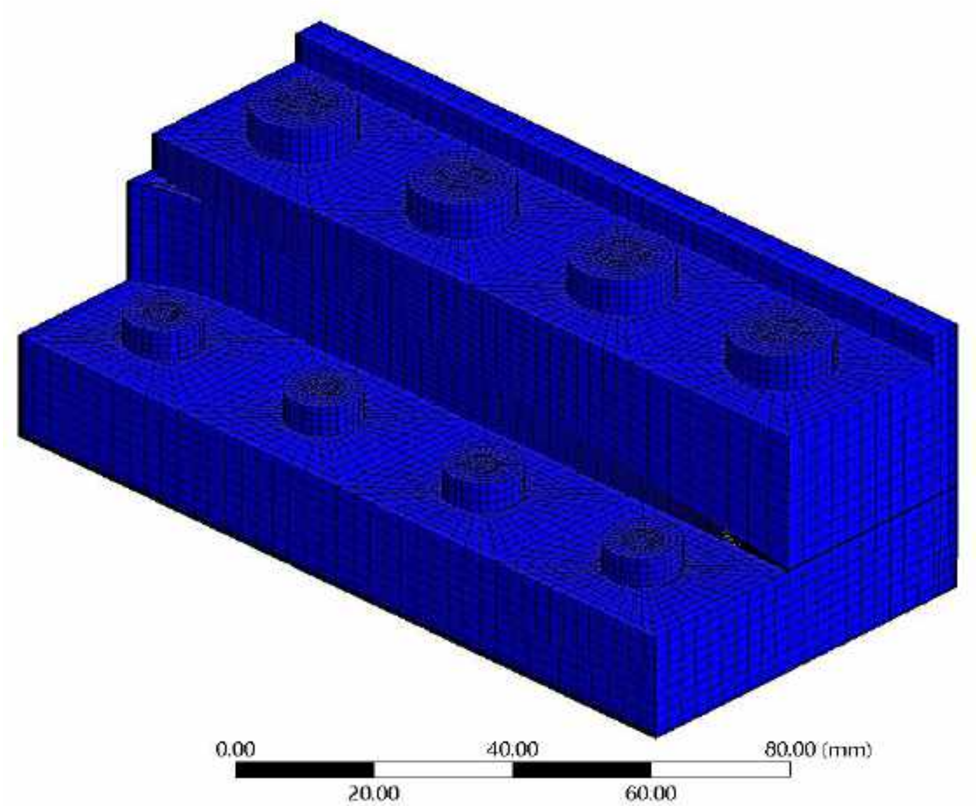

Fig. 3.10 The finite element model of II fitting joint

The finite element models of I fitting joint and II fitting joint are composed of hexahedral elements and a small number of tetrahedral elements. In order to decrease the number of meshes to reduce the amount of calculation, only the mesh size close to the functional holes is set smaller. Since the fitting joint structure is symmetrical, only the stress-strain state of half model can be analyzed to obtain the general stress-strain state of the fitting joint. It should be noted that in this paper, when each finite element model is calculated, the grid independence is first verified, and the convergence tolerance of stress and strain is set to 0.03. The mesh size after convergence is a minimum of 0.2mm and a maximum size of 1mm, and the grid quality is good.

The finite element models of the local fitting joints are subject to the following boundary conditions according to the actual working conditions.

1) The bolts are also subjected to axial pre-tightening force, the pre-tightening

force of the M18 bolt is 66000N, the pre-tightening force of the M8 bolt is 12400N, and the pre-tightening force of the M6 bolt is 6750N.

2) The contact between the bolts and fitting of center section, intermediate panel, fitting of outer wing section, stringer of outer wing section, lower panel of outer wing section is frictionless.

3) The contact between the nuts and fitting of center wing section, fitting of outer wing section, stringer of outer wing section is frictional contact, and the friction coefficient is 0.2.

4) The constraints on the two sides of the model of the local fitting joints are frictionless. The right side of the model of I fitting joint is a fixed constraint. The fitting of outer wing section on the right side of the model of II fitting joint is a fixed constraint.

5) The end of the I fitting joint has a shear force -3545.2 N, a bending moment of 1510 N*m, and an axial stress 22.6 MPa. The end of the II fitting joint has a shear force -3941.9 N, a bending moment of 924.5 N*m, and an axial stress 38.86 MPa. The shear force here is caused by the different positions of the center of gravity of the segments of the fitting joint, and partial bending occurs due to eccentricity during load transmission.

The stress-strain states of the local fitting joints are obtained using Workbench, as shown in Fig. 3.11-3.14.

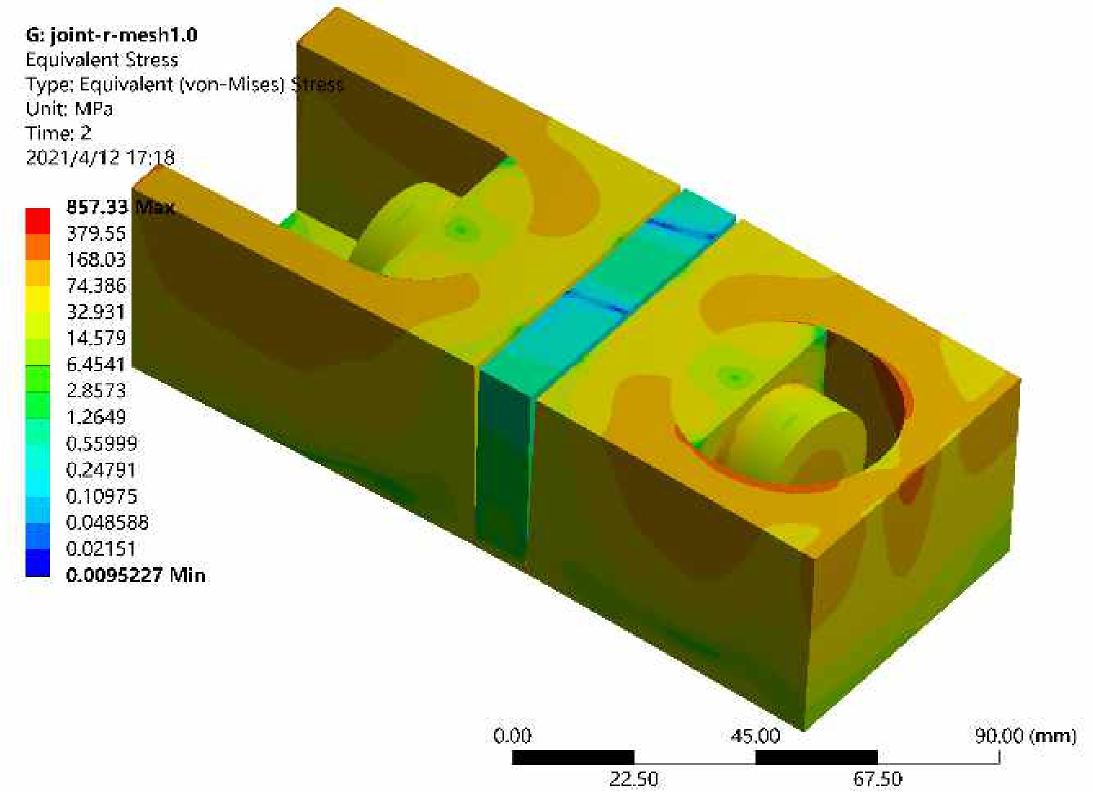

Fig. 3.11 The stress state of I fitting joint

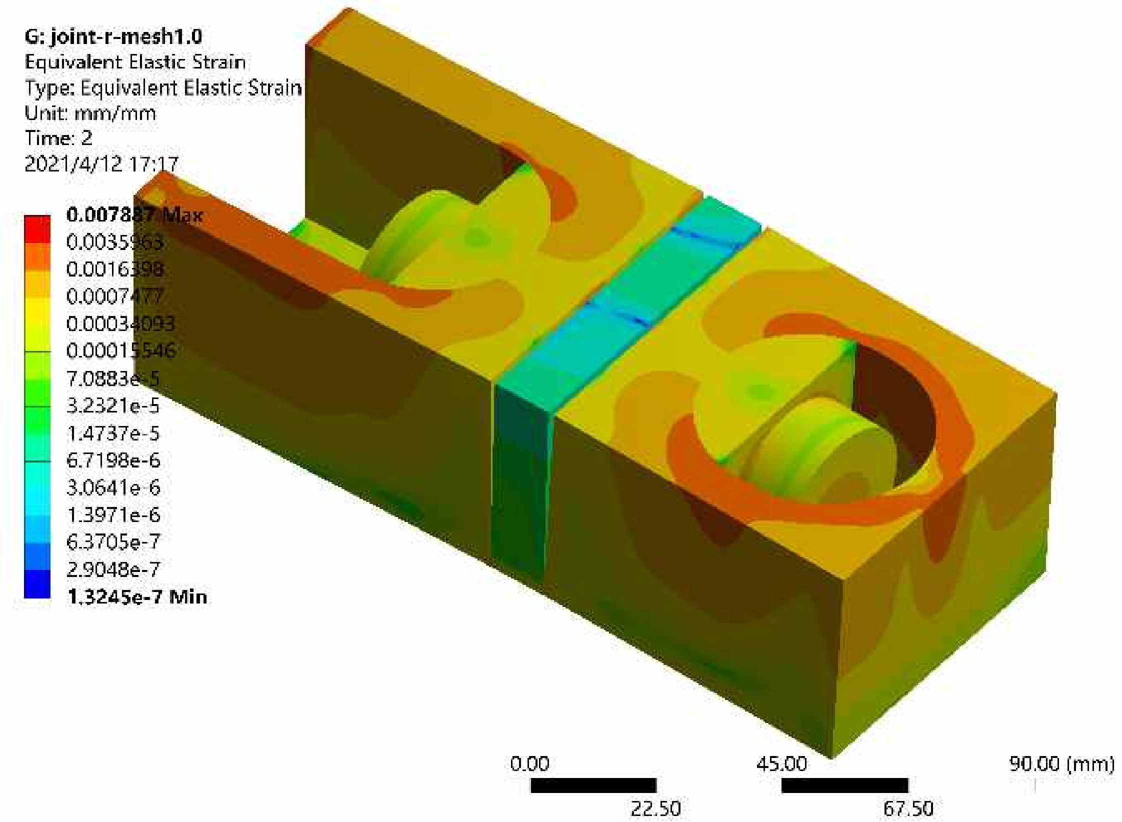

Fig. 3.12 The stress state of I fitting joint

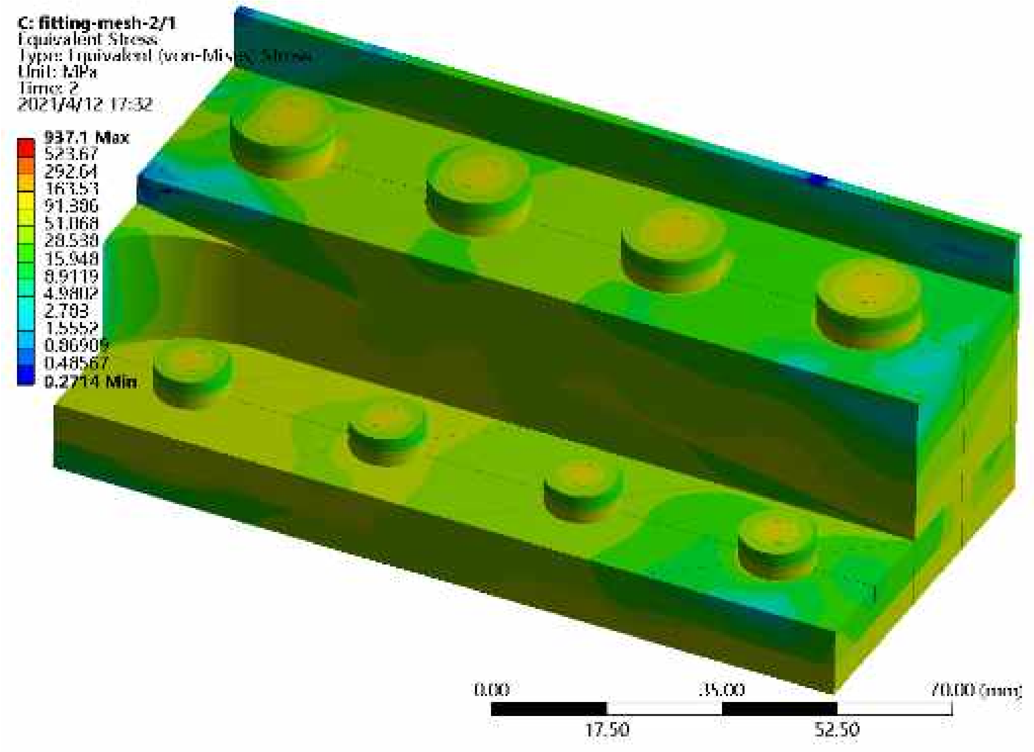

Fig. 3.13 The strain state of II fitting joint

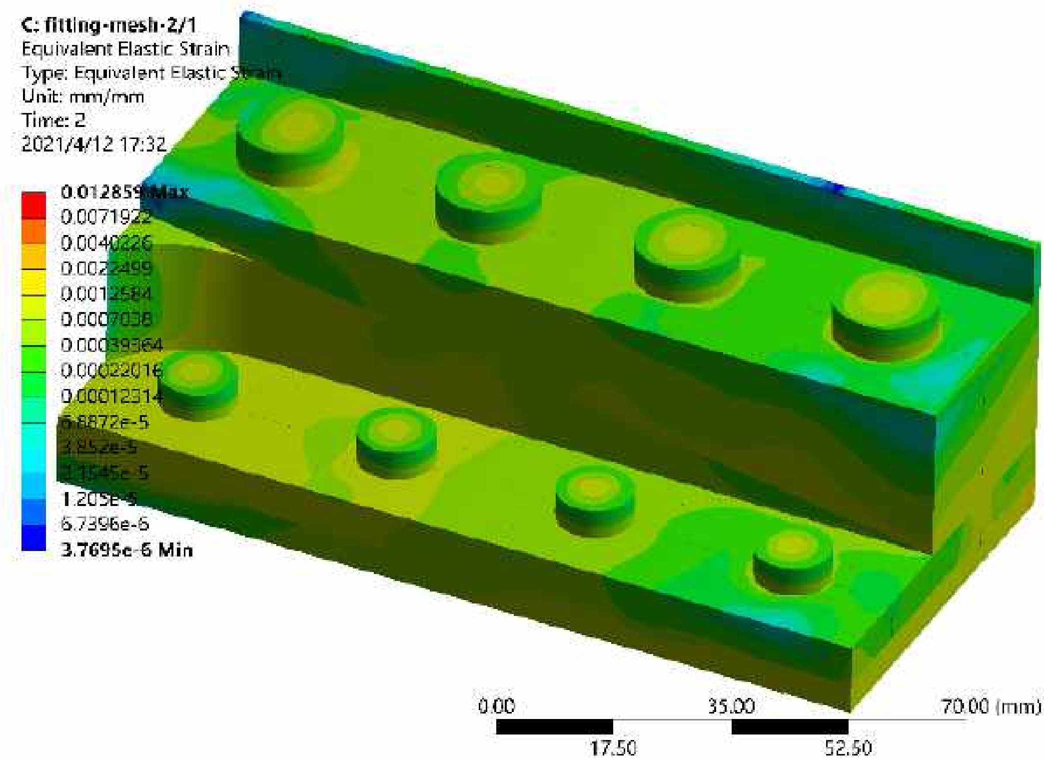

Fig. 3.14 The strain state of II fitting joint

3.3 Direct method to calculate stress-strain state of the fitting joint

When calculating the stress-strain state of the fitting joint, the three-dimensional model of the fitting joint is directly imported into Workbench for calculation without simplifying the model. This calculation method is called the direct method to calculate the stress-strain state of the fitting joint. Fig. 3.15 shows the calculation process of the direct method. During the execution of the direct method, first the 3D model of the fitting joint is created using CATIA, and then the 3D model is imported into Workbench for meshing and setting the boundary conditions to obtain the finite element model of the fitting joint. The three-dimensional model of the fitting joint is shown in Fig. 2.2.

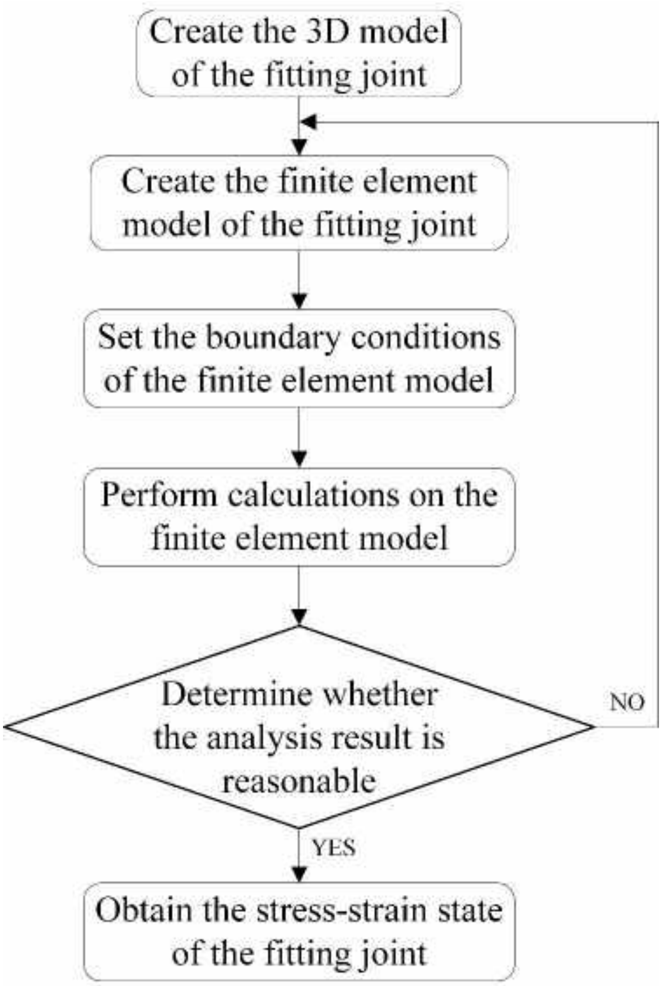

Fig. 3.15 Direct method to calculate stress-strain state of the fitting joint

The finite element models of fitting joint (overall) is composed of hexahedral elements and a small number of tetrahedral elements. In order to decrease the number of meshes to reduce the amount of calculation, only the mesh size close to the holes and bolts are set smaller. It should be noted that in this paper, when each finite element model is calculated, the grid independence is first verified, and the convergence tolerance of stress and strain is set to 0.03. The mesh size after convergence is a minimum of 0.2mm and a maximum size of 1mm, and the grid quality is good. The finite element model of the fitting joint is shown in Fig. 3.16.

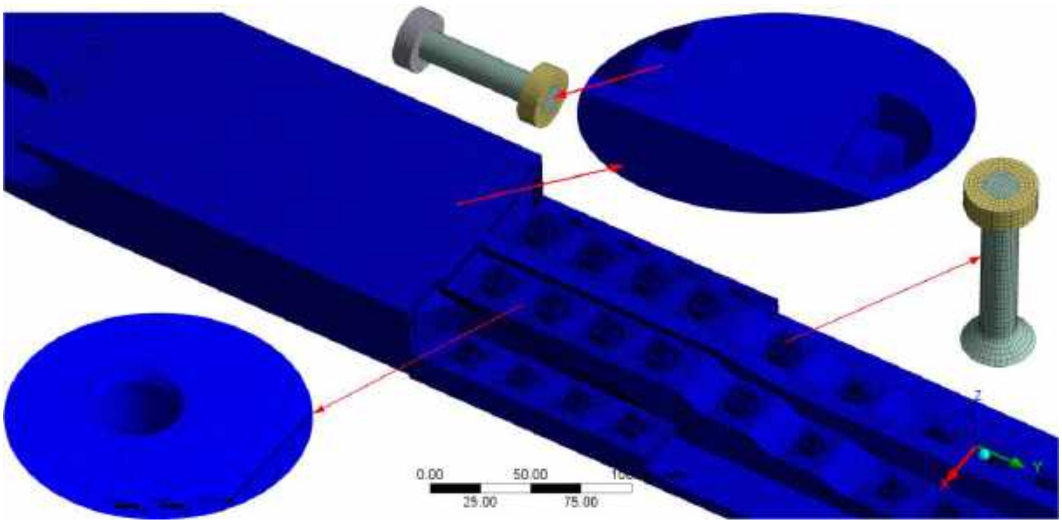

Fig. 3.16 The finite element model of the fitting joint

The finite element models of the fitting joints are subject to the following boundary conditions according to the actual working conditions.

1) The bolts are also subjected to axial pre-tightening force, the pre-tightening force of the M18 bolt is 66000N, the pre-tightening force of the M8 bolt is 12400 N, and the pre-tightening force of the M6 bolt is 6750 N.

2) The contact between the bolts and fitting of center section, intermediate panel, fitting of outer wing section, stringer of outer wing section, lower panel of outer wing section is frictionless.

3) The contact between the nuts and fitting of center section, fitting of outer wing section, stringer of outer wing section is frictional contact, and the friction

coefficient is 0.2.

4) The constraints on the two sides of the model of the local fitting joints are frictionless. The right side of the model of the fitting joint is a fixed constraint. The lower section of the intermediate panel is a fixed constraint.

5) The end of the fitting joint of the outer wing section has a force 127140 N.

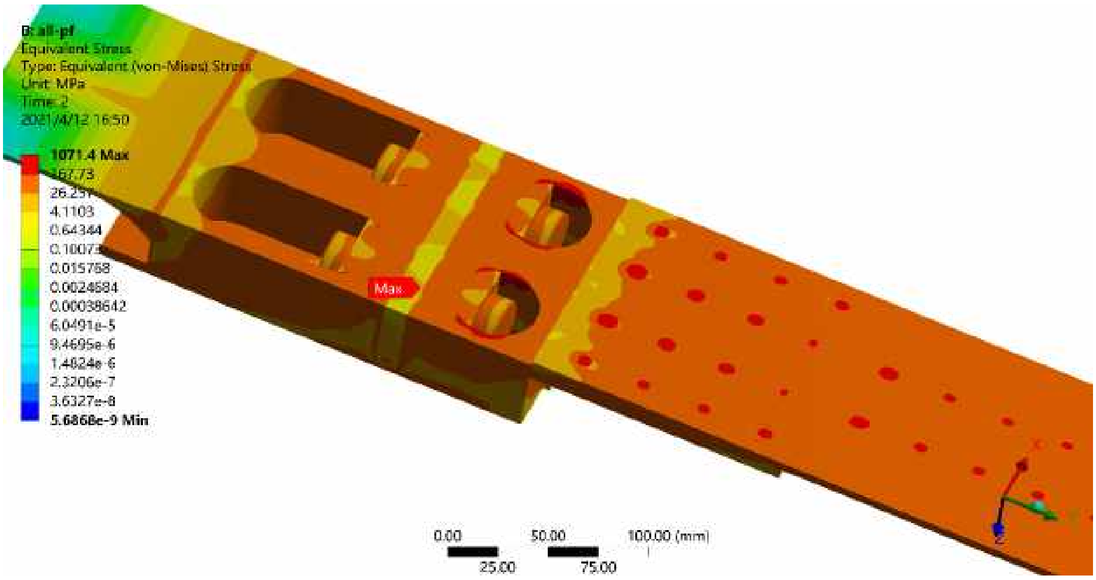

Fig. 3.17 The stress state of the fitting joint

The stress-strain states of the fitting joints are obtained using Workbench, as shown in Figs 3.17-3.18. The stress cloud diagram of the fitting joint is shown in Fig. 3.17, the strain cloud diagram of the fitting joint is shown in Fig. 3.18.

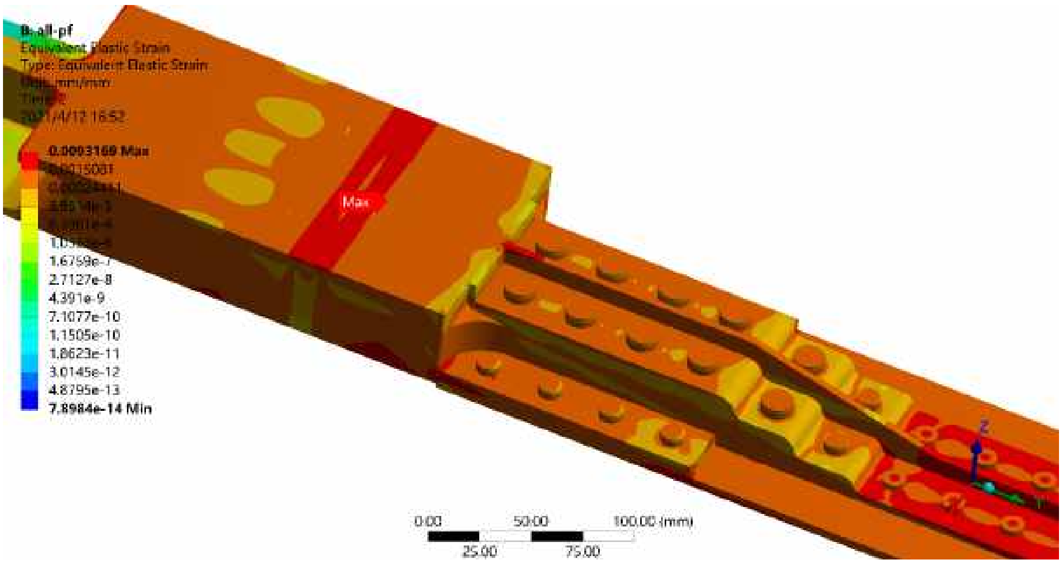

Fig. 3.18 The strain state of the fitting joint

3.4 Results and discussion

The results of the indirect method show that when the fitting joint is loaded with 150 MPa, the fitting of center section has a maximum stress of 146.21 MPa and a maximum strain of 0.0023012, the intermediate panel has a maximum stress of 129.73 MPa and a maximum strain of 0.0018345, the fitting of outer wing section has a maximum stress of 323.82 MPa and a maximum strain of 0.004625, the stringer of outer wing section has a maximum stress of 342.76 MPa and a maximum strain of 0.0048149, the lower panel of outer wing section has a maximum stress of 320.28 MPa and a maximum strain of 0.004556. The connecting bolts (M18) have a maximum stress of 700.34 MPa and a maximum strain of 0.006984. The connecting bolts (M8 and M6) have a maximum stress of 833.77 MPa and a maximum strain of 0.0067211.

The results of the direct method show that when the fitting joint is loaded with 150 MPa, the fitting of center wing section has a maximum stress of 156.44 MPa and a maximum strain of 0.0021744, the intermediate panel has a maximum stress of 143.08 MPa and a maximum strain of 0.0020548, the fitting of outer wing section has a maximum stress of 353.95 MPa and a maximum strain of 0.0049405, the stringer of outer wing section has a maximum stress of 350.86 MPa and a maximum strain of 0.0050585, the lower panel of outer wing section has a maximum stress of 349.19 MPa and a maximum strain of 0.00485012. The connecting bolts (M18) have a maximum stress of 737.65 MPa and a maximum strain of 0.0068203. The connecting bolts (M8 and M6) have a maximum stress of 803.14 MPa and a maximum strain of 0.0069841.

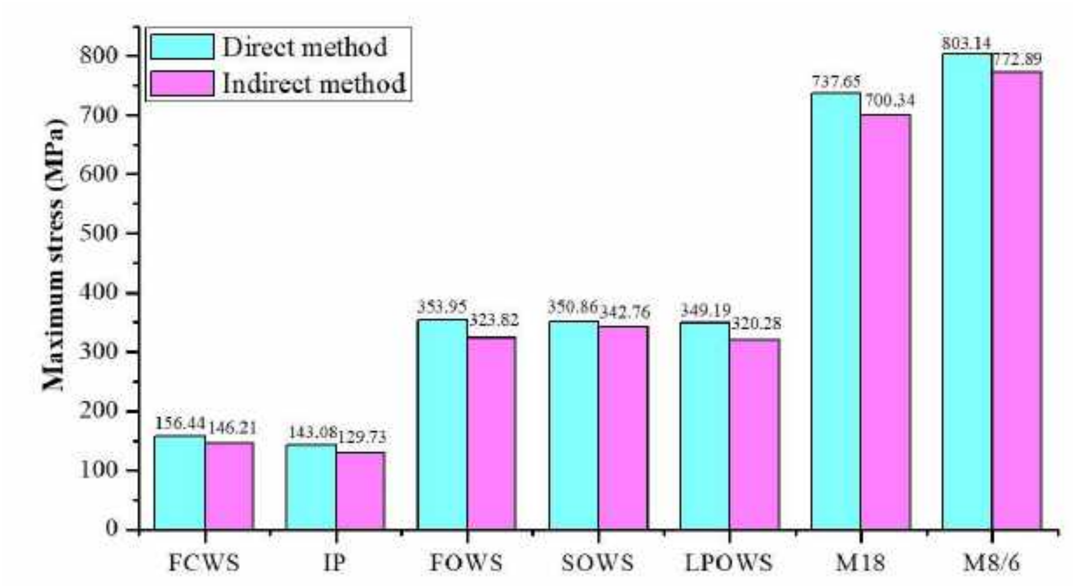

Fig. 3.19 Comparison of stress calculation results by direct method and indirect method

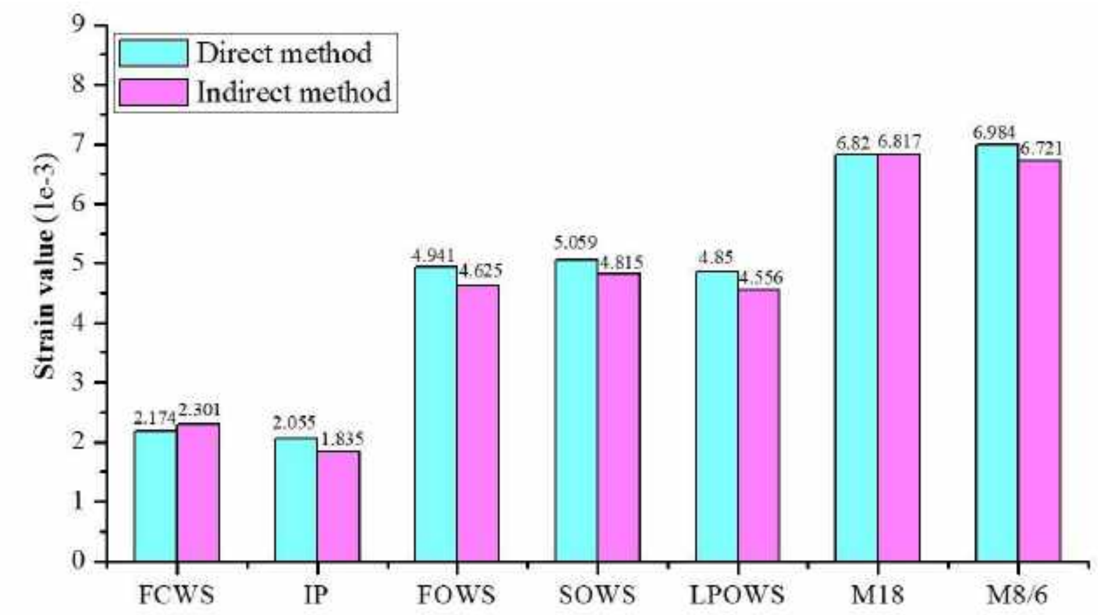

Fig. 3.20 Comparison of strain calculation results by direct method and indirect method

Figs 3.19 and 3.20 show the comparison between the results of the direct method and the results of the indirect method. It can be seen that the results of the stress-strain state of the fitting joint obtained by the direct method and the indirect method are consistent.

3.5 Conclusion of this chapter

1. An indirect method for calculating the stress-strain state of fitting joint between center section and outer wing is developed in this chapter. In this indirect method, three-dimensional modeling software and finite element analysis software are used to calculate the stress-strain state of the fitting joint. In the three-dimensional modeling software CATIA, the solid model is segmented and simplified according to geometrical and mass properties of the solid model cross section. In the finite element analysis software ANSYS Workbench, the solid model of the fitting joint is performed by two finite element calculations. First, beam elements are used to replace segmented and simplified models to obtain the general finite element model. The general finite element model is executed finite element calculation to obtain the internal force distribution of the solid model. Second, according to the internal force distribution of the solid model, the boundary conditions of the single segmented model can be obtained, and then the finite element analysis can be performed on the single segmented model to obtain its stress-strain state (local stress-strain state). When the finite element analysis of each segmented model is completed, the integral stress-strain state can be obtained according to the local stress-strain state.

2. It is a very feasible method to use the indirect method to calculate the stress and strain state of the assembled joint. The result calculated by the indirect method is compared with the result calculated by the direct method, the comparison results show that the two results are in good agreement. Compared with the direct method, the indirect method has the advantages of small calculation amount and fast calculation speed.

3. The stress-train state of the fitting joint between center wing section and outer wing section meets the strength requirements of the design. According to the stress-strain state results of the fitting joint, it can be seen that the stringer of outer wing section has the most stress and will be damaged first. when the fitting joint is loaded

with 150 MPa, the stringer of outer wing section has a maximum stress of 293.17 MPa and a maximum strain of 0.0047. The connecting bolts (M18) have a maximum stress of 830.81 MPa and a maximum strain of 0.0056. The connecting bolts (M8 and M6) have a maximum stress of 686.81 MPa and a maximum strain of 0.0063. However, the yield stress of D16T is 447 MPa, the yield stress of VT22 is 1380 MPa, so the maximum stress of the components are within the allowable range of the material.

This chapter completes the dissertation work task: develop new methods for strength calculation and analysis of the fitting joint between the center wing section and the outer wing section of a regional aircraft by means of simulation technologies. For the first time, an indirect method for calculating the stress-strain state of the fitting joint between the center wing section and the outer wing section of a regional aircraft is proposed. The indirect method obtains the stress-strain state of the fitting joint through two finite element calculations. The results are consistent with those calculated by direct method.

CHAPTER 4

METHOD FOR FATIGUE LIFE EXTENSION OF WING PANELS WITH FUNCTIONAL HOLES: THE EXTRUDED ARC GROOVES

In order to obtain more loading space, the modern aircrafts usually adopt a compact structural layout. However, due to the numerous structural components on the aircraft, some functional holes must be made to ensure the reasonable installation of each structure and the efficient use of space. For example, in modern regional aircraft, almost all of the fuel is stored in the wings. However, the requirements for reliable operation of the fuel system are not always consistent with the "interests" of the wing design. In order to ensure the smooth fuel supply for the aircraft, some functional holes must be made on the panels of some wings. These functional holes on the wing panel will inevitably lead to a decrease in the fatigue life of the aircraft wing structure. Fig. 4.1 shows the wing panel with functional holes [46]. In response to the problem of the low life of the panels with functional holes, the researchers used cold extrusion [47-48], shot peening [49-50], laser strengthening [51-52] and other methods to strengthen the hole wall. It is concluded that the method of the cold extrusion strengthening is still the most concise and effective anti-fatigue manufacturing technology for the panels with functional holes.

In the past few decades, the cold extrusion strengthening technology has been widely used in the anti-fatigue design of the aircrafts. A large number of studies have shown that the residual stress generated by the cold extrusion strengthening process can effectively reduce the tensile stress caused by the external load and improve the fatigue strength and effectively reduce the stress intensity factor at the crack tip, thereby slow down the fatigue crack growth speed and significantly improve the fatigue life of the connector [53-54]. However, due to the limitation of the measurement method, the three-dimensional distribution of the extrusion residual stress in the material is still an unsolved problem [53].

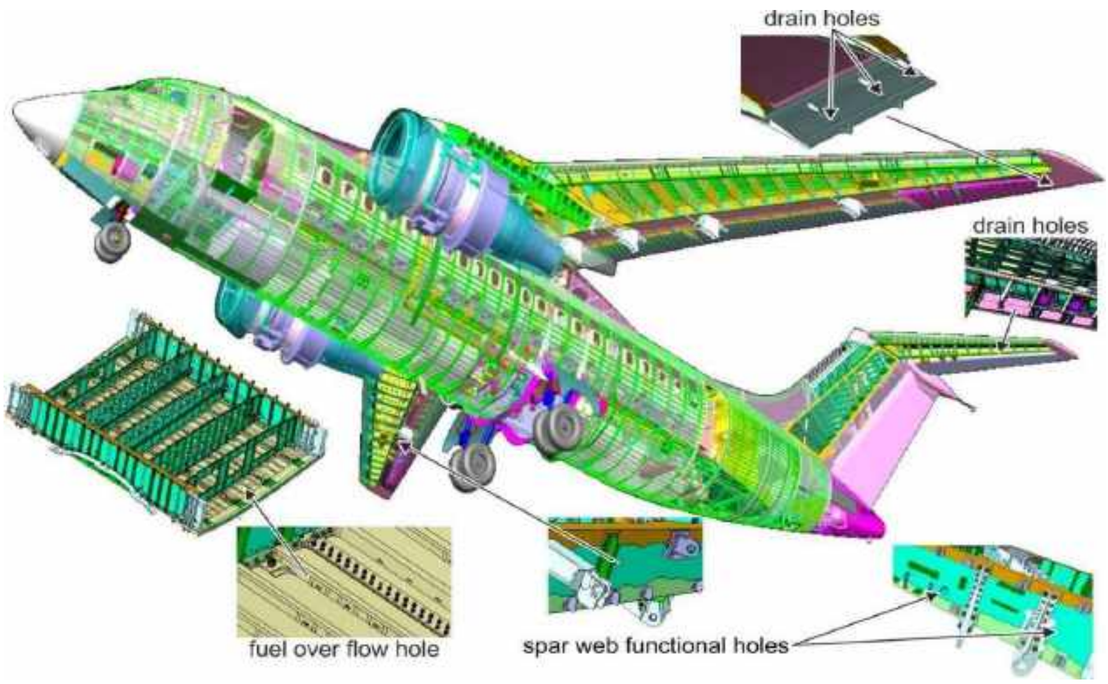

Fig. 4.1 Wing panel with functional holes [46]

In recent years, with the rapid development of computer technology, researchers have conducted a lot of researches on the residual stress distribution of parts after extrusion through finite element analysis [55-64]. Zhang et al. [55] obtain the residual stress distribution on the lugs of the wing by reasonably simplifying the geometric structures, boundary conditions and loading methods in the finite element analysis. Liu et al. [56-57] investigate the residual stress and fatigue performance of the wing panel under the action of cold expansion holes with different radial interference values through finite element analysis and experiment. Babu et al. [58] study the change law of tangential residual stress in the thickness direction of the panels. Seifi [59] and Kumar et al. [60-61] research the residual stress distribution caused by the cold expansion of two adjacent holes, as well as the influence of hole geometry, expansion ratio and crack position parameters on fatigue behavior. Zhang et al. [62-63] use neutron diffraction technology and finite element simulation to study the relationship between residual stress and overload ratio, overload position and load ratio in the large residual plastic strain caused by overload. Geiglou and Chakherlou [64-65] investigate the effect of cold expansion process on fatigue behavior of 7075-T6 aluminum alloy through numerical modeling and experimental tests, and obtain the stress distribution and the initial position of fatigue cracks in the process. Tian et al. [66] studied the influence of countersunk depth of riveting hole (functional hole) on the fatigue life of connecting samples, and concluded that the high cycle fatigue life of samples with countersunk depth of 1.2 mm was far less than the other samples. Zeng et al. [67] studied the effect of residual stress due to interference fit on the fatigue behavior of a fastener hole (functional hole) with edge cracks. Based on the above researches, it is found that the extrusion process is a complex elastic-plastic deformation process, and after the component is extruded, the residual stress distribution on the component is uneven, and different residual stress distributions have different effects on the fatigue life of the component.

Kiva et al. [68] propose a method of the extruded arc grooves to strengthen parts with functional holes, which is verified by experiments. According to this method, the arc grooves are formed by extrusion near the edge of the hole in the force direction of the component, so that the periphery of the hole is plastically deformed and then residual stress is generated. The residual stress can offset the stress damage caused by the component under the tension or compression, thereby achieving the purpose of extending fatigue life of the component. Therefore, the method is simple to operate, easy to implement, and presents great engineering application value. However, in Kiva`s research, only simple qualitative analysis and experimental verification are performed without detailed and in-depth quantitative analysis. Based on Kiva`s research, this article will deeply discuss the influence of the process parameters of the extruded arc grooves on extending the fatigue life of the component.

4.1 Experiment

4.1.1 Specimen

In order to ensure the validity of the experiment, the experimental specimen in this chapter is same as the specimen in Kiva`s study. The sizes of specimen are shown in Fig. 4.2. The specimen has a symmetrical structure, with a total length of 330 mm, a center width of 48 mm, and an end width of 70 mm. The three holes in the middle of the specimen are the functional holes with a diameter of 8 mm, and the two holes at both ends of the specimen are the clamping holes with a diameter of 32 mm. The centers of the functional holes are located on the central axis of the specimen, and the distances between them are 12 mm. The center of the extrusion arc groove is at the same position as the center of the functional hole at the end. The angle of the extrusion arc groove is θ, and its outer diameter is 16mm, the width is 2 mm, the given extrusion depth is h, and the actual extrusion depth is h_1. The h_1 is slightly less than h, that is because the specimen undergoes plastic deformation and elastic deformation during the extrusion process, after the extrusion punches are released, the elastic deformation disappears and only the plastic deformation remains. The manufacturing process of the extrusion arc groove is shown in Fig. 4.3.

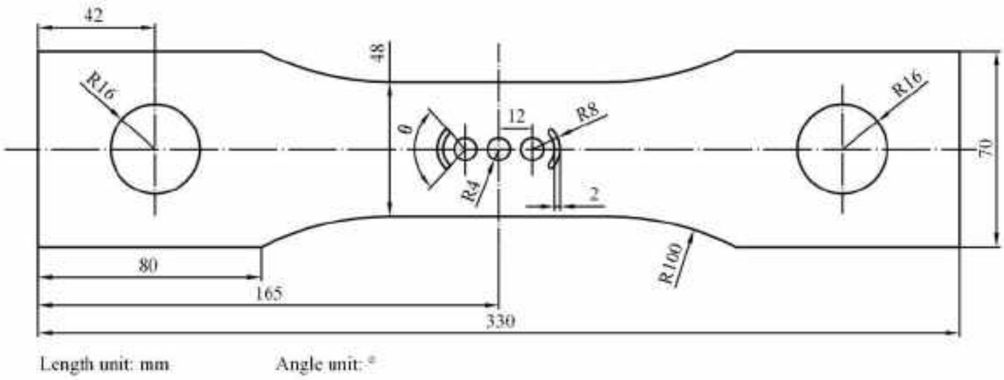

Fig. 4.2 The dimensions of the experimental specimen

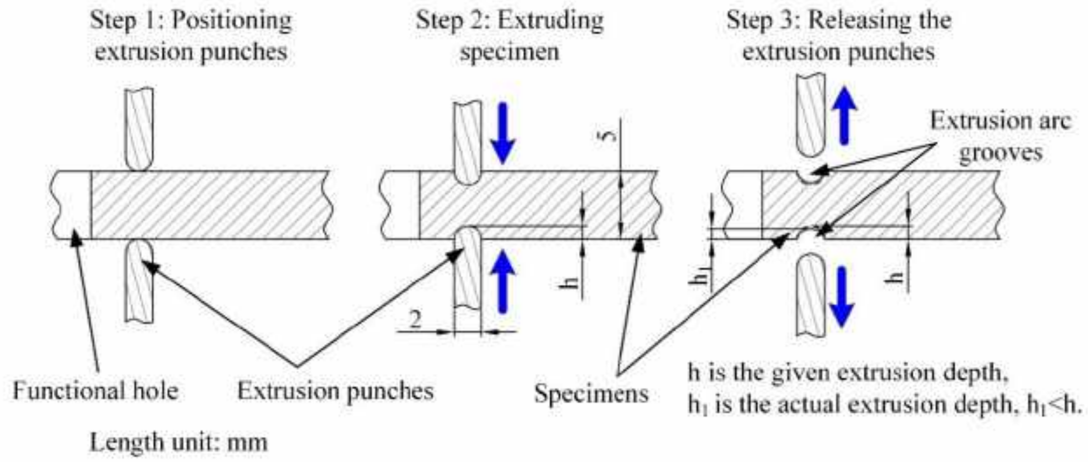

Fig. 4.3 The manufacturing process of the extruded arc grooves

4.1.2 Material

The material of the experimental specimen is same as that of the AN-148 aircraft wing panel, and the material is aluminum alloy D16T [69]. The main performance parameters of aluminum alloy D16T are shown in Table 4.1. D16T is one of the most popular duralumin alloys in the shipbuilding, aviation and aerospace industries. Its main advantages are: stable structure; high strength characteristics; low density; strong resistance to deformation; good processability. The extrusion punches are made of chromium alloy Cr12MoV [70], and its main performance parameters are shown in Table 4.1.

Table 4.1 The mechanical properties of materials

Material	Density (kg/m^3)	Young's Modulus (GPa)	Ultimate Strength (MPa)	Yield Strength (MPa)	Poisson's Ratio
D16T	2780	73.264	564	447	0.33
Cr12MoV	7700	200.00	880	550	0.31

4.1.3 Experimental principle and process

In the experiment, the experiment equipment is the fatigue testing machine МУП-50 and its working principle is shown in Fig. 4. The working frequency is 12 Hz. The loading load is a cyclic stress, and the method is a sine wave. The load on the wing panels can be obtained referring to the simplified segmentation method [71]. The five working conditions are set as shown in Table 4.2.

Table 4.2 Five working conditions

Working condition	Maximum load σ_{max} (MPa)	Minimum load σ_{min} (MPa)
1	100	0
2	114	0

3	130	0
4	150	0
5	170	0

Due to the inevitable defects of the specimen, four specimens are tested under each working condition, and the fatigue life is the average of the four test results to reduce errors. The maximum load can be calculated by the following formula:

$$\sigma_{max} = \frac{F_{max}}{A_m} \tag{4.1}$$

Where F_{max} is the maximum tensile force loaded on the specimen, and A_m is the area of the cross section of the specimen without functional holes.

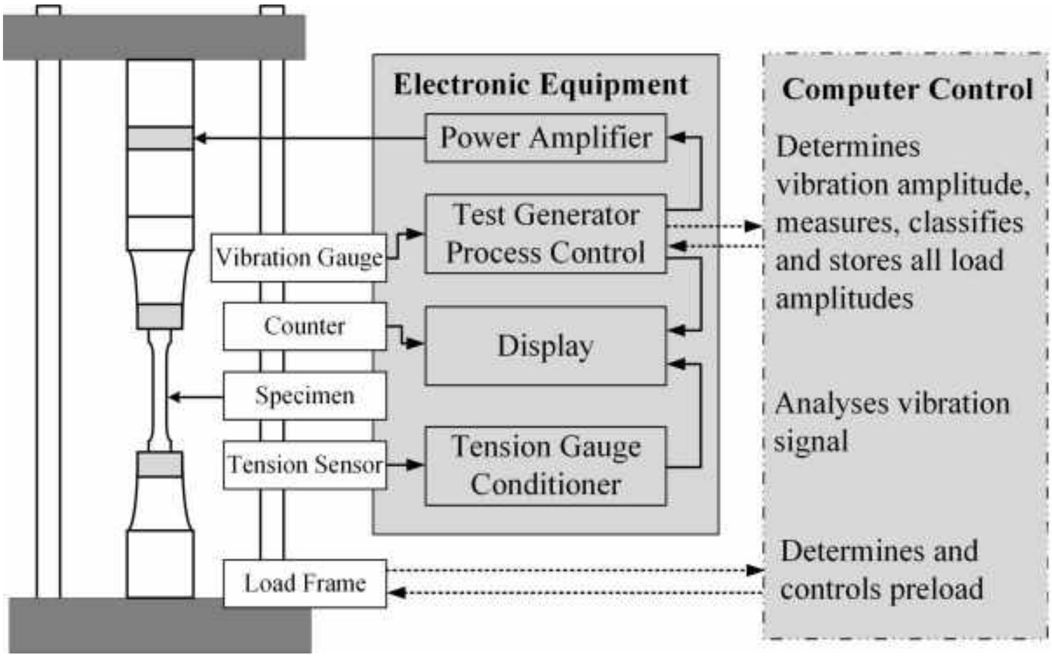

Fig. 4.4 Working principle of the fatigue testing machine

4.2 Finite element analysis

4.2.1 Finite element model

The finite element model includes two parts: a model of specimen and a model of extrusion punches, which are composed of hexahedral elements and a small number of tetrahedral elements. In order to decrease the number of meshes to reduce the amount of calculation, only the mesh size close to the functional holes is set smaller. Since the specimen and the extrusion punches have a symmetrical structure, only a quarter of their structure is used for finite element analysis in ANSYS, as shown in Fig. 4.5. It should be noted that in this paper, when each finite element model is calculated, the grid independence is first verified, and the convergence tolerance of stress and strain is set to 0.03. The mesh size after convergence is a minimum of 0.2 mm and a maximum size of 1 mm, and the number of elements along the thickness direction is 25.

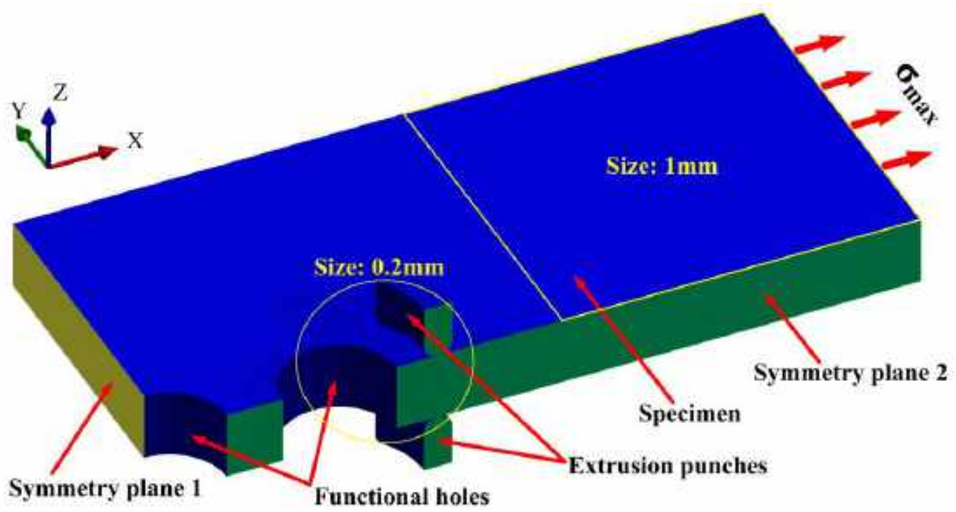

Fig. 4.5 Finite element model of the specimen and the extrusion punches

4.2.2 Simulation process

In order to ensure the accuracy of the calculation results, a step-by-step method is used to analyze the stress-strain state and fatigue life of the model. The calculation steps of the simulation are as follows:

STEP I: Set the boundary conditions: the end of the model of specimen is loaded with a maximum load σ_{max}, the symmetry plane 1 and symmetry plane 2 are set as frictionless support, the contacts between the model of specimen and the model of extrusion punches are set to frictional contact, the friction coefficient is 0.2 [68], and the given extrusion displacement of the model of extrusion punches is h. This step is the preparation stage.

STEP II: The model of extrusion punches squeezes the model of specimen to the given extrusion depth h (during the extrusion process). In this step, the stress distribution and deformation on the model of specimen can be gained during the forming of the arc grooves.

STEP III: The extrusion punches are released to obtain the extruded arc grooves (after the extrusion process). In this step, the residual stress distribution, deformation and the actual extrusion depth h_1 on the model of specimen can be gained after the arc grooves are extruded.

STEP IV: Apply the maximum load σ_{max} on the end of the model of specimen with the extrusion grooves. In this step, the stress distribution and deformation on the specimen with the extrusion grooves can be gained under the action of the maximum load σ_{max}.

STEP V: Apply the maximum load σ_{max} on the end of the model of specimen without the extrusion grooves. The purpose of this step is to compare the stress distribution of the specimens with extrusion arc groove and without extrusion arc groove under the action of the maximum load σ_{max}.

4.3 Results

4.3.1 Experimental results

For the specimens with three functional holes, under working condition 1, the average fatigue life is 858000 cycles; under working condition 2, the average fatigue life is 387000 cycles; under working condition 3, the average fatigue life is 180500 cycles; under working condition 4, the average fatigue life is 101000 cycles; under working condition 5, the average fatigue life is 65000 cycles. According to these experimental results, the curve of the relationship between the maximum load and the fatigue life of the specimens is shown in Fig. 4.6.

For the specimens with three functional holes and the extruded arc grooves (h = 0.3mm, θ = 90°), under working condition 1, the average fatigue life is 4500000 cycles; under working condition 2, the average fatigue life is 1805000 cycles; under working condition 3, the average fatigue life is 701000 cycles; under working condition 4, the average fatigue life is 335000 cycles; under working condition 5, the average fatigue life is 181000 cycles. According to these experimental results, the curve of the relationship between the maximum load and the fatigue life of the specimens is shown in Fig. 6.

It can be seen from the results in Fig. 4.6 that under the same fatigue load, the specimens with three functional holes and the extruded arc grooves (h = 0.3mm, θ = 90°) have a longer fatigue life than the specimens only with three functional holes. Therefore, it can be proved that the extruded arc grooves can extend the fatigue life of the wing panel with functional holes.

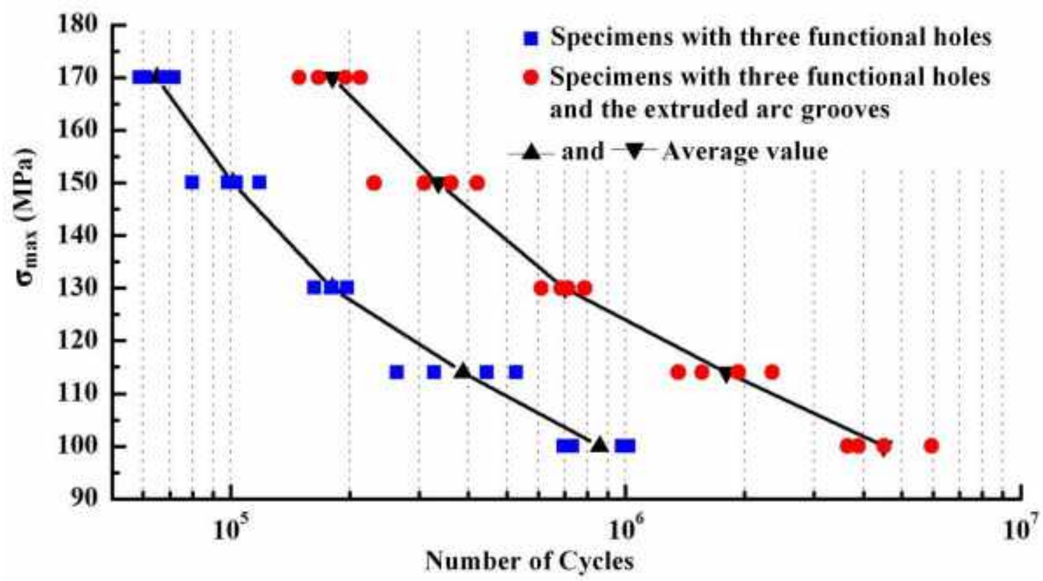

Fig. 4.6 The relationship between the maximum load (σ_{max}) and the fatigue life

4.3.2 Simulation results

Take the simulation of the specimens with three functional holes and the extruded arc grooves (h = 0.3mm, θ = 90°, σ_{max} = 100MPa) as an example. After the above simulation process is executed, the simulation results are shown in Figs 4.7 through 4.11. Fig. 4.7 shows the z-directional deformation of the specimen. Fig. 4.8 shows the z-directional normal stress distribution of the specimen in STEP III. Fig. 4.9 shows the von-Mises stress distribution of the specimen. Fig. 4.10 shows the x-directional normal stress distribution of the specimen. Fig. 4.11 shows the x-directional normal stress distribution on the hole wall. The direction of the X axis is the same as the direction of the maximum load σ_{max}. The direction of the Z axis is the same as the thickness direction of the specimen, and upward is the positive direction.

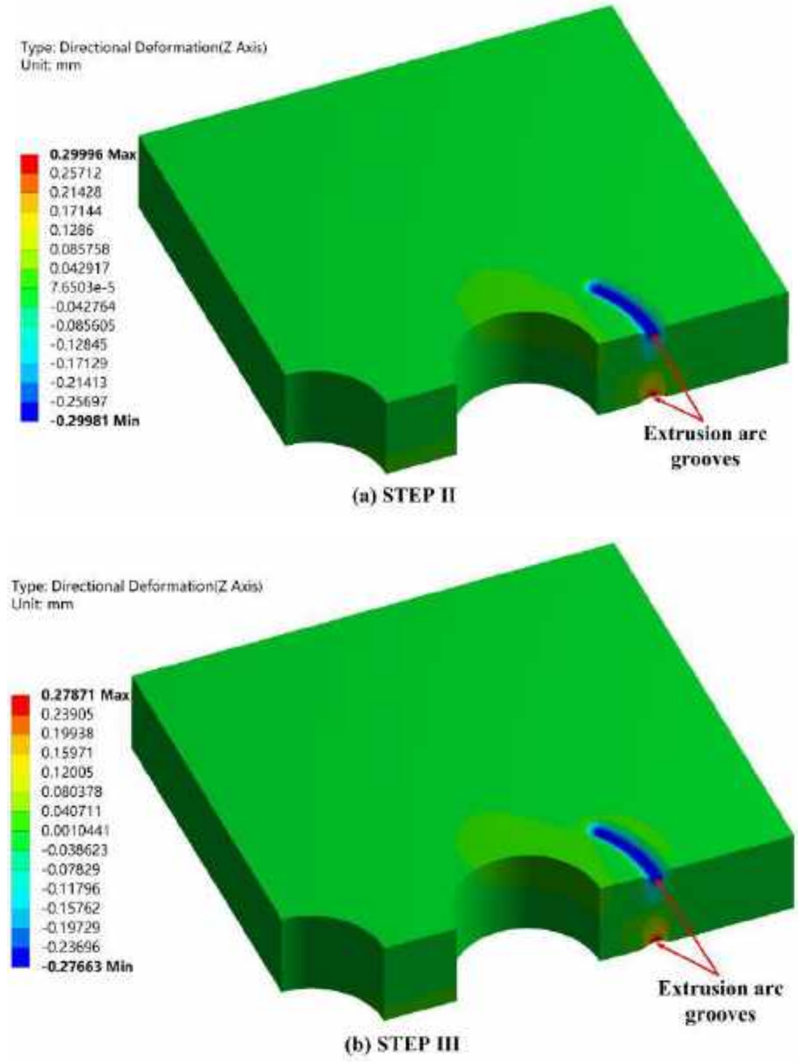

Fig. 4.7 The z-directional deformation of the specimen

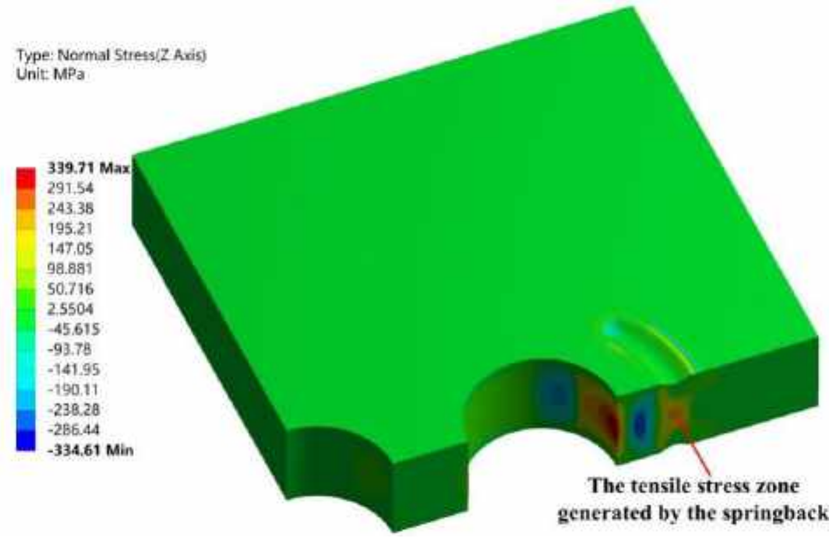

Fig. 4.8 The z-directional normal stress distribution of the specimen in STEP III

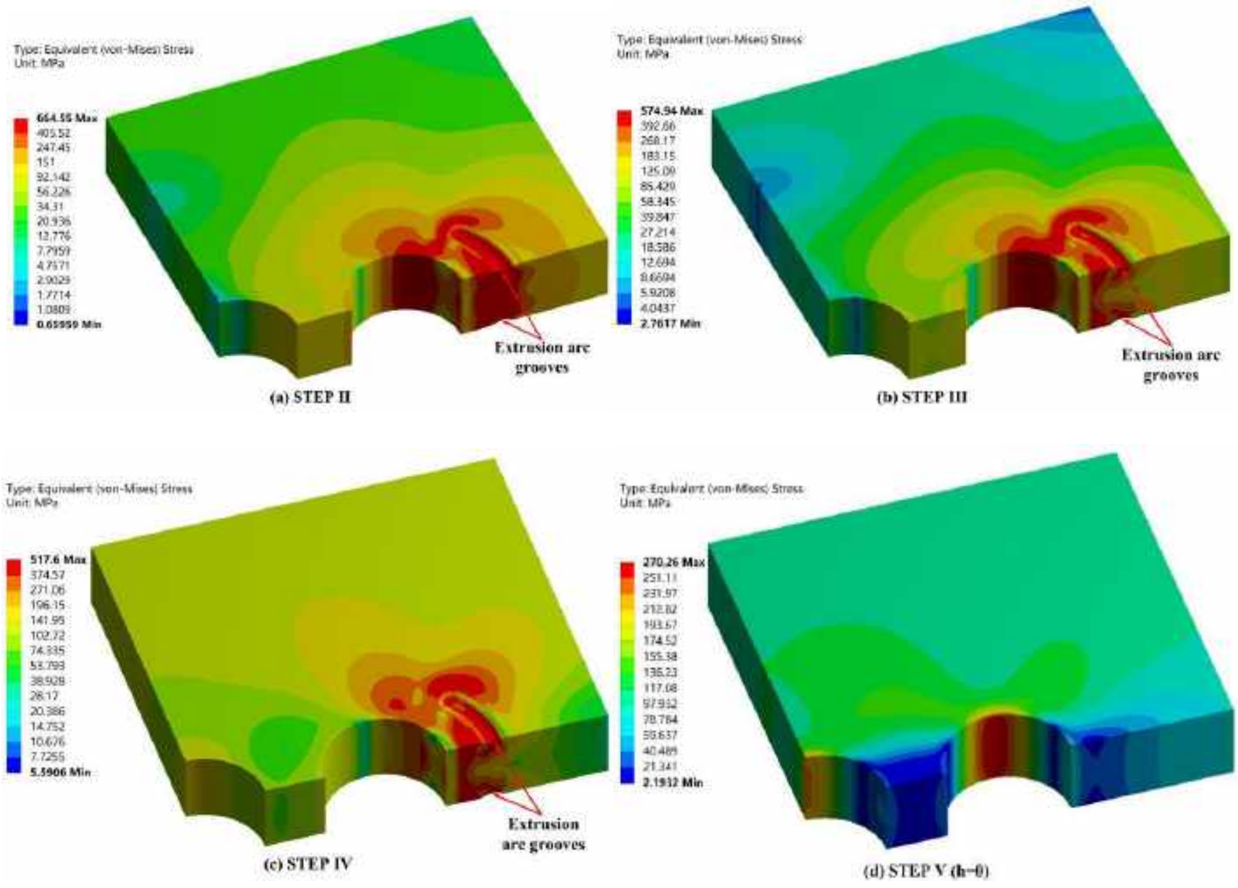

Fig. 4.9 The von-Mises stress distribution of the specimen

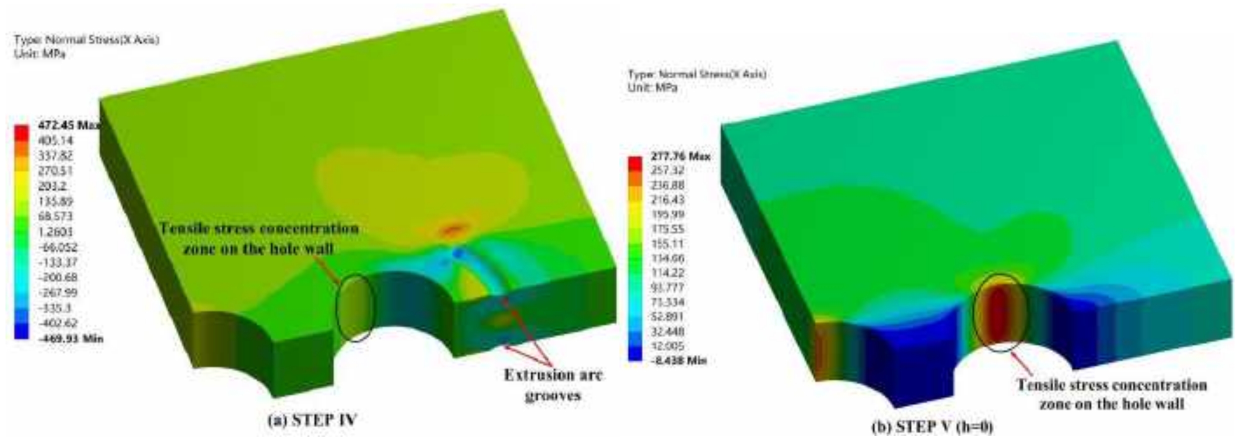

Fig. 4.10 The x-directional normal stress distribution of the specimen

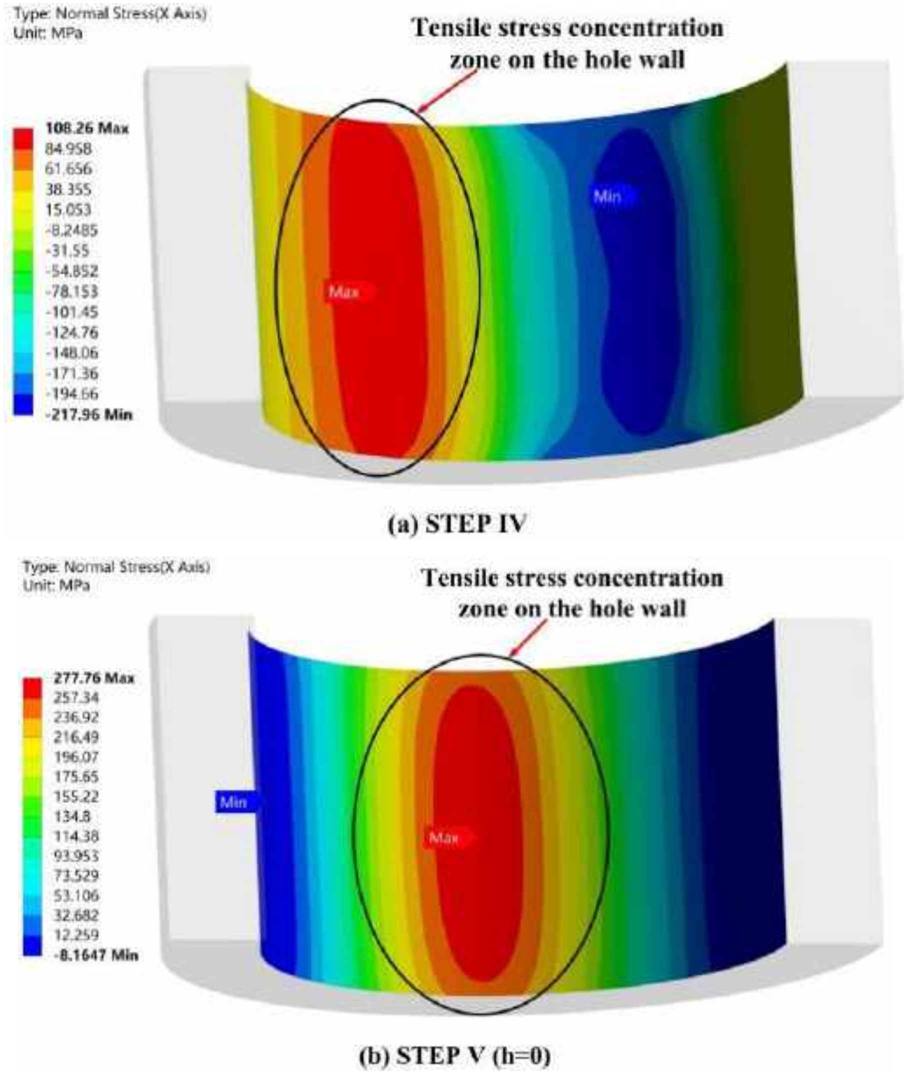

Fig. 4.11 The x-directional normal stress distribution on the hole wall

It can be seen from Fig. 4.7 that when the given extrusion depth is 0.3 mm, the actual extrusion depth is 0.279 mm. The reason for this phenomenon is the springback of the material after the extrusion, which results in the formation of a z-direction tensile stress zone in the middle of the two extrusion grooves, as shown in Fig. 4.8. It can be seen from Fig. 4.9(a) that the maximum stress on the specimen is 664.55 MPa (greater than the yield strength of the material (438 MPa)), which indicates that the specimen undergoes the plastic deformation. It can be seen from Fig. 4.9(b) that the specimen bears the maximum residual stress of 574.94 MPa after the extrusion punches are released, and the residual stress mainly occurs around the extruded arc grooves. Comparing Fig. 4.9 (a) and Fig. 4.9 (b), it can be concluded that after the extrusion punches are released, the residual stress is generated on the specimen. It can be seen from Fig. 4.9(c) that the maximum stress on the specimen is reduced to 517.6 MPa under the action of the maximum load σ_{max}. Comparing the stress distribution of the specimen without extrusion groove, as shown in Fig. 4.9(d), it can be seen that the stress distribution on the specimen with extrusion groove has changed due to the effect of the extruded grooves.

In order to better analyze the effect of the extrusion grooves on the specimen under the action of the maximum load, the x-directional normal stress on the specimen is presented in Figs 4.10 and 4.11. It can be seen from Fig. 4.10 and 4.11, the tensile stress concentration zone on the hole wall is located on the left of the hole wall for the specimen with the extrusion grooves, while the zone is located in the middle of the hole wall for the specimen without the extrusion grooves. It can be concluded that the tensile stress concentration zone on the hole wall has shifted due to the effect of the extrusion grooves. It can be seen from Fig. 4.11 that the maximum value of the tensile stress on the hole wall is 108.26 MPa for the specimen with the extrusion grooves, while the maximum value is 277.76 MPa for the specimen without the extrusion grooves. It can be concluded that the maximum tensile stress on the hole wall is greatly reduced due to the effect of the extrusion grooves.

4.3.3 Comparison of simulation and experimental results

The comparison between the experimental specimens and the simulated specimens is presented in Fig. 4.12, which shows the fracture position and shape of the experimental specimen after the fatigue test (part of the results), and the tensile stress concentration zone on the hole wall of the simulated specimen. The position of the initial crack is obtained by analyzing the position and shape of the fracture of the specimen. It can be seen that the position of the initial crack is consistent with the location of the tensile stress concentration zone. In engineering, the tensile stress concentration zone is often the location where fatigue failure occurs. Therefore, the stress in the tensile stress concentration zone can be used as the basis for judging the fatigue life of the specimen. From Figs 4.12 (a) and 4.12 (b), it can be seen that for the specimens without the extrusion grooves, the tensile stress concentration zone and the position of the initial crack are on the central axis. From Fig. 4.12 (c) and 4.12(d), it can be seen that for the specimens with the extrusion grooves, the tensile stress concentration zone and the position of the initial crack have shifted.

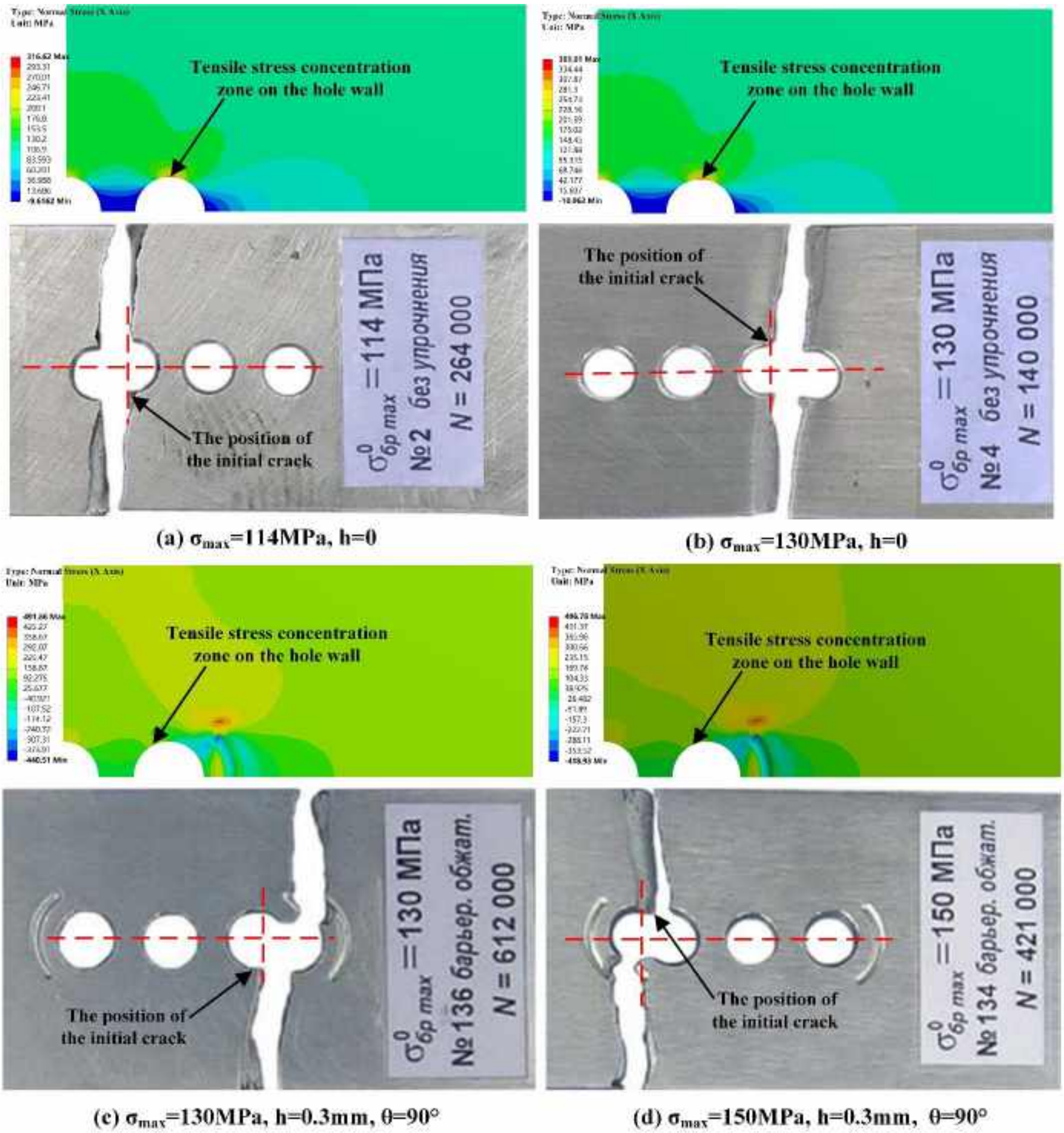

Fig. 4.12 Comparison of simulation and experimental results

4.4 Discussion

4.4.1 Theory of critical distance

It is conservative that the maximum tensile stress is used as the basis to judge the fatigue life of the specimen. In order to improve the accuracy of judgment, the theory of critical distance is used to extract the corresponding stress as the basis. Critical distance theory is a new method for the fatigue assessment of the notched components based on fracture mechanics. Its concept is that the fatigue failure of the notched components not only depends on the peak stress of the stress concentration zone, but also depends on the stress distribution within a certain distance near the stress concentration zone. This distance range is called "critical distance L_0". The characteristic stress is the control parameter of the fatigue failure of the notched component. When the characteristic stress reaches the threshold, the fatigue damage will occur. According to the different methods of calculating the characteristic stress, the critical distance theory is divided into point method, line method, area method and volume method [72-73]. In this paper, the point method is used to calculate the characteristic stress. The point method considers that the characteristic stress is the stress at $L_0/2$ from the hole edge, and the corresponding characteristic stress is:

$$\sigma_c = \sigma_1 \tag{4.2}$$

Where: σ_c is the characteristic stress, and σ_1 is the stress at $L_0/2$ from the tip of the notch.

The key parameter in the critical distance theory is the critical distance L_0, which is defined by the fatigue limit $\Delta\sigma_0$ of the material and the crack growth threshold ΔK_{th}, which can be calculated by the following formula:

$$L_0 = \frac{1}{\pi}\left(\frac{\Delta K_{th}}{\Delta\sigma_0}\right)^2 \tag{4.3}$$

The ΔK_{th} and $\Delta\sigma_0$ are both material property parameters, so L_0 is a parameter that depends on the material itself. The specimen is made of the D16T aluminum alloy, and its ΔK_{th} is 7.26 MPa $\sqrt{\mathrm{m}}$ [74], $\Delta\sigma_0$ is 120 MPa [75], so the critical distance L_0 can be calculated by Formula 3, which is 1.167mm.

After the specimen is affected by the extrusion grooves, the tensile stress concentration zone has shifted, which means that the position of the "notch tip" has changed. Therefore, the maximum tensile stress on the cylindrical surface (critical distance surface) at the position $L_0/2$ from the wall of the functional hole is taken as the characteristic stress, as shown in Fig. 4.13.

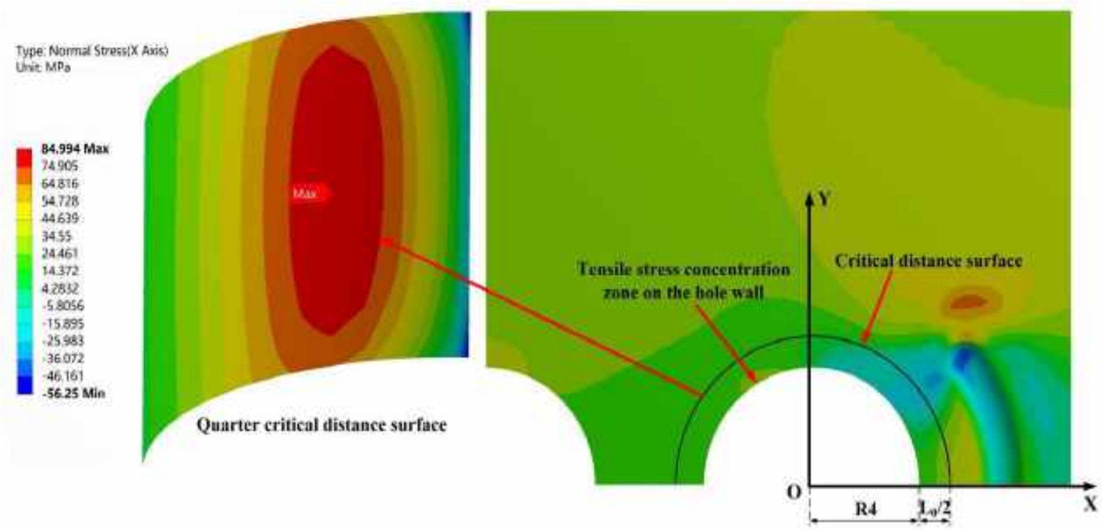

Fig. 4.13 The characteristic stress

4.4.2 Numerical analysis

Through the characteristic stress acquisition method introduced in Chapter 4.2, the relationship between the maximum load σ_{max} and the characteristic stress σ_c generated on the specimen is shown in Fig. 4.14. It can be clearly seen from the figure that due to the effect of the extruded arc grooves, under the same maximum load σ_{max}, the characteristic stress σ_c generated on the specimen with the extruded arc grooves (h = 0.3mm, θ = 90°) is significantly lower than that of the specimen without the extruded arc grooves.

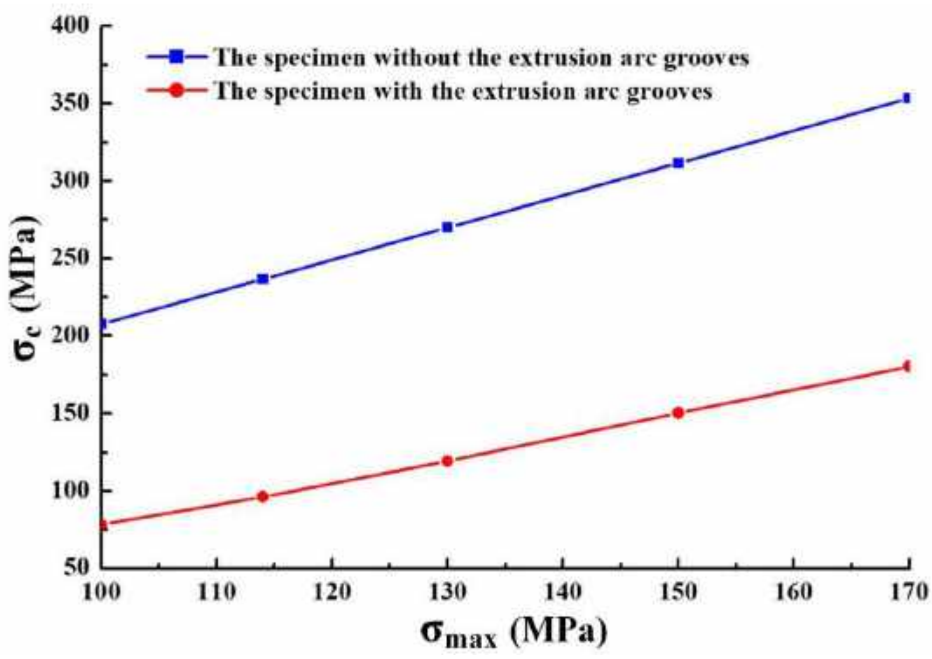

Fig. 4.14 The relationship between the maximum load and the characteristic stress

The relationship between the characteristic stress σ_c generated on the specimen and the average fatigue life of the corresponding specimen is shown in Fig. 4.15. In order to further analyze the influence of the extrusion process on the fatigue life of the specimen and determine the relationship between the average fatigue life and the characteristic stress, the Allometric 1 function model (Classical Freundlich Model in the ORIGIN) is used to fit this relationship. The Allometric 1 function model is as follows:

$$y = a * x^b \tag{4.4}$$

Where a and b are undetermined coefficients, y is the average fatigue life of specimen, x is the characteristic stress.

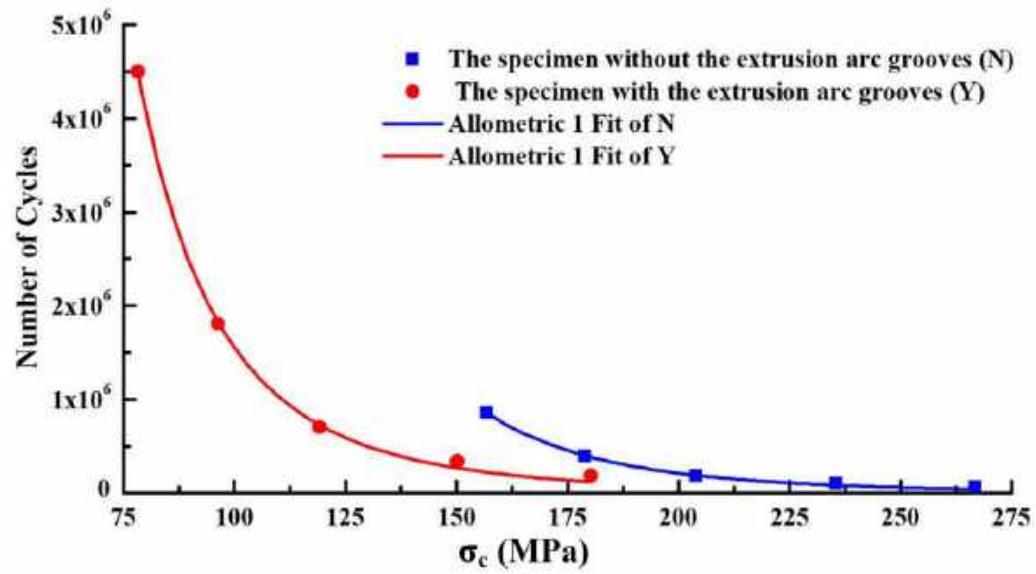

Fig. 4.15 The relationship between the average fatigue life and the characteristic stress

Through the numerical analysis and function fitting, the fitting function of the relationship between the average fatigue life and the characteristic stress of specimen without the extruded arc grooves is gained as follows:

$$y = 3.53764E18x^{-5.74678} \tag{4.5}$$

Where y is the average fatigue life of specimen without the extruded arc grooves, x is the characteristic stress.

Through the numerical analysis and function fitting, the fitting function of the relationship between the average fatigue life and the characteristic stress of specimen with the extruded arc grooves is gained as follows:

$$y = 7.18081E14x^{-4.3326} \tag{4.6}$$

Where y is the average fatigue life of specimen with the extruded arc grooves, x is the characteristic stress.

In Fig. 4.15, Allometric 1 Fit of N shows the fitting relationship between the average fatigue life and the characteristic stress of the specimen without the extruded arc grooves, while Allometric 1 Fit of Y shows the fitting relationship between the average fatigue life and the characteristic stress of the specimen with the extruded arc grooves. It can be seen that the Allometric 1 function model can fit these experimental data well. In this way, the functional relationship between the average fatigue life and the characteristic stress can be used to predict the fatigue life of the specimen under different working conditions.

4.4.3 Optimization of the extrusion arc groove depth

From the experimental results of the specimen without the extruded arc grooves and the specimen with the extruded arc grooves shown in Fig. 4.6, it can be seen that the extruded arc grooves can extend fatigue life of the specimen. Different depths of the extruded arc grooves result in different residual stresses, which have different effects on fatigue life of the specimen. In order to explore the effect of the depth of the extruded arc grooves on fatigue life of specimens in detail, the finite element models of specimens with different depths of the extruded arc grooves are implemented. It should be noted that during the extrusion process, the specimen undergoes both elastic deformation and plastic deformation. Therefore, the actual extrusion depth is less than the given extrusion depth of the specimen. The relationship between the actual extrusion depth and the given extrusion depth is shown in Fig. 4.16.

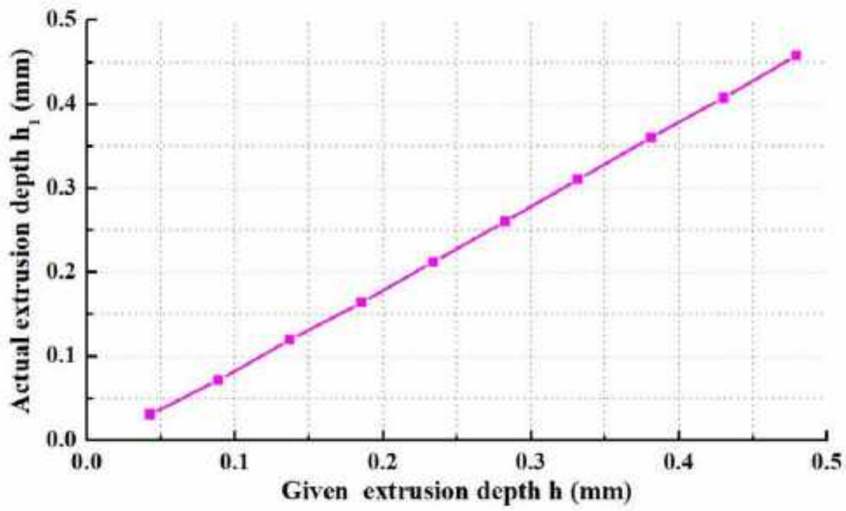

Fig. 4.16 The relationship between the actual extrusion depth and the given extrusion depth

During the extrusion process, the extrusion stress is generated on the specimen, and after the extrusion process (the extrusion punches are released), the residual stress remains on the specimen. The relationships between the maximum x-directional extrusion stress of the specimen during the extrusion process, the maximum x-directional residual stress of the specimen after the extrusion process and the given extrusion depth are shown in Fig. 4.17. The x-directional positive stress is the tensile stress, and the x-directional negative stress is the compressive stress.

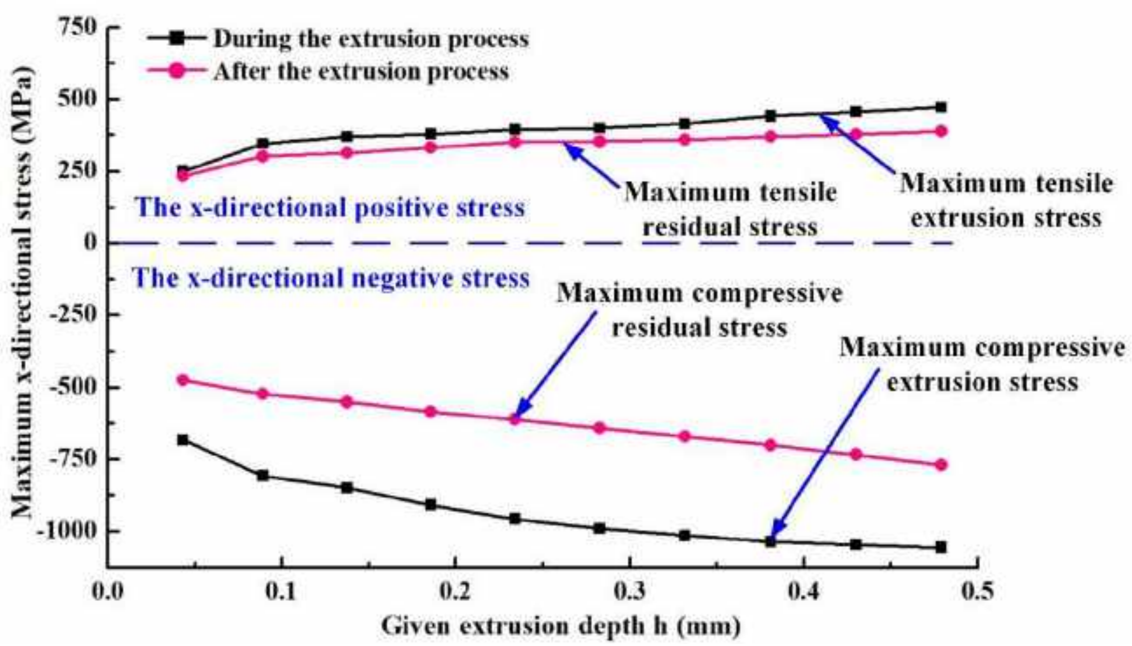

Fig. 4.17 The relationship between the maximum x-directional stress and the given extrusion depth (θ = 90°)

It can be seen from Fig. 4.17 that the maximum (tensile and compressive) extrusion stress and the maximum (tensile and compressive) residual stress increase with the increase of the given extrusion depth. After the extrusion process, the maximum compressive residual stress value is greater than the maximum tensile residual stress value on the specimen. The compressive residual stress can counteract part of the effect of the maximum load σ_{max}, so the characteristic stress generated on the specimen with the extruded arc grooves is reduced compared to the specimen without the extruded arc grooves. The variation of characteristic stress σ_c on the specimen with the given extrusion depth under the different maximum load σ_{max} is shown in Fig. 4.18.

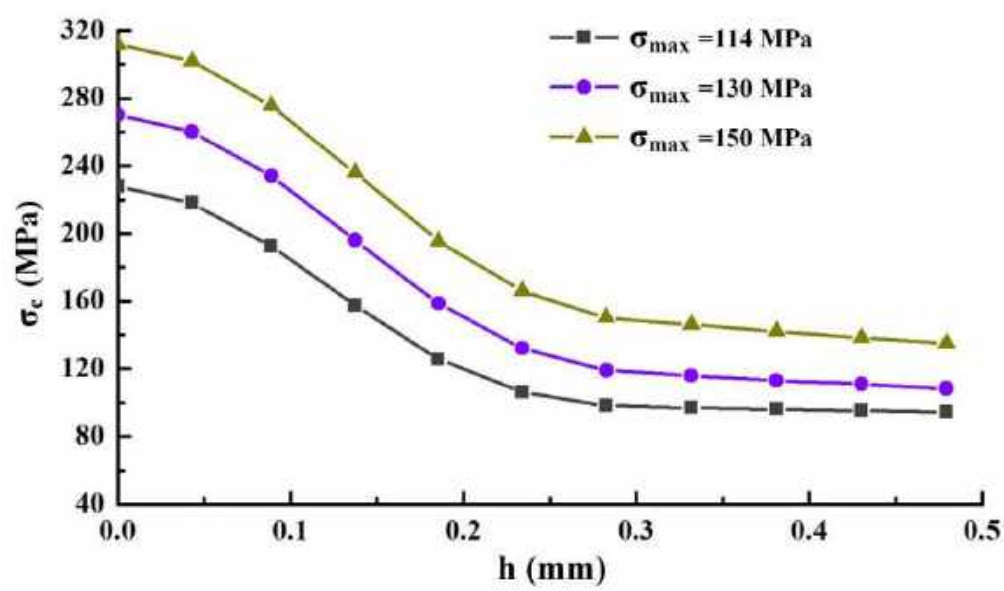

Fig. 4.18 The relationship between the characteristic stress and the given extrusion depth ($\theta = 90°$)

It can be seen from Fig. 4.18 that when the given extrusion depth is 0-0.3mm, the characteristic stress generated on the specimen rapidly decreases, and when the given extrusion depth is 0.3-0.5mm, the characteristic stress generated on the specimen decreases slowly. According to the results of the characteristic stress on the specimen with different depths of the extruded arc grooves, the predicted fatigue lives of the specimens can be gained by using the fitting function (4.5). The predicted fatigue lives of the specimens with different depths of the extrusion grooves are shown in Fig. 4.19.

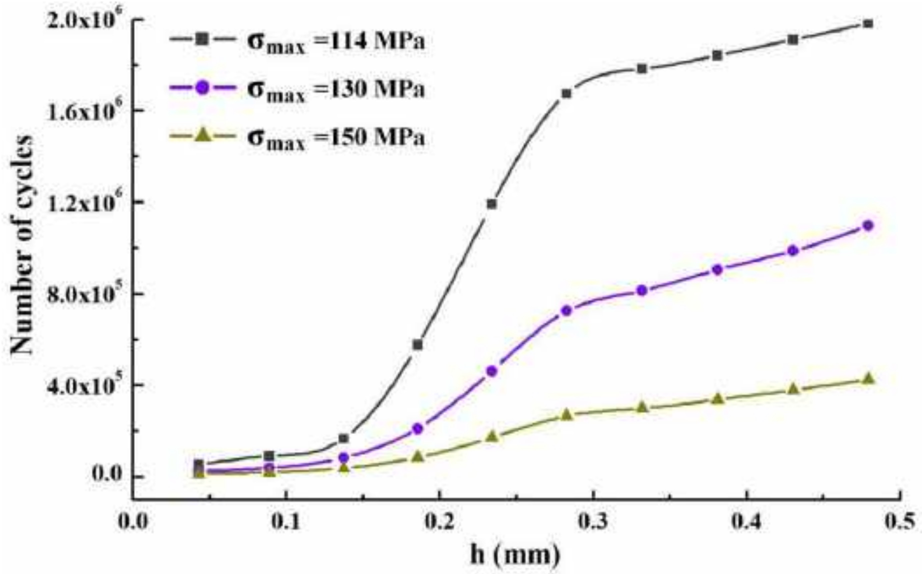

Fig. 4.19 The relationship between the fatigue life
and the given extrusion depth (θ = 90°)

It can be seen from Fig. 4.19 that the fatigue lives of the specimens are affected by the depths of the extrusion grooves (θ = 90°). When the depths are shallow (0-0.15 mm), their fatigue lives are extended slightly; when the depths are deep (0.15-0.3 mm), their fatigue lives are greatly extended; when the depths are too deep (>0.3mm), their fatigue lives are extended slowly, on the other hand, the excessively deep extrusion arc groove will lead to excessive residual stress on the wing panel, and even cause the wing plate to be damaged. Therefore, for the wing panel made of D16T with the thickness of 5 mm and the angle of the extrusion arc groove of 90°, the optimal depth of the extrusion arc groove is 0.3 mm and the lifetime can be extended by more than 2.3 times.

4.4.4 Optimization of the extrusion arc groove angle

From the experimental results of the specimens with the extruded arc grooves shown in Fig. 4.6, it is seen that the fatigue life of specimen can be extended by the extruded arc grooves. Different angles of the extruded arc grooves result in different residual stresses, which have different effects on the fatigue lives of the specimens. In order to explore the influence of the angle of the extrusion arc groove on the fatigue life of specimen in detail, a batch of specimens with the depth of 0.3 mm and different angles of the extruded arc grooves are established for finite element simulation. The simulation results are shown in Figs 4.20-4.22, which respectively present that the maximum x-directional stress， the maximum compressive residual stress and the characteristic stress of the specimen under different extrusion arc groove angles.

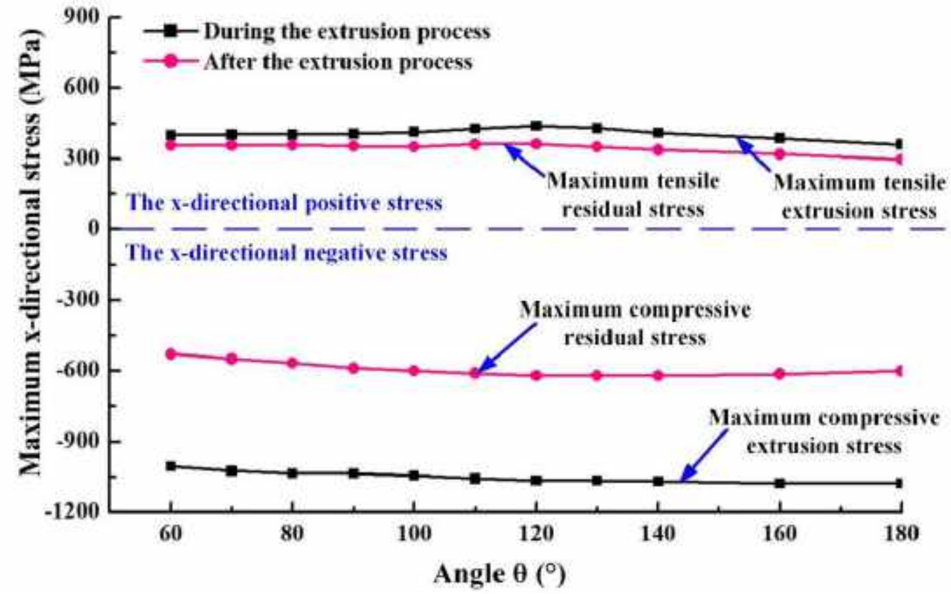

Fig. 4.20 The relationship between the fatigue life and the given extrusion depth (θ = 90°)

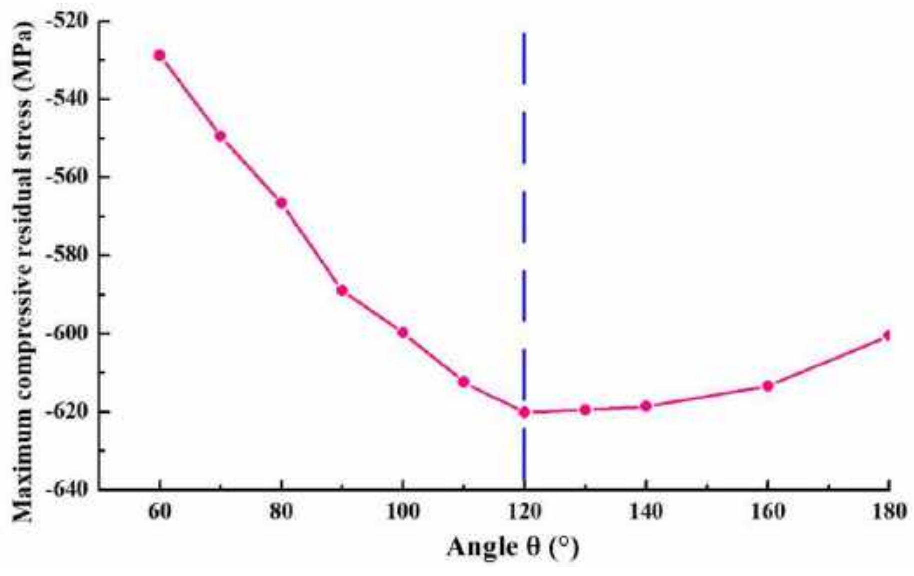

Fig. 4.21 The relationship between the maximum compressive residual stress and the angle (h=0.3mm)

As can be seen from Fig. 4.20 that after the extrusion process, the maximum compressive residual stress value is greater than the maximum tensile residual stress value on the specimen. The compressive residual stress can counteract the part of the effect of the maximum load σ_{max}, so the characteristic stress σ_c generated on the specimen with the extruded arc grooves is reduced compared to the specimen without the extruded arc grooves.

As can be seen from Figs 4.20 through 4.21 that as the angle θ increases, the maximum (tensile and compressive) compressive stress and the maximum (tensile and compressive) residual stress first increase and then decrease, and 120° is the turning point. This means that the effect of the extrusion arc groove is reduced when the angle of the extrusion arc groove is greater than 120°. Therefore, the maximum angle of the extrusion arc groove is 120°.

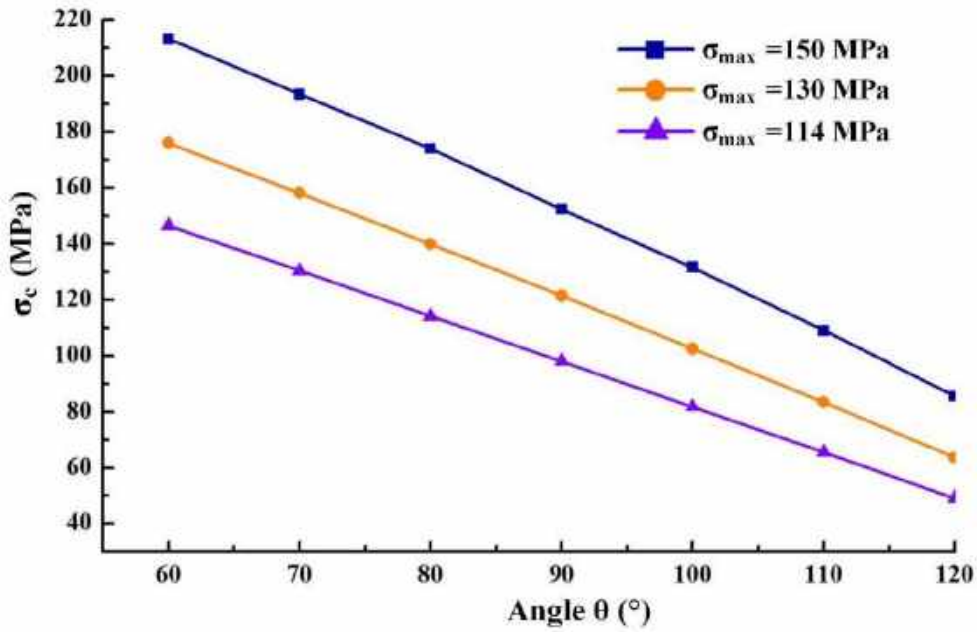

Fig. 4.22 The relationship between the characteristic stress and the angle (h=0.3 mm)

It can be seen from Fig. 4.22 that with the increase of the angle, the characteristic stress σ_c on the specimen gradually decreases, and under the same angle, the greater the maximum load σ_{max}, the greater the characteristic stress σ_c.

According to the characteristic stress σ_c on the specimen with different angles of the extruded arc grooves, the predicted fatigue lives of the specimens can be gained by using the fitting function (4.5), as shown in Fig. 4.23.

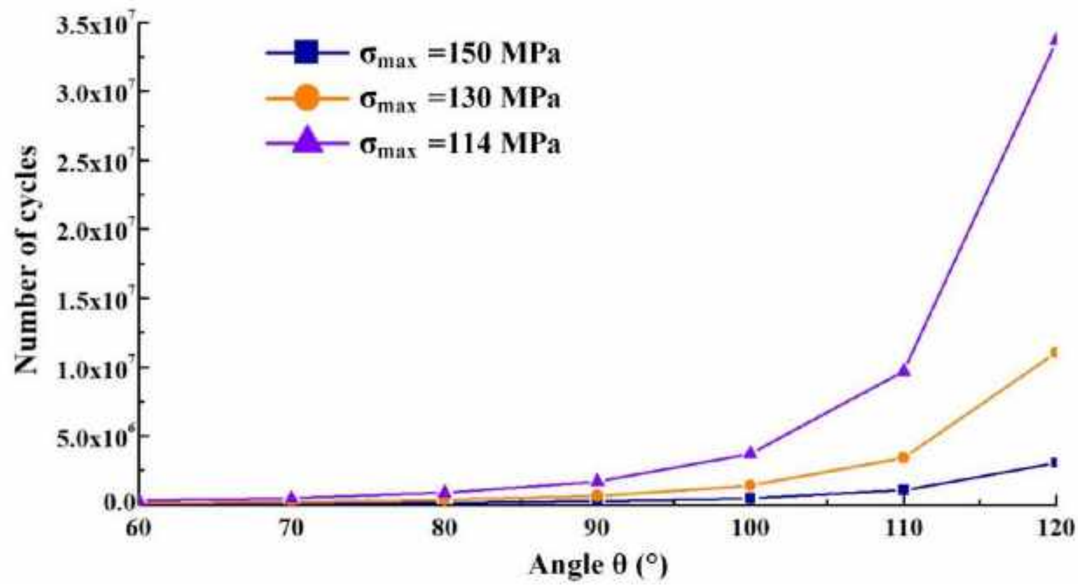

Fig. 4.23 The relationship between the predicted fatigue life and the angle (h=0.3mm)

It can be seen from Fig. 4.23 that when the angle of the extrusion arc groove is less than 120°, the fatigue life of the specimen is gradually extended with the increase of the angle. Therefore, for the wing panel made of D16T, with the thickness of 5 mm and the depth of the extrusion arc groove of 0.3 mm, the optimal angle of the extrusion arc groove is 120° and the lifetime can be extended by more than 2.34 times.

4.5 Conclusion of this chapter

1. For the wing panel with functional holes, the fatigue life can be extended by the extruded arc grooves, which is due to the residual stress is generated on the wing panel after extrusion process, that counteracts the part of the effect of the maximum load σ_{max}, so that the characteristic stress is reduced and the fatigue life is extended.

2. The fatigue life of the wing panel with functional holes is affected by the depth of the extruded arc grooves. When the depth is 0-0.15 mm, the fatigue life is

extended slightly; when the depth is 0.15-0.3 mm, the fatigue life is greatly extended; when the depth is more than 0.3 mm, the fatigue life is extended slowly. For the wing panel made of D16T with the thickness of 5 mm and the angle of the extrusion arc groove of 90°, the optimal depth of the extrusion arc groove is 0.3 mm and the lifetime can be extended by more than 2.3 times.

3. The fatigue life of the wing panel with functional holes is affected by the angle of the extruded arc grooves. The fatigue life is extended with the increase of the angle until the angle reaches the optimal angle 120°. For the wing panel made of D16T, with the thickness of 5 mm and the depth of the extrusion arc groove of 0.3 mm, the optimal angle of the extrusion arc groove is 120° and the lifetime can be extended by more than 2.34 times.

This chapter completes the dissertation work task: work out new methods of the extruded arc groove to increasing the fatigue life of the fitting joint between the center wing section and the outer wing section of a regional aircraft. The influence of the depth and angle of the extruded arc groove on the fatigue life of the wing panel is studied in detail by experimental and new finite element simulation methods. The results show that the extruded arc groove can improve the fatigue life of the wing panel and the optimal extruded arc groove depth and angle are obtained. This conclusion has been applied in engineering practice in the design process of Chinese aircraft

CHAPTER 5

METHOD FOR EXTENDING FATIGUE LIFE OF DOUBLE SHEAR JOINT IN WING

According to the method proposed in Chapter 4 to extend fatigue life of the wing panel with holes by the extruded arc grooves, this chapter proposes a new method to extrude annular grooves to extend fatigue life of the double shear joints of the wing panel. There are two main purposes for setting the extruded annular groove. One is to extend fatigue life of the double shear joint of the wing panel by retaining the residual stress after extruding the annular groove. The other is to reduce the effect of fretting corrosion on the wing panel by adding anti-fretting paste in the annular groove to further extend fatigue life of the double shear joint of the wing panel. This chapter will conduct experimental verification and explanation from three parts: the effect of extruded annular grooves on the fatigue life of wing panel with holes, the effect of extruded annular grooves on the fatigue life of double shear joints of wing panels, and the effect of extruded annular grooves and anti-fretting paste on the fatigue life of double shear joints of wing panels.

5.1 The effect of extruded annular groove on the fatigue life of wing panel with functional holes

In order to study the effect of extruded annular groove on the fatigue life of wing panel with holes, the following experimental verification is carried out.

5.1.1 Test specimen

This chapter draws on the research methods of Kiva, Sun and others to propose a method of the extruded annular groove to improve the fatigue life of panels with functional holes. This method is to make an annular groove on the edge of the hole in the component through cold extrusion, so that plastic deformation occurs around the hole and thereby generates residual stress. This residual stress can offset the tension of the component. Or the stress damage generated during pressing can achieve the purpose of extending the life of the component. In order to verify the correctness of the method of the extruded annular groove improving the life of wing panels with functional holes, the following test was carried out for verification.

The specific parameters of the test specimen are shown in Fig. 5.1, and the actual object is shown in Fig. 5.2.

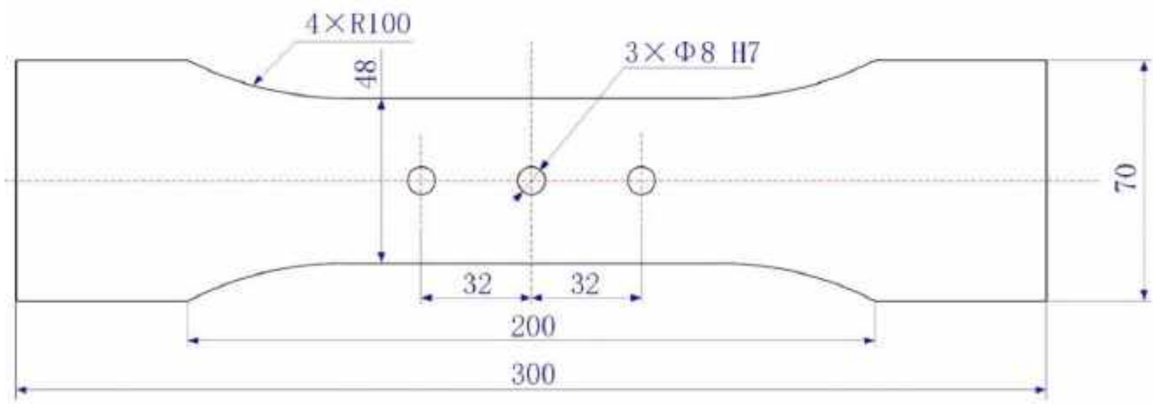

Fig. 5.1 Parameters of specimen

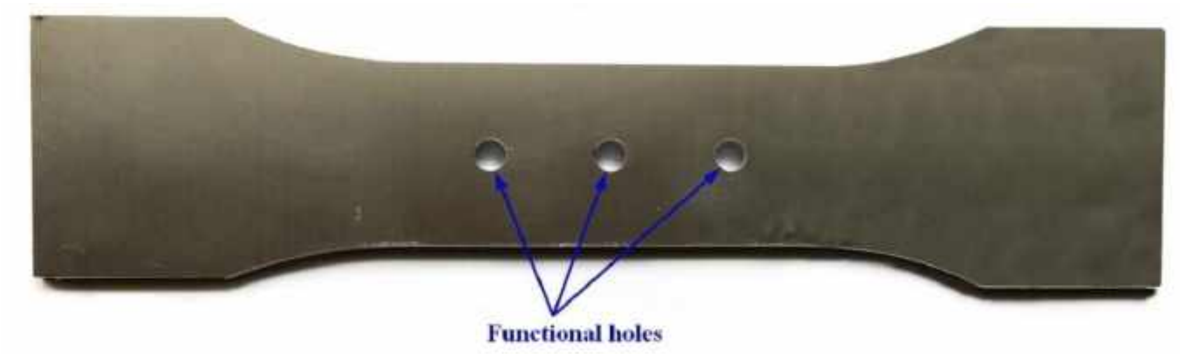

Fig. 5.2 Specimen

The three holes in the middle of the specimen are simulated functional holes. The total length of the specimen is 300 mm, the center width is 48 mm, and the thickness is 5 mm. The functional hole is located on the central axis of the specimen, with a hole diameter of 8 mm. The center distance between holes is 32 mm, and the tolerance level of functional holes is H7.

The test specimen is made of 6061 aluminum alloy plate. The main performance parameters of 6061-T6 aluminum alloy are shown in Table 5.1. 6061 aluminum alloy is one of the most popular duralumin alloys in the shipbuilding, aviation and aerospace industries. It has good formability, weldability and machinability, and is widely used in the production of aircraft skins, fuselage frames, beams, rotors, propellers, fuel tanks, wall panels and landing gear struts, as well as rocket forging rings, spacecraft Spaceship siding, etc.

Table 5.1 The mechanical properties of materials 6061-T6

Materials	Density	Young's Modulus	Ultimate Strength	Yield Strength	Poisson's Ratio
6061-T6	2700(kg/m^3)	71 (GPa)	310(MPa)	276(MPa)	0.33

5.1.2 The extruded annular groove

In order to obtain annular grooves on the specimen, the extrusion die was designed. The extrusion die is made of 30CrMnSiA. The mechanical properties of 30CrMnSiA are shown in Table 5.2.

Table 5.2 The mechanical properties of materials 30CrMnSiA

Materials	Density	Young's Modulus	Ultimate Strength	Yield Strength	Poisson's Ratio
30CrMnSiA	7900(kg/m^3)	206(GPa)	1080(MPa)	835(MPa)	0.3

30CrMnSiA steel plate is medium carbon steel, with high strength and poor welding performance. After quenching and tempering, 30CrMnSiA steel has high strength, sufficient toughness and good hardenability, and can be used as grinding wheel shaft, gear and sprocket. 30CrMnSiA steel plate has excellent machinability, small deformation and good fatigue resistance. It is used for shafts, pistons and other parts, as well as various special wear-resistant parts of cars and airplanes.

The specimen extrusion equipment is the WANCE universal testing machine, which can output a maximum extrusion force of 1000kN. The specimen extrusion site is shown in Fig. 5.3.

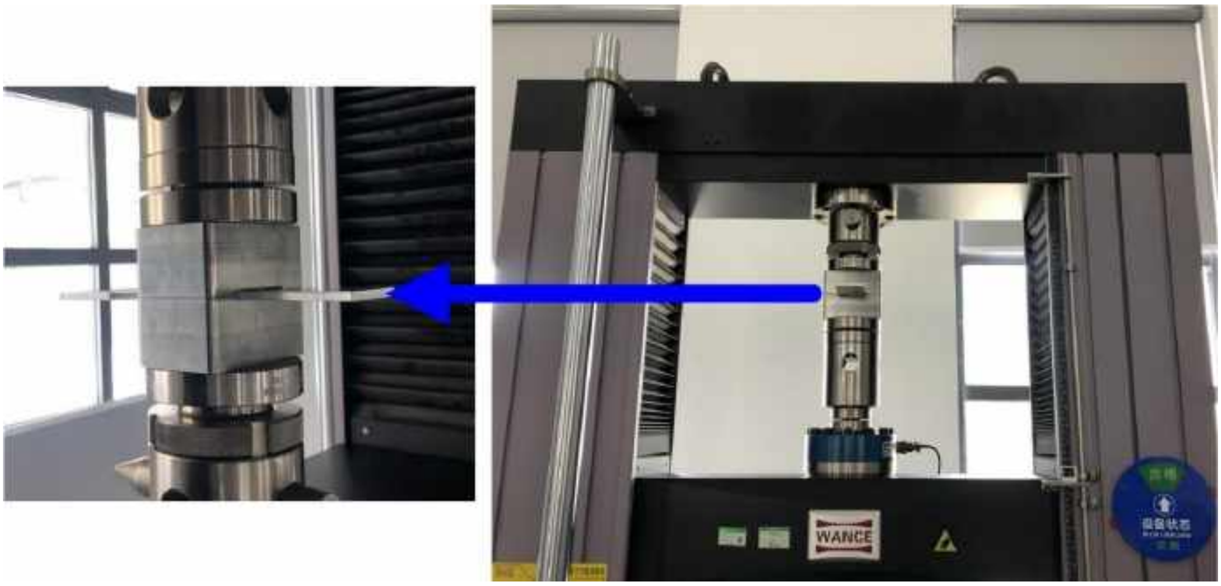

Fig. 5.3 WANCE universal testing machine

The extrusion die is divided into an upper extrusion die and a lower extrusion die. Actual product is shown in Fig. 5.4

Fig. 5.4 The cold extrusion die

. The two-dimensional drawing is shown in Fig. 5.5. The height of the annular punch of the upper extrusion die is 0.33 mm and the height of the annular punch of the lower extrusion die is 0.34 mm as measured by the depth gauge.

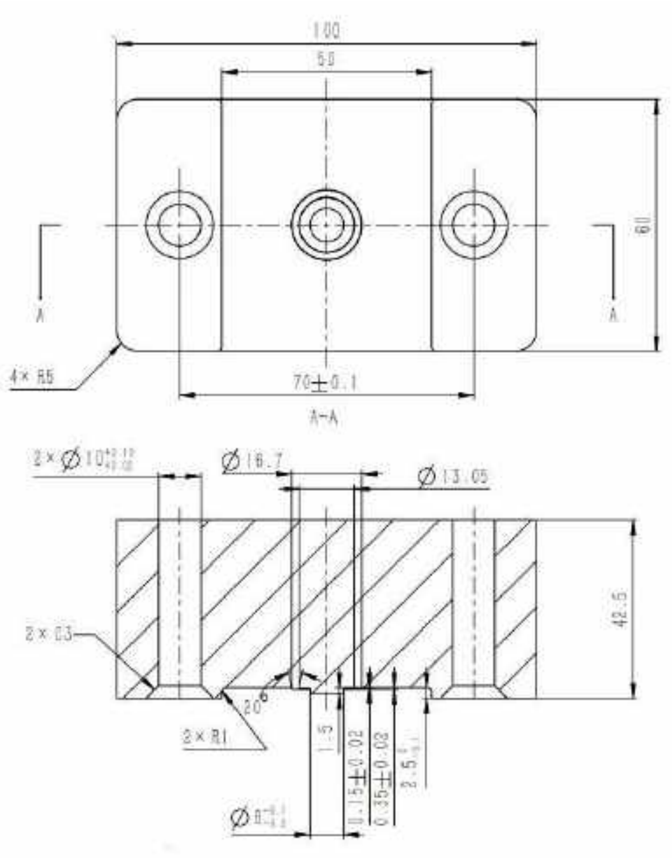

a) The upper extrusion die

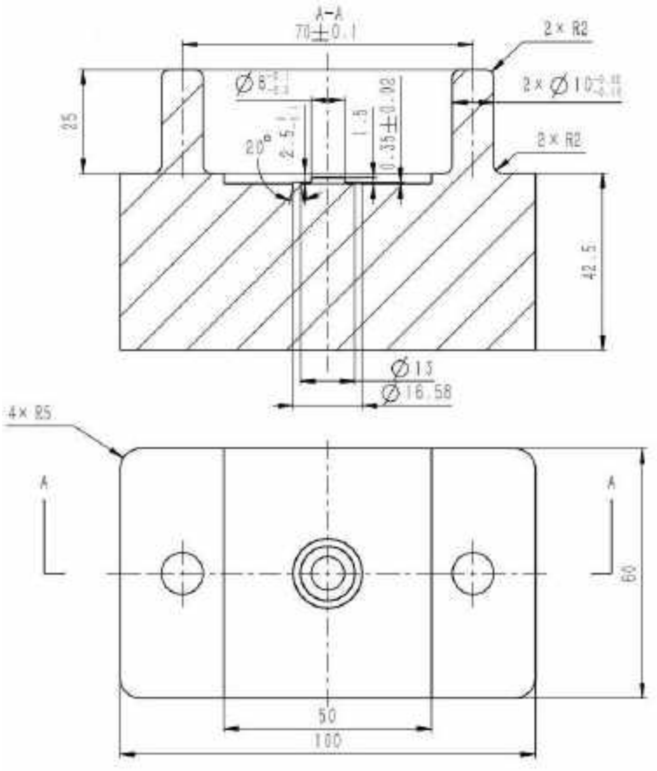

b) The lower extrusion die

Fig. 5.4 Two-dimensional dimensions of the extrusion die

The test steps for extruding annular grooves on the specimen are as follows:

1) Place the specimen in the groove between the upper extrusion die and the lower extrusion die, adjust any functional hole on the specimen to align with the positioning piles on the upper extrusion die and the lower extrusion die;

2) Place the extrusion die with the specimen installed in the center of the lower extrusion table, and adjust the upper extrusion table to contact the extrusion die;

3) Set the testing machine parameters: extrusion speed and extrusion force;

4) Click Start to extrude the specimen to obtain the extruded annular groove;

5) Remove the specimen from the extrusion die;

6) Repeat steps 1–5 to obtain the annular grooves corresponding to the other two functional holes on the specimen.

The upper and lower dies are squeezed by a universal testing machine to obtain a specimen with an annular groove in the extrusion test, as shown in Fig. 5.6.

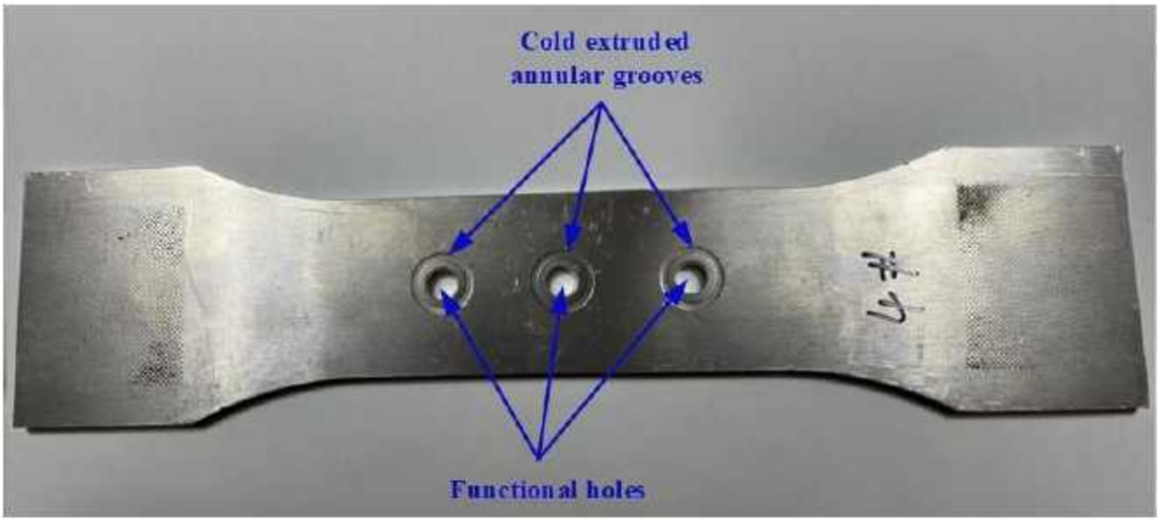

Fig. 5.6 Specimen with annular grooves

The specimens are extruded with extrusion forces of 0, 20 kN, 40 kN, 60 kN, 80 kN and 100 kN respectively. Use a depth gauge to measure the depth of the annular groove formed by extrusion of the specimen, as shown in Fig. 5.7. Measure three different places and average the results to obtain the results in Table 5.3 below.

Fig. 5.7 Measuring the depth of the annular groove

Table 5.3 Annular groove depth of specimen

Working conditions	Specimen number	Extrusion speed (mm/min)	Squeeze force (kN)	Extrusion depth (mm)	Average extrusion depth (mm)
1	I-0-1, I-0-2, I-0-3, II-0-1, II-0-2, II-0-3	0	0	0	0
2	I-20-1, I-20-2, I-20-3 II-20-1, II-20-2, II-20-3	1	20	0.06/0.07/0.05	0.06
3	I-40-1, I-40-2, I-40-3 II-40-1, II-40-2, II-40-3	1	40	0.13/0.14/0.13	0.133
4	I-60-1, I-60-2, I-60-3 II-60-1, II-60-2, II-60-3	1	60	0.26/0.25/0.27	0.26
5	I-80-1, I-80-2, I-80-3 II-80-1, II-80-2, II-80-3	1	80	0.31/0.32/0.33	0.32
6	I-100-1, I-100-2, I-100-3 II-100-1, II-100-2, II-100-3	1	100	0.33/0.34/0.33	0.333

It can be seen from the results of the extrusion depth of the specimen that when the extrusion forces are 0, 20 kN, 40 kN, and 60 kN, the extrusion depth increases linearly with the extrusion force. When the extrusion force is 80 kN or 100 kN, the extrusion depth of the specimen is close to the maximum height of the extrusion punch of the cold extrusion die, and the extrusion depth remains basically unchanged. However, the extrusion depth is slightly different due to the influence of extrusion force.

5.1.3 Fatigue test

During the test process, the WANCE-100 fatigue machine is used as the test equipment as shown in Fig. 5.8. The fatigue machine can be used to mechanically test metal samples, individual parts, through compression, tension, longitudinal and transverse bending under static and cyclic loading. During the test, different load forces are loaded on the specimen (the load on the wing component can be determined according to the simplified segmentation method [6-7]) for fatigue testing, the working frequency is 20 Hz, and 3 specimens are tested under each working condition.

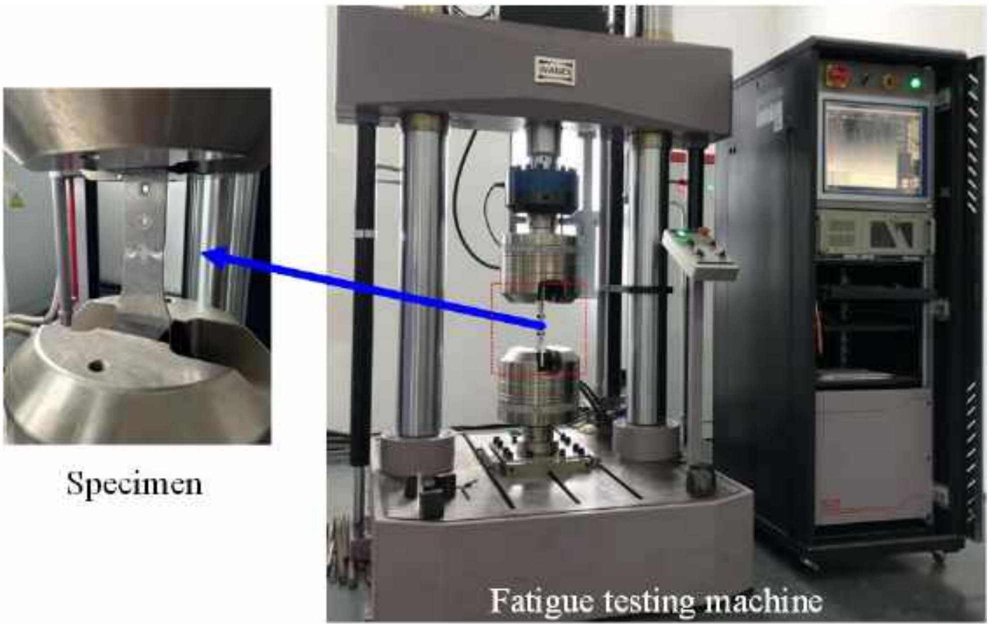

Fig. 5.8 WANCE-100 fatigue testing machine

Under different working conditions, the fatigue life results of the specimens are shown in Table 5.4, and the specimens after fatigue fracture are shown in Fig. 5.9. The loading force is determined based on the ultimate tensile force of the specimen without the annular extruded grooves. Two specimens were used for tensile testing and the ultimate tensile forces were 43.12 kN and 43.07 kN respectively, so the average ultimate tensile force was 43.095 kN. The loading force was 25.85 kN according to 60 % of the ultimate tensile force, and 34.48 kN according to 80 % of the ultimate tensile force.

Table 5.4 Fatigue life of specimens

Working conditions	Specimen number	Working frequency, HZ	Loading force, kN	Fatigue life	Average fatigue life
I-1	I-0-1, I-0-2, I-0-3	20	25.85	5490/7408/21526	11474.7
I-2	I-20-1, I-20-2, I-20-3	20	25.85	19378/32771/27026	26391.7
I-3	I-40-1, I-40-2, I-40-3	20	25.85	137795/105450/70923	104722.7
I-4	I-60-1, I-60-2, I-60-3	20	25.85	379797/337384/415450	377543.7
I-5	I-80-1, I-80-2, I-80-3	20	25.85	189778/178839/144559	171058.7
I-6	I-100-1, I-100-2, I-100-3	20	25.85	176103/150050/115800	147317.7
II-1	II-0-1, II-0-2, II-0-3	20	34.48	6086/5233/7800	6373
II-2	II-20-1, II-20-2, II-20-3	20	34.48	10545/11200/12020	11255
II-3	II-40-1, II-40-2, II-40-3	20	34.48	11912/15506/13033	13483.7
II-4	II-60-1, II-60-2, II-60-3	20	34.48	12388/17578/14996	14987.3
II-5	II-80-1, II-80-2, II-80-3	20	34.48	7408/12300/11053	8033.7
II-6	II-100-1, II-100-2, II -100-3	20	34.48	7063/10360/9043	8822

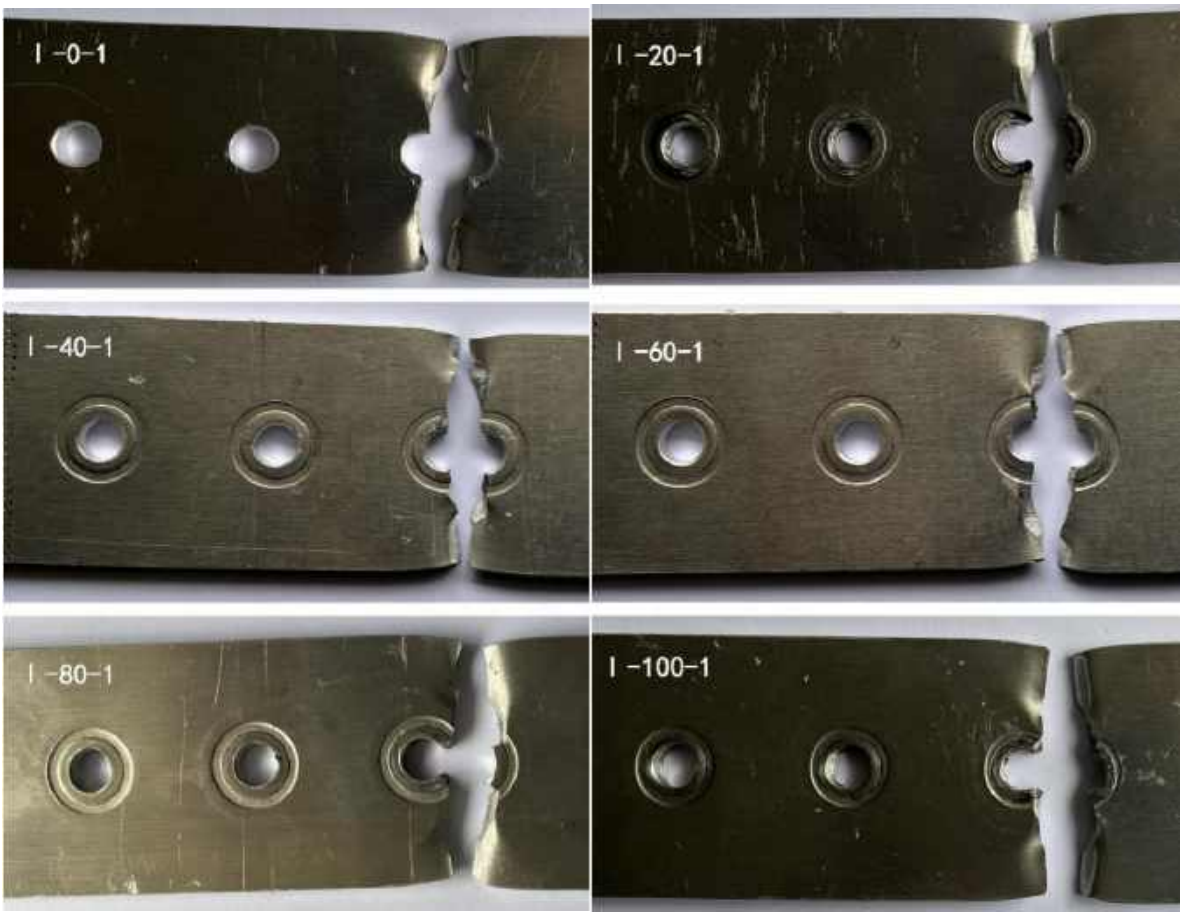

Fig. 5.9 Specimens after fatigue fracture

Fig. 5.9 shows some specimens that broke after fatigue testing. It can be seen that the specimens all broke from the hole on the right side of the specimen, and the shape of the fracture notch of each specimen is different. This is because the specimens themselves have differences in manufacturing processes and materials. In order to eliminate the influence of inconsistency, the average of the fatigue life of 3 specimens under each working condition is taken as the result for analysis. Through data processing, it can be obtained that the relationship between the extrusion depth and the fatigue life of the specimen under a load of 25.85 kN as shown in Fig. 5.10.

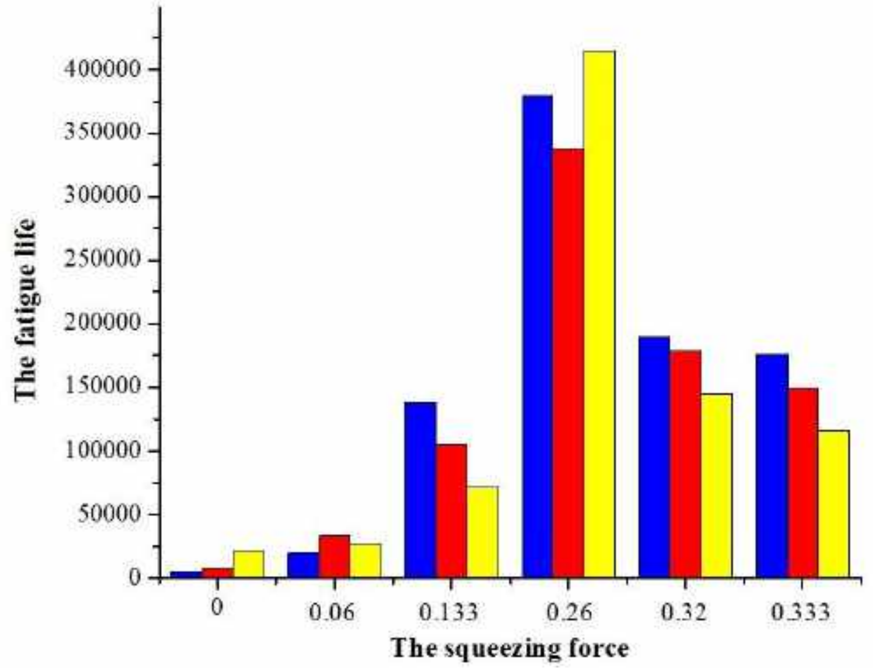

Fig. 5.10 The relationship between extrusion depth and specimen fatigue life under loading 25.85 kN

The relationship between the extrusion depth and the fatigue life of the specimen under a load of 34.48 kN is shown in Fig. 5.11.

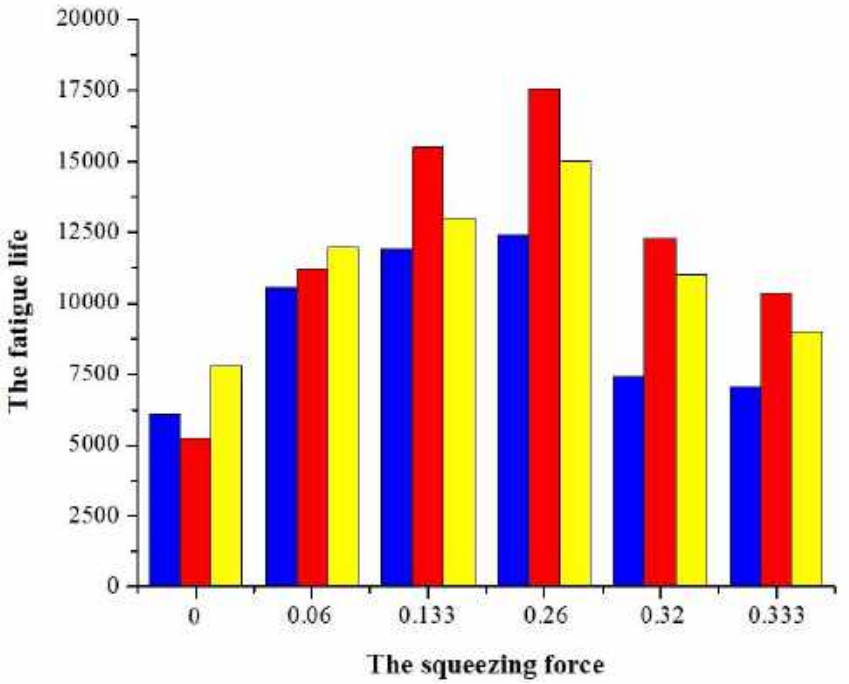

Fig. 5.11 The relationship between extrusion depth and specimen fatigue life under loading 34.48 kN

It can be seen from the results in Figs 5.10 and 5.11 that there are differences in the fatigue life of different specimens under the same working conditions. This is caused by factors such as differences in the material of the test piece itself, differences in the processing technology of the test piece, and differences in the trial extrusion process, which is a normal phenomenon. Therefore, the average fatigue life of three specimens is taken to eliminate the influence of these differences.

Under different working conditions, the average fatigue life of the specimen is affected by the extrusion depth of the annular groove. The fatigue life of the specimen changes in an inverted "V" shape as the depth of the cold extruded annular groove increases. When the groove depth is 0.26 mm, the fatigue life of the aircraft wing panel with functional holes is the longest, which can be increased by 2.35~32.9 times.

5.1.4 Results and discussion

1) 6061 aluminum alloy is a widely used aviation material. Fatigue tests on specimens made of 6061 aluminum alloy can well reflect the mechanical properties of aircraft wing panels.

2) For aircraft wing panels with functional holes, the fatigue life of the wing panels can be improved by the extruded annular grooves around the functional holes.

3) The fatigue life of aircraft wing panels with functional holes is affected by the depth of the extruded annular groove. The fatigue life of the wing panel changes in an inverted "V" shape as the depth of the cold extruded annular groove increases. When the groove depth is 0.26 mm, the fatigue life of the aircraft wing panel with functional holes is the longest, which can be increased by 2.35~32.9 times.

5.2 The effect of extruded annular groove on the fatigue life of double shear joint in wing

In order to study the effect of extruded annular groove on the fatigue life of double shear joint in wing, the following experimental verification was carried out.

5.2.1 Test specimen

The comparison specimen is a double shear joint specimen without the extruded annular groove, which consists of two wing panels without the extruded annular groove, one wing wall panel without an extruded annular groove, and three M8 bolts, as shown in Fig. 5.12.

Fig. 5.12 Components of double shear joint specimen without extruded annular groove

The tolerance level of the functional hole on the specimen is H7. The bolt is an 8.8-grade M8 bolt, and the maximum tightening torque of the coarse-threaded metric bolt is 28.8 Nm. During the specimen assembly process, the specimen is tightened by a torque wrench, as shown in Fig. 13. The assembly process is to stack three plates and tighten them by inserting three bolts into the holes.The assembled specimen is shown in Fig. 5.14, including specimens III-1, III-2, and III-3.

Fig. 5.13 Torque wrenches for test piece installation

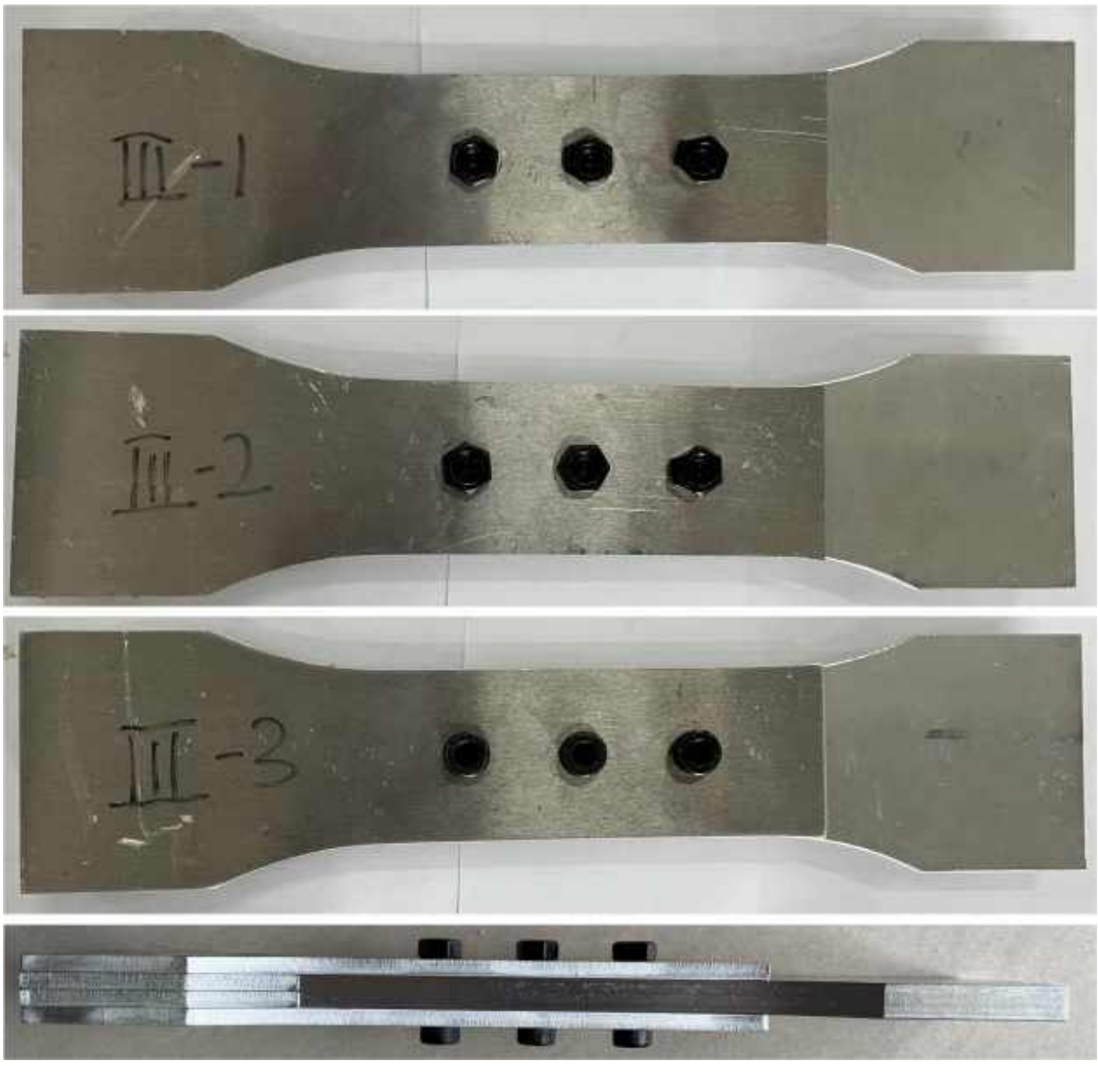

Fig. 5.14 The double shear joint specimen without the extruded annular groove

The test specimen is a double shear joint specimen with the extruded annular groove. The specimen consists of two wing panels with the extruded annular grooves, one wing wall panel with the extruded annular grooves, and three M8 bolts, as shown in Fig. 5.15. According to the conclusion of Chapter 4, the maximum extended fatigue life can be obtained when the extrusion force is 60 kN. Therefore, the extrusion force of the double shear joint specimen with the extruded annular groove is set to 60 kN, and the extrusion depth is about 0.26 mm. The production process of the extruded annular groove is shown in Section 5.1.2. The assembly process is as in Section 5.2.1, and the assembled specimen is shown in Fig. 5.16, including specimens IV-1, IV-2, and IV-3.

Fig. 5.15 Components of double shear joint specimen with the extruded annular grooves

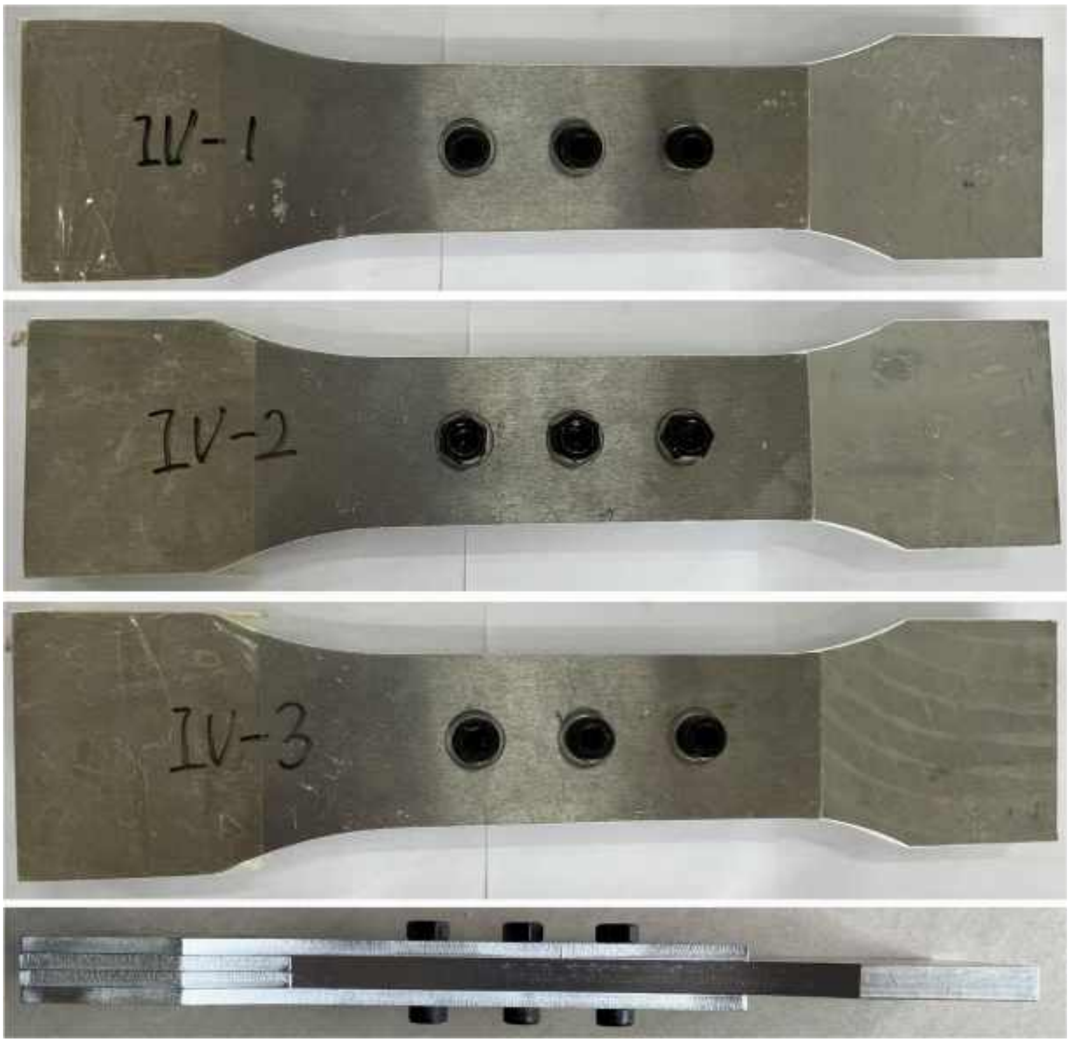

Fig. 5.16 The double shear joint specimen with the extruded annular grooves

5.2.2 Fatigue test

Fatigue test methods and test equipment are described in Section 5.1.3. Under different working conditions, the fatigue life results of the specimens are shown in Table 5.5. The loading force is determined based on the ultimate tensile force of the double shear joint specimen without the extruded annular grooves. Two specimens were used for tensile testing and the ultimate tensile forces were 94.16 kN and 93.93 kN respectively, so the average ultimate tensile force was 94.05 kN. The loading force was 56.43 kN according to 60 % of the ultimate tensile force. The double shear joint specimen without the extruded annular groove after fatigue fracture is shown in Fig. 5.17. The double shear joint specimen with the extruded annular groove after fatigue fracture is shown in Fig. 5.18.

Table 5.5 Fatigue life of specimens

Working conditions	Specimen number	Working frequency, HZ	Loading force, kN	Fatigue life	Average fatigue life
III-1	III-60-1	20	56.43	13542	17646
III-1	III-60-2	20	56.43	18042	
III-1	III-60-3	20	56.43	21355	
IV-1	IV-60-1	20	56.43	38428	40305
IV-1	IV-60-2	20	56.43	40456	
IV-1	IV-60-3	20	56.43	42332	

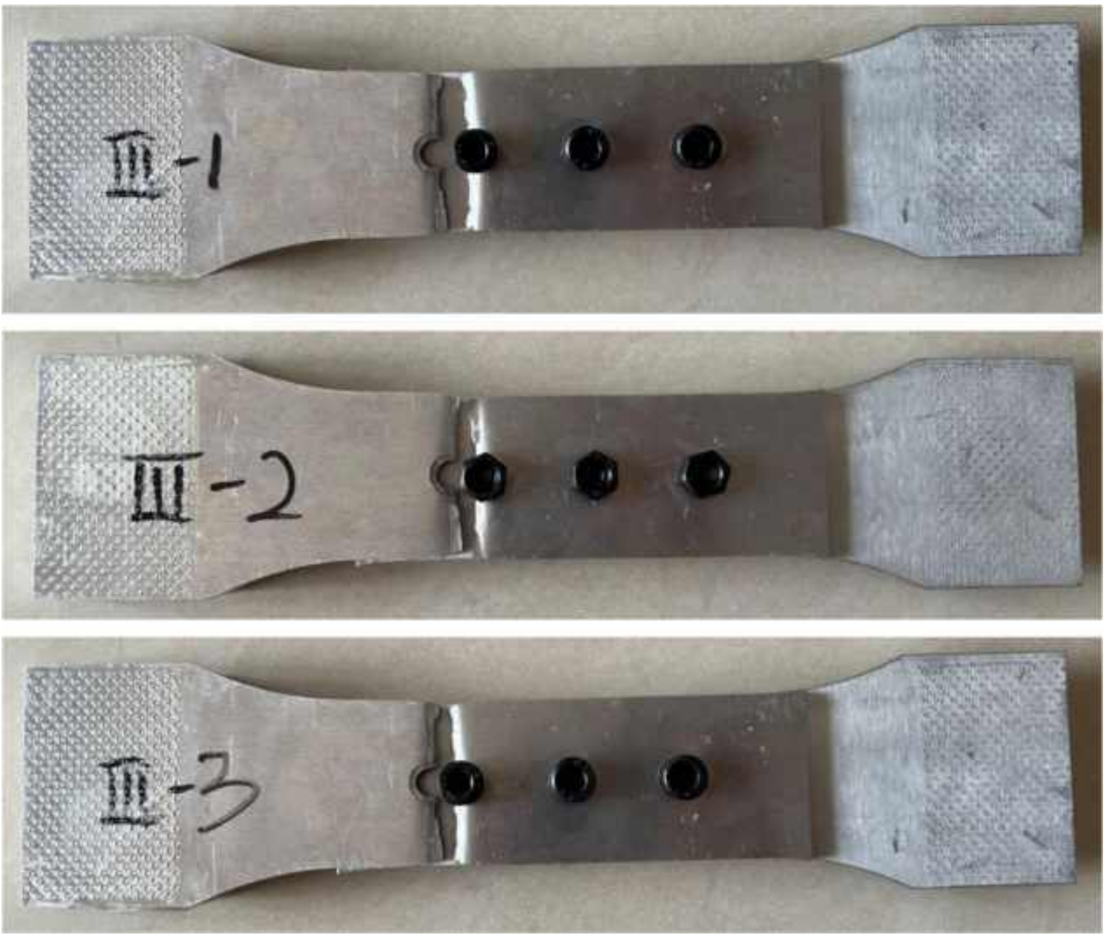

Fig. 5.17 The double shear joint specimen without the extruded annular groove after fatigue fracture

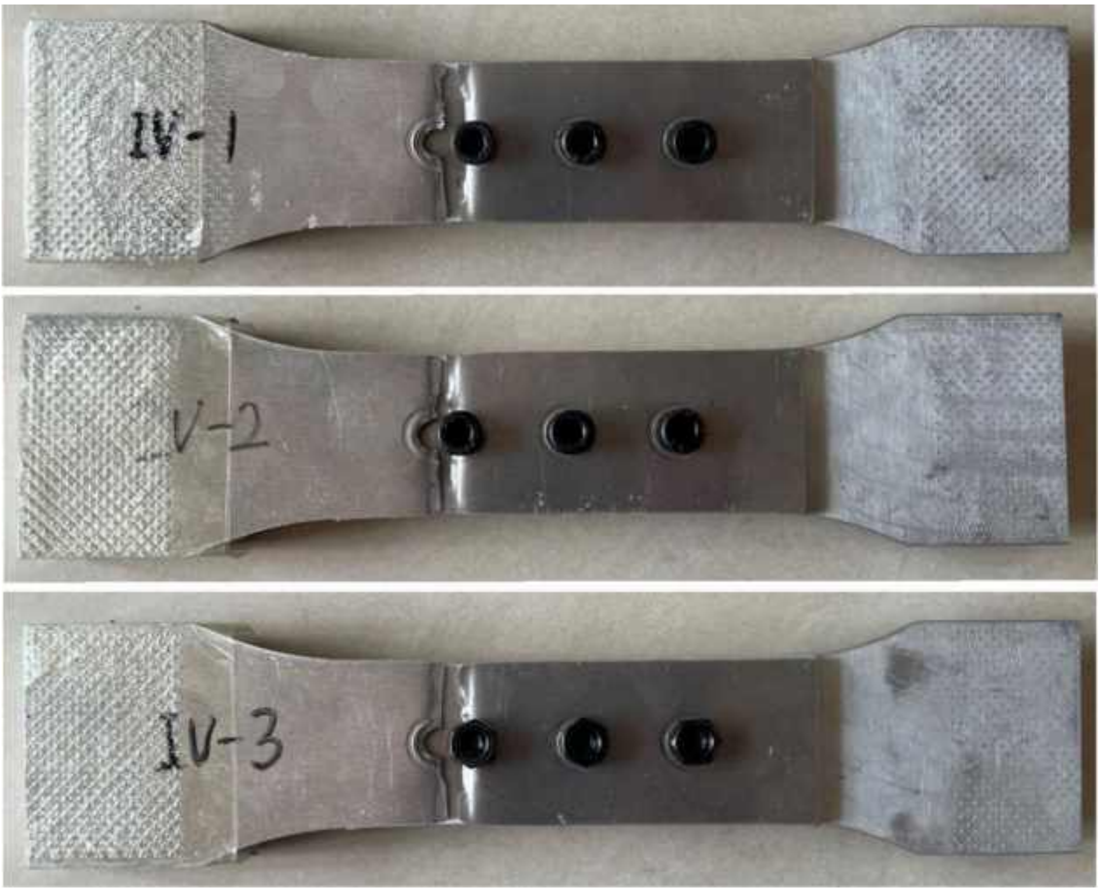

Fig. 5.18 The double shear joint specimen with the extruded annular groove after fatigue fracture

Under the same working conditions, the fatigue life of different specimens is different. This is due to the differences in the material of the specimens themselves, the processing technology of the specimens, the test extrusion process, etc., which is a normal phenomenon. Therefore, the average fatigue life of the three specimens is taken to eliminate the influence of these differences. Through data processing, the comparison results of III-1, III-2, III-3 and IV-1, IV-2, IV-3 in Fig. 5.19 are obtained. The fatigue life of the double shear joint with an extruded annular groove is about 2.28 times that of the double shear joint without an extruded annular groove.

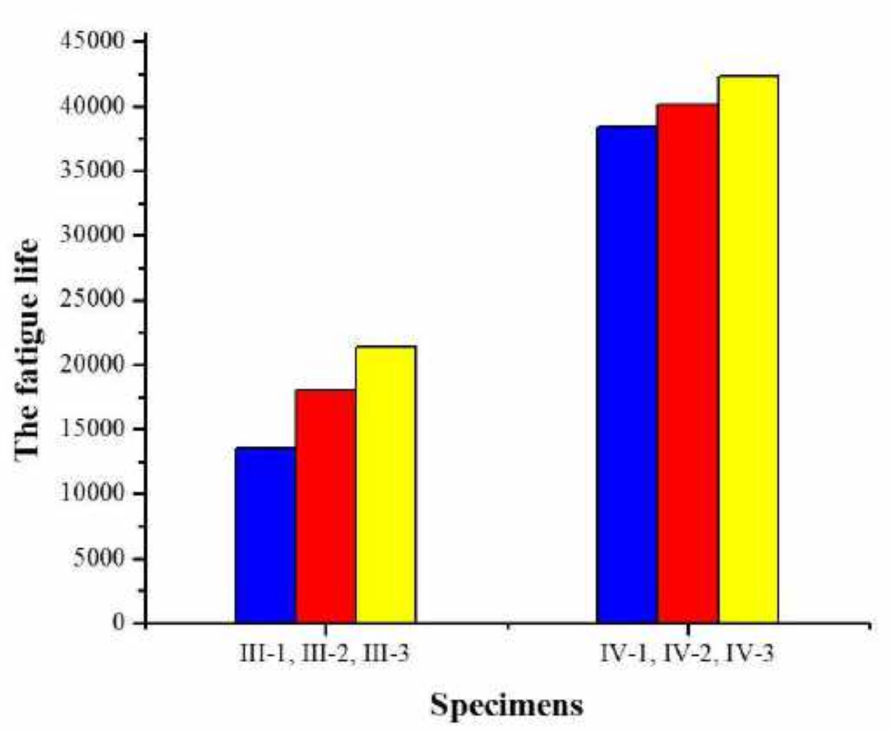

Fig. 5.19 Comparison of test results of specimens III-1, III-2, III-3 and IV-1, IV-2, IV-3

5.2.3 Results and discussion

1) Extruded annular grooves can improve the fatigue life of double shear joints.

2) The fatigue life of double shear joints with extruded annular grooves is about 2.28 times that of double shear joints without extruded annular grooves.

5.3 The effect of extruding annular grooves and anti-fretting paste on the fatigue life of double shear joint

In order to study the effect of extruding annular grooves and anti-fretting corrosion glue on the fatigue life of double shear joint of wing panels, the following experimental verification is carried out.

5.3.1 Test specimen

The test specimen is a double shear joint specimen with an extruded annular groove and the extrusion groove is coated with anti-fretting paste. The specimen consists of two wing panels with extruded annular grooves, one wing wall panel with extruded annular grooves, and three M8 bolts. The anti-fretting paste is coated on the butt surface of the wing panel and the wing wall panel, as shown in Fig. 5.20. The production process of the extruded annular groove is shown in Chapter 5.1.2. According to the conclusion of Chapter 4, the maximum extended fatigue life can be obtained when the extrusion force is 60 kN. Therefore, the extrusion force of the double shear joint specimen with an extruded annular groove is set to 60 kN, and the extrusion depth is about 0.26 mm. The assembly process is as in Section 5.2.1, the butt surfaces of the two plates are coated with anti-fretting paste. The anti-fretting paste is NTN Anti-fretting paste. The assembled specimen is shown in Fig. 5.21, including specimens Anti-fretting-1, Anti-fretting-2, and Anti-fretting-3.

Fig. 5.20 Components of double shear joint specimen with the extruded annular grooves and anti-fretting paste

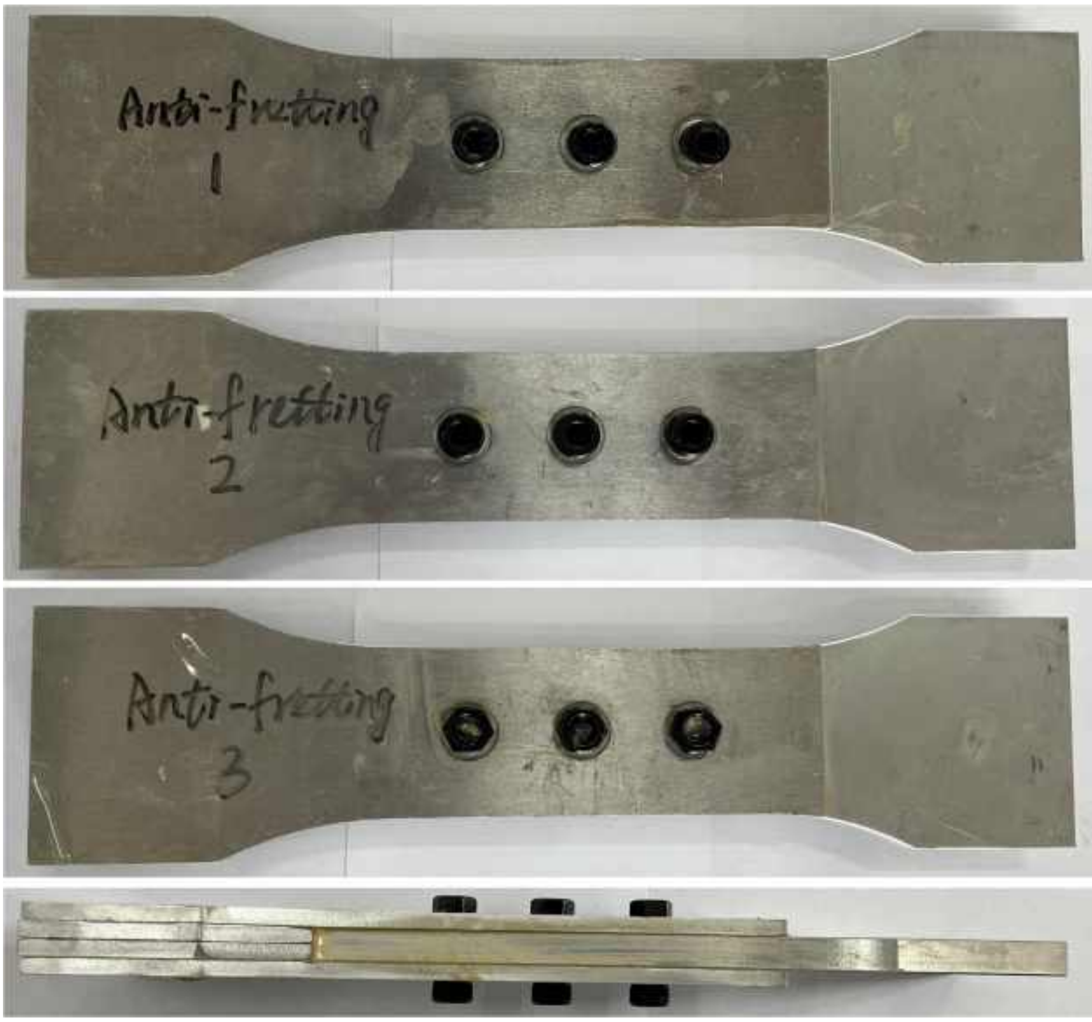

Fig. 5.21 The double shear joint specimen with the extruded annular grooves and anti-fretting paste

5.3.2 Fatigue test

Fatigue test methods and test equipment are described in Section 5.1.3. Under different working conditions, the fatigue life results of the specimens are shown in Table 5.6. The loading force is determined based on the ultimate tensile force of the double shear joint specimen without the extruded annular grooves. Two specimens were used for tensile testing and the ultimate tensile forces were 94.16 kN and 93.93 kN respectively, so the average ultimate tensile force was 94.05 kN. The loading force was 56.43 kN according to 60 % of the ultimate tensile force. The specimens of Anti-fretting-1, Anti-fretting-2, and Anti-fretting-3 after fatigue fracture are shown in Fig. 5.22.

Table 5.6 Fatigue life of specimens

Working conditions	Specimen number	Working frequency, HZ	Loading force, kN	Fatigue life	Average fatigue life
V-1 (Anti-fretting-1)	V-60-1	20	56.43	47256	51578
V-1 (Anti-fretting-2)	V-60-2	20	56.43	51620	
V-1 (Anti-fretting-3)	V-60-3	20	56.43	55860	

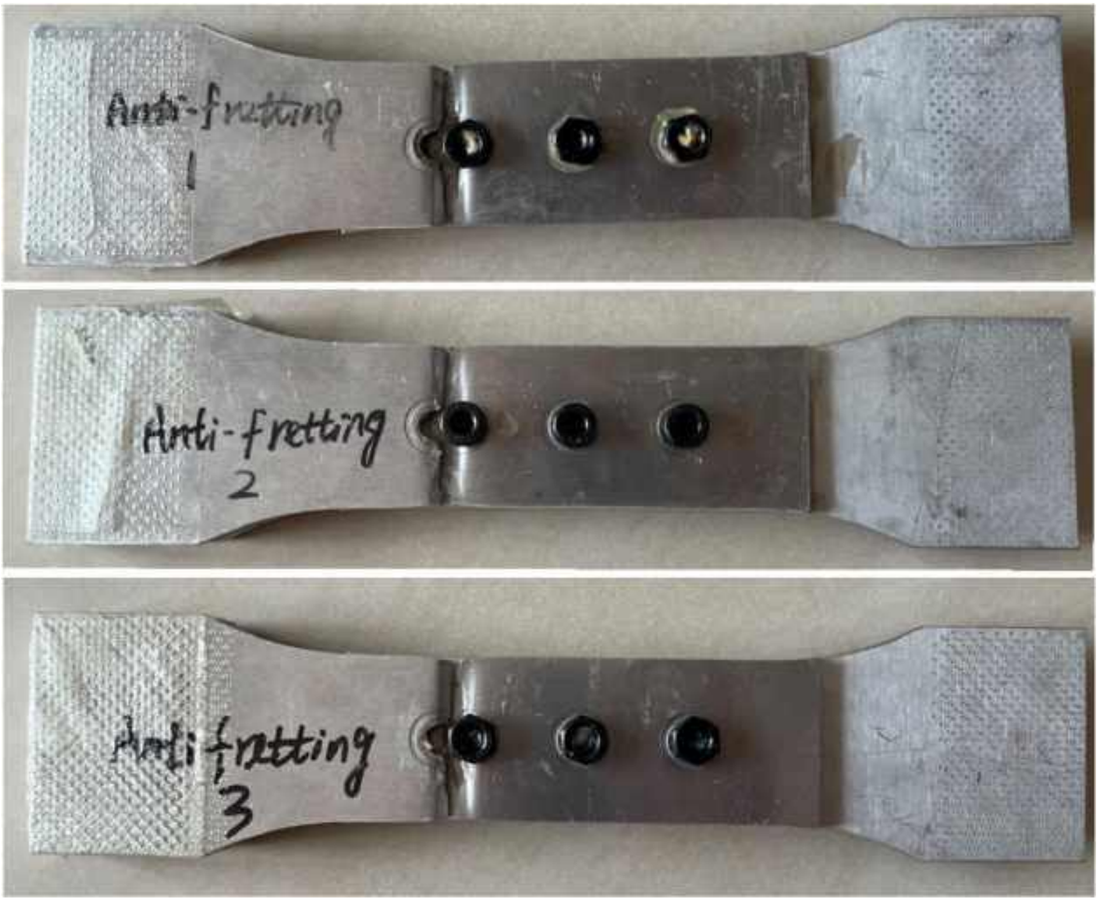

Fig. 5.22 The double shear joint specimen with the extruded annular grooves and anti-fretting paste after fatigue fracture

Under the same working conditions, the fatigue life of different specimens is different. This is due to the differences in the material of the specimens themselves, the processing technology of the specimens, the test extrusion process, etc., which is a normal phenomenon. Therefore, the average fatigue life of the three specimens is taken to eliminate the influence of these differences. Through data processing, the comparison results of Anti-fretting-1, Anti-fretting-2, and Anti-fretting-3 in Fig. 5.23 are obtained. The fatigue life of the double shear joint with extruded annular groove and micro-dynamic glue is about 2.9 times the fatigue life of the double shear joint without extruded annular groove.

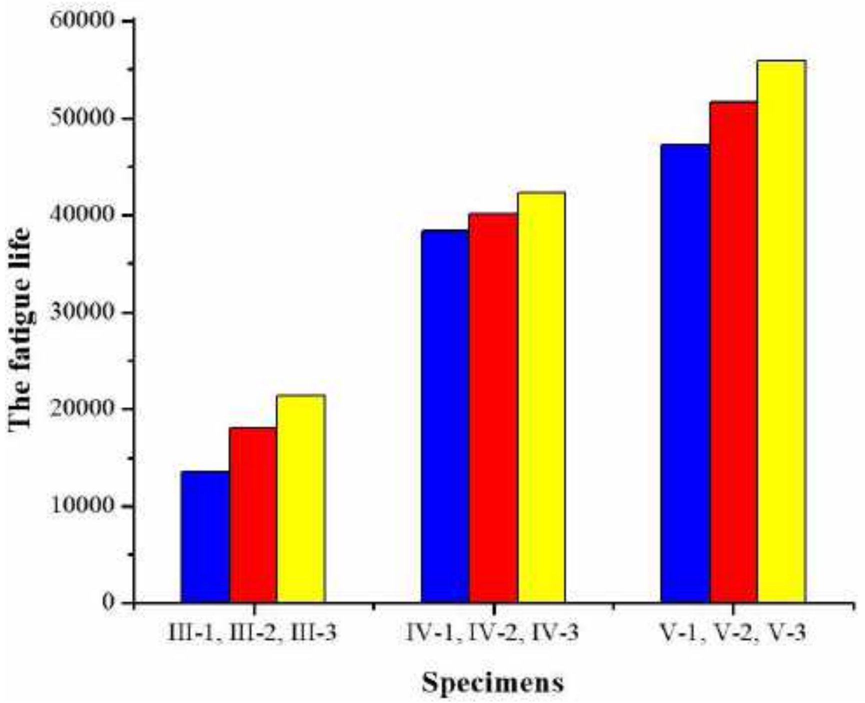

Fig. 5.23 Comparison of test results of specimens
III-1, III-2, III-3 and IV-1, IV-2, IV-3 and V-1, V-2, V-3

5.3.3 Results and Discussion

1) Anti-fretting paste can improve the fatigue life of double shear joints.

2) The fatigue life of double shear joints coated with anti-fretting paste is about 1.28 times that of double shear joints not coated with anti-fretting paste.

5.4 Conclusion of this chapter

1) 6061 aluminum alloy is a widely used aviation material. Fatigue tests on specimens made of 6061 aluminum alloy can well reflect the mechanical properties

of aircraft wing panels.

2) For aircraft wing panels with functional holes, the fatigue life of the wing panels can be improved by the extruded annular grooves around the functional holes.

3) The fatigue life of aircraft wing panels with functional holes is affected by the depth of the cold extruded annular groove. The fatigue life of the wing panel changes in an inverted "V" shape as the depth of the cold extruded annular groove increases. When the groove depth is 0.26 mm, the fatigue life of aircraft wing panels with functional holes is maximum, increasing the fatigue life by 2.35 to 32.9 times when specimen thickness is 5 mm.

4）Extruded annular grooves can improve the fatigue life of double shear joints. The fatigue life of double shear joints with extruded annular grooves is about 2.28 times that of double shear joints without extruded annular grooves.

5）Anti-fretting paste can improve the fatigue life of double shear joints. The fatigue life of double shear joints coated with anti-fretting paste is about 1.28 times that of double shear joints not coated with anti-fretting paste.

This chapter completes the dissertation work task: Implement the methods for designing the fitting joint between the center wing section and the outer wing section and methods for extending the fatigue life in the design and production of promising regional aircraft in the process of production and education at the National Aerospace University "Kharkov Aviation Institute" and in the process of design and production of Chinese aircraft. For the first time, the extruded annular groove is proposed to extend the fatigue life of the wing panel with functional holes, and it is verified by experiments, and a method of the extruded annular grooves in combination with anti-fretting paste to extend the fatigue life of the double shear joint of the wing panel is proposed. The study shows that the combination of the extruded annular grooves and anti-fretting paste can improve the fatigue life of the double shear joint of the wing panel.

GENERAL CONCLUSIONS

According to the established goals and tasks of the dissertation, the following results are achieved.

1. The design types, methods and principles of the fitting joint between the center wing section and the outer wing section of international regional aircraft are investigated. The difficulty analysis, load transfer characteristics analysis, root rib arrangement method and characteristics analysis, and comparative analysis of different root fitting joint design schemes of regional aircraft wing root connection design are given. A flexible compensation design method to alleviate structural assembly stress is proposed, and the feasibility of the relevant flexible compensation design method is verified through experimental results.

2. An effective solution for the design, quality and static strength calculation of joints in the modeling stage is proposed for the first time. The method and its application are introduced by taking the preliminary analysis and design calculation of the flange connection design of a regional aircraft wing as an example. The method is based on the calculation of stress caused by the discreteness of force transmission between units. The calculation method obtains a simplified hyperstatic joint model based on the geometric characteristics and force transmission characteristics of the cross section at each node in the flange connection design. During the calculation process, the curves of bending moment and axial force obtained by the force method and the force load distribution of each part of the model are determined to further analyze the static strength reserve. The calculation results obtained are compared with the requirements of the airworthiness standards to determine whether the design requirements are met. For components with large static strength or that do not meet the requirements, it is recommended to change the design parameters additionally to ensure the effective design of the fitting joint between the center wing section and the outer wing section and subsequent recalculation. The calculation method used has practical value as a preliminary

engineering analysis.

3. An indirect method for calculating the stress-strain state of the fitting joint between the center wing section and the outer wing section is proposed for the first time. The indirect method obtains the stress-strain state of the through two finite element calculations. In order to prove the validity of the calculation results, the stress-strain state results calculated by the indirect method are compared with results calculated by the direct method. The results show that the calculation results of the indirect method are consistent with results of the direct method. Therefore, the indirect method is a very feasible method for obtaining the stress-strain state of the fitting joint. Compared with the direct method, the indirect method has the advantages of small calculation amount and fast calculation speed.

4. The influence of the depth and angle of the extruded arc groove on the fatigue life of the wing panel is studied by experimental and finite element simulation methods. The study shows that for wing panels with functional holes, the fatigue life can be extended by extruding the arc groove. This is because the residual stress generated after the extrusion process offsets the effect of part of the load, reducing its characteristic stress. The fatigue life of the wing panel with functional holes is affected by the depth of the extruded arc groove. When the depth is 0~0.15 mm, the fatigue life is not extended much; when the depth is 0.15~0.3 mm, the fatigue life is greatly extended; when the depth is greater than 0.3 mm, the fatigue life is extended slowly. The fatigue life of the wing panel with functional holes is also affected by the angle of the extruded arc groove. The fatigue life increases with the increase of the angle until the optimal angle is 120 °. The use of the optimal extruded arc groove can extend the fatigue life of the studied wing panel by more than 2.34 times.

5. The effect of extruded annular groove on the fatigue life of wing panels with holes is studied by experimental methods. The study shows that for aircraft wing panels with functional holes, extruding annular grooves around the functional holes can improve the fatigue life of the wing panels. The depth of the extruded annular

groove has an effect on the fatigue life of aircraft wing panels with functional holes. As the depth of the extruded annular groove increases, the fatigue life of the wing panels changes in an inverted "V" shape. For specimens with a thickness of 5 mm, when the groove depth is 0.26 mm, the fatigue life of the aircraft wing panels with functional holes is the largest, which can be increased by 2.35~32.9 times.

6. The effect of extruded annular groove on the fatigue life of double shear joints of wing panels was studied by experimental methods. The results show that extruded annular grooves can improve the fatigue life of double shear joints. The fatigue life of double shear joints with extruded annular grooves is about 2.28 times that of double shear joints without extruded annular grooves. Anti-fretting paste can improve the fatigue life of double shear joints. The fatigue life of double shear joints coated with anti-fretting paste is about 1.28 times that of double shear joints without anti-fretting paste.

7. Methods of extending the wing life, such as extruding arc grooves, extruding annular grooves, and applying anti-fretting paste, have all been applied in actual engineering with good results. The results of the work are implemented in the educational process of the National Aerospace University "Kharkiv Aviation Institute" and in the process of design and production of Chinese aircraft.

REFERENCES

1. Huang Jianguo, Design of trailing edge flaps moving along the airflow // Civil Aircraft Design and Research. 1996, 3:30-33.

2. Zhang Xun, overview and analysis of the docking structure of the outer wing and center wing of foreign civil aircraft // Civil Aircraft Design and Research. 2009, 3.

3. Tang Ping, Li Qingfei, Research on the docking selection of composite upper wall panel and 1# rib of civil aircraft center wing // Civil Aircraft Design and Research, 2012 (Supplement): 99-101.

4. Cui Weijun, Li Qingfei, Li Nian, Design and analysis of the docking area of composite wing lower wall panel // Civil Aircraft Design and Research, 2012, 3: 49-50.

5. Tang Ping, Zhu Senhu, Zhao Yi, Research on the docking form between the outer wing and the lower wall of the central wing of a civil aircraft // Civil Aircraft Design and Research, 2014 (1): 30-34.

6. Zhang Xun, Fang Fang, Docking structure design and optimization analysis based on HyperWorks // Civil Aircraft Design and Research, 2012(Supplement): 147-149.

7. Zhang Xun, Liu Ting, Tang Ping, Analysis and experimental study on the docking structure of outer wing and lower wall panel of central wing of civil aircraft // Civil Aircraft Design and Research, 2013, 4: 41-44.

8. Fang Caiwen, Zhang Shujun, Jia Dawei, Li Tong, Research on the connection form between the outer wing and the upper wall panel of the central wing of civil aircraft // Civil Aircraft Design and Research, 2015 (1): 19-22

9. Aircraft design manual editorial committee. aircraft design manual volume 10 [M]. Beijing: Aviation Industry Press, 2000.

10. Zhai Bin, Wu Tiefeng, Analysis of typical out-of-tolerance strength of civil aircraft wing-fuselage joints // Science and Technology Innovation Herald,

2013(15): 38-40.

11. Qian Yibin, Effect of forced assembly on fatigue quality of aircraft metal structure based on experiment // China Science and Technology Information, 2017, 8: 28-29.

12. Shu Maosheng, He Yuting, Durability test and analysis of forced assembly butt beams // The 6th China Aeronautical Society Youth Science and Technology Forum, 2014: 387-390.

13. Deng Chengyang, Xu Huanyu, Wang Jianhua, Stress corrosion and protection of an aircraft joint // Corrosion Science and Protection Technology, 2015, 27(4): 393-395.

14. Long Xiaoqing, Stress corrosion and protection of aircraft // Journal of China Civil Aviation University, 1995, 13(1): 62-7.

15. Zhao Xiang, Zhang Nina, Zhang Junlong, Research on the influence of the root connection form of the outer wing upper wall panel on the aircraft's load-bearing capacity // Aviation Manufacturing Technology, 2016, 22: 103-106.

16. Jiang Qilin, An Luling, Yun Yishen, Effects of gap compensation and liquid gasket parameters on single-layer and interlaminar stresses of laminates // Mechanical Science and Technology, 2017, 36(10): 1633-1640.

17. Li Dongsheng, Zhai Yunong, Li Xiaoqiang, Research and application progress of stress-free assembly method for aircraft composite structures // Aerospace Manufacturing Technology, 2017, 9: 30-34.

18. Liu Dongxing, Tao Hua, Liu Zaoli, Effect of interference on fatigue life of composite laminates // Aeronautical Manufacturing Technology, 2011, 8: 80-82.

19. Zhang Junqi, Liu Longquan, Chen Kunkun, Effect of interference fit on the bearing capacity of composite mechanical connection structures // Journal of Shanghai Jiaotong University, 2013, 47 (11), 1795-1806.

20. Grebenikov, A. G. Methodology of integrated designing and modelling of aircraft assembly structures: training guide // A. G. Grebenikov / Kharkov:

National Aerospace University “Kharkov Aviation Institute”. – 2010. – 425 pages.

21. Zipay JJ, Modlin CT, Larsen CE. The ultimate factor of safety for aircraft and spacecraft-its history, applications and misconceptions. In57th AIAA/ASCE/AHS/ASC Structures, Structural Dynamics, and Materials Conference 2016 (p. 1715).

22. Aviation Regulations - 25.303 Factor of safety.

23. Yakimenko, S. I. Calculation of transverse joint of flange and shear type panels: methodology // S. I. Yakimenko / ANTK "Antonov". - 2000. - 25 pages.

24. Vasilevskij, E. T. Method of integrated design, construction and modeling of high-core fitting strut of a roof with a central plan of a transport category aircraft / E. T. Vasilevskij, A. G. Grebenikov, A. Yu. Efremov, N. V. Efremova // Open Information and Integrated Computer Technologies. – 2010. – Vol. 46. – P. 277 – 292.

25. Plácido JC, Miranda PE, Antoun Netto T, Pasqualino IP, Miscow GF, Pinheiro BD. Fatigue analysis of aluminum drill pipes. Materials Research. 2005;8:409-15.

26. Ivasyshyn OM, Vasylevs’ kyi ET, Antonyuk SL, Velychko VV, Markovs’ kyi PE, Havrysh IM. Specific Features of Fracture of High-Strength Bolts of VT22 Alloy. Materials Science. 2015 Nov;51:366-71.

27. Grebenikov, A. G. Issues of designing a medium bolted jointed wing with allowance for wear / A. G. Grebenikov, L. D. Arson // National Aerospace University "Kharkiv Aviation Institute". – 1981. – 112 p.

28. Zhang Shaoshi. New Material Mechanics [Kniga] / Zhang Shaoshi. // Machinery Industry Press – 2010. – 374 pages.

29. Liu Shikui. Structural Mechanics / Liu Shikui // Tsinghua University Press, 2008. – 204 pages.

30. Vasilevskij E. T. Basic provisions of the Ukrainian air code and the standard of airworthiness of aircraft of the transport category / E. T. Vasilevskij,

A. G. Grebenikov, V. N. Nikolayenko // National Aerospace University “Kharkiv Aviation Institute”. – 2006. – 331 p.

31. Influence of the Rivet Type on the Fatigue Life of Samples of Riveted Joints of Plates with Filled Unloaded Holes / A. G. Grebenikov, A. K. Myalitsa, A. M. Gumenny, V. M. Andryushchenko, A. S. Chumak, L. Yu. Buyval, S. S. Kapustin // Open Information and Computer Integrated Technologies: Coll. sci. t. / N. E. Zhukovsky National Aerospace University "Kharkiv Aviation Institute". Kharkov, 2017. Issue 76. Pp. 119–125.

32. Andrianov IK, Stankevich AV. The stress-strain state simulation of the aircraft fuselage stretch forming in the ANSYS. In Journal of Physics: Conference Series 2019 Oct 1 (Vol. 1333, No. 8, p. 082002). IOP Publishing.

33. Oskouei RH, Keikhosravy M, Soutis C. A finite element stress analysis of aircraft bolted joints loaded in tension. The aeronautical journal. 2010 May;114(1155):315-20.

34. Prakash RU, Kumar GR, Vijayanandh R, Kumar MS, Ramganesh T. Structural analysis of aircraft fuselage splice joint. InIOP Conference Series: Materials Science and Engineering 2016 Sep 1 (Vol. 149, No. 1, p. 012127). IOP Publishing.

35. Babu TN, Kumar ER, Mageshvaran R, Shankar T, Prabha DR. Structural analysis on wing box spliced joint for an aircraft using the finite element method. Int J Civil Eng Technol. 2017; 8:2302-13.

36. Pavan G, Kishore N. Static and Fatigue Analysis on a Wing Spar Joint for a Light Jet Aircraft Structure Using 2024 T351 Material. In Applied Mechanics and Materials 2019 (Vol. 895, pp. 244-252). Trans Tech Publications Ltd.

37. Vasilevsky E. T., Grebennikov A. G., Efremov A. Y., and Svetlichny S. P. Analysis of the characteristics of the general stress-strain state in the elements of the fitting joint of the wing with the center wing section, Open Information and Computer Integrated Technologies, vol. 24, pp. 78–89, 2004.

38. Vasilevsky E. T., Grebennikov A. G., Efremov A. Y., and Svetlichny S. P. Methods for determining the characteristics of local stress-strain state in the zone of the monolithic profile of the fitting joint of a wing with a center section, Open Information and Computer Integrated Technologies, vol. 28, pp. 177–193, 2005.

39. Vasilevsky E. T., Grebennikov A. G., Efremov A. Y., and Efremova N. V. The method of integrated design, construction and modeling of a high-resource fitting junction of a wing with a center section of a transport category aircraft, Open Information and Computer Integrated Technologies, vol. 46, pp. 277–293, 2010.

40. Sun Y, Grebenikov OG, Li C. Analysis of Force Distribution of Four Rows of Bolts in Aircraft Fitting Joint. International Journal of Aerospace Engineering. 2021 Jul 14;2021.

41. Doru MO, Özel A, Akpinar S, Aydin MD. Effect of the spew fillet on adhesively bonded single-lap joint subjected to tensile loading: experimental and 3-D non-linear stress analysis. The Journal of Adhesion. 2014 Mar 4;90(3):195-209.

42. Vinogradov YI, Menkov GB. Study of Stress-Strain State of an Aircraft Body at Steering Loads. Mechanics of Solids. 2020 May;55(3):423-36.

43. Balalayeva E, Artiukh V, Kukhar V, Tuzenko O, Glazko V, Prysiazhnyi A, Kankhva V. Researching of the stress-strain state of the open-type press frame using of elastic compensator of errors of “press-die” system. InEnergy Management of Municipal Transportation Facilities and Transport 2017 Apr 10 (pp. 220-235). Springer, Cham.

44. Zeng C, Tian W, Liu XY, Xue JT. Experimental and numerical studies of stress/strain characteristics in riveted aircraft lap joints. Journal of Mechanical Science and Technology. 2019 Jul;33(7):3245-55.

45. Zhao K, Wang L, Chang Y, Yan J. Identification of post-necking stress–strain curve for sheet metals by inverse method. Mechanics of Materials. 2016 Jan 1; 92:107-18.

46. V.O. Boguslayev, S.A. Bychkov, O.G. Grebenikov, Scientific grounds of

structural and production concepts to provide aircraft life time. National aerospace university, KhAI, Ukraine, 2019.

47. B.N. Du, Z.P. Xiao, Y.X. Qiao, L. Zheng, B.Y. Yu, D.K. Xu, and L.Y. Sheng, Optimization of microstructure and mechanical property of a Mg-Zn-Y-Nd alloy by extrusion process. Journal of Alloys and Compounds, 2019 Feb 15;775:990-1001.

48. Y.L. Wang, Y.L. Zhu, S. Hou, H.X. Sun, Y. Zhou, Investigation on fatigue performance of cold expansion holes of 6061-T6 aluminum alloy. International journal of fatigue. 2017 Feb 1; 95:216-228.

49. H. Soyama, Comparison between the improvements made to the fatigue strength of stainless steel by cavitation peening, water jet peening, shot peening and laser peening. Journal of Materials Processing Technology. 2019 Jul 1; 269:65-78.

50. Q. Lin, H. Liu, C. Zhu, D. Chen, S. Zhou, Effects of different shot peening parameters on residual stress, surface roughness and cell size. Surface and Coatings Technology. 2020 Sep 25; 398:126054.

51. X.D. Ren, Q.B. Zhan, H.M. Yang, F.Z. Dai, C.Y. Cui, G.F. Sun, L. Ruan, The effects of residual stress on fatigue behavior and crack propagation from laser shock processing-worked hole. Materials & Design. 2013 Feb 1; 44:149-54.

52. R. Li, M. Wang, Z. Li, P. Cao, T. Yuan, H. Zhu, Developing a high-strength Al-Mg-Si-Sc-Zr alloy for selective laser melting: crack-inhibiting and multiple strengthening mechanisms. Acta Materialia. 2020 Jul 1; 193:83-98.

53. E. Ge, H. Su, Y. Cheng, Y. Fu, J. Xu, R. Xiao. Residual stress fields and fatigue life of cold expansion hole in titanium alloy TC4. China Mechanical Engineering. 2015 Apr 10;26(7):971.

54. X. Wang, W. Xu, X.J. Zhang, L.N. Zhang, B.R. Hu, Numerical prediction and experimental verification of fatigue life of TC4 plate strengthened by cold expansion. Journal of Zhejiang University (Engineering Science). 2017 Aug 16;51(8):1610-1618.

55. Y. Zhang, Y. Xu, Z. Yang, Y. Wu. Residual Stress Analysis of Double Cold Extrusion for Titanium Alloy Lug. In2018 IEEE International Conference on Mechatronics, Robotics and Automation (ICMRA) 2018 May 18 (pp. 122-126). IEEE.

56. J. Liu, X.J. Shao, Y.S. Liu, Z.F. Yue. Effect of cold expansion on fatigue performance of open holes. Materials Science and Engineering: A. 2008 Mar 25;477(1-2):271-276.

57. Y.S. Liu, X.J. Shao, J. Li, Z.F. Yue. Finite element method and experimental investigation on the residual stress fields and fatigue performance of cold expansion hole. Materials & Design. 2010 Mar 1;31(3):1208-15.

58. N.M. Babu, T. Jagadish, K. Ramachandra, S.N. Sridhara, A simplified 3-D finite element simulation of cold expansion of a circular hole to capture through thickness variation of residual stresses. Engineering failure analysis. 2008 Jun 1;15(4):339-48.

59. R. Seifi, Total fatigue lives, crack growth paths and cycles in cold expanded adjacent holes. International Journal of Fatigue. 2018 Aug 1; 113:69-77.

60. A. Kumar, M. Babu, The Effect of Cold Expansion on Fatigue Life of Closely Spaced Adjacent Fastener Holes. Sas Tech Journal of RUAS. 2017;16(1):17-20.

61. S.A. Kumar, N.M. Babu, Effect of proximity hole on induced residual stresses during cold expansion of adjacent holes. Materials Today: Proceedings. 2018 Jan 1;5(2):5709-15.

62. W. Zhang, W. Jiang, H. Li, M. Song, Y. Yu, G. Sun, J. Li, Y. Huang, Effect of tensile overload on fatigue crack behavior of 2205 duplex stainless steel: Experiment and finite element simulation. International Journal of Fatigue. 2019 Nov 1; 128:105199.

63. A.K. Syed, X. Zhang, J.E. Moffatt, R. Maziarz, L. Castelletti, M.E. Fitzpatrick, Fatigue performance of bonded crack retarders in the presence of cold

worked holes and interference-fit fasteners. International Journal of Fatigue. 2017 Dec 1; 105:111-8.

64. E.Z. Geiglou, T.N. Chakherlou, Investigating the effect of cold expansion process on the fatigue behavior of aluminum alloy 7075-T6 in double-lap shear joints. Proceedings of the Institution of Mechanical Engineers, Part L: Journal of Materials: Design and Applications. 2019 Aug; 233(8):1645-60.

65. Z.E. Geiglou, T.N. Chakherlou, Numerical and experimental investigation of the effect of the cold expansion process on the fatigue behavior of hybrid (bonded-bolted) double shear lap aluminum joints. International Journal of Fatigue. 2019 Sep 1; 126:30-43.

66. S. Tian, C. Li, W. Dai, D. Jia, H. Zhang, M. Xu, Y. Yuan, Y. Liu, Y. Zhang, Effect of the countersunk hole depth on tensile-tensile fatigue behavior of riveted specimens of AA2024-T3 alloy. Engineering Failure Analysis. 2020 Sep 1; 115:104639.

67. C. Zeng, W. Tian, W.H. Liao, The effect of residual stress due to interference fit on the fatigue behavior of a fastener hole with edge cracks. Engineering Failure Analysis. 2016 Aug 1; 66:72-87.

68. D.S. Kiva, G.A. Krivov, V.F. Sementsov, et al. Construction and technological methods of increasing the fatigue durability of the airplane planer structure elements in the area of functional holes. National aerospace university, KhAI, Ukraine, 2015.

69. N.V. Boychenko, Elastic and plastic stress intensity factor in specimen of aluminum alloys under tension and bending in the temperature range. Procedia Structural Integrity. 2018 Jan 1; 13:908-13.

70. Tool Steel and Hard Alloy: Cr12MoV. // https://www.steelgr.com/Steel-Grades/Tool-Steel-Hard-Alloy/cr12mov.html.

71. Y. Sun, O.G. Grebenikov, C. Li, Analysis of Force Distribution of Four Rows of Bolts in Aircraft Fitting Joint. International Journal of Aerospace

Engineering. 2021 Jul 14; 2021:9962645.

72. Z. Luo, H. Chen, J. Wang, R. Zheng. Fatigue life calculation of notched specimens by modified Wöhler curve method and theory of critical distance under multiaxial random loading. Fatigue & Fracture of Engineering Materials & Structures. 2022 Feb;45(2):514-529.

73. G. Härkegård, Critical-distance fatigue analysis of limiting cases of ellipsoidal cavities. Engineering Fracture Mechanics. 2021 Nov 1; 257:108011.

74. J.C. He, S.P. Zhu, D. Liao, X.P. Niu, J.W. Gao, H.Z. Huang, Combined TCD and HSV approach for probabilistic assessment of notch fatigue considering size effect. Engineering Failure Analysis. 2021 Feb 1; 120:105093.

75. P. Luo, W. Yao, L. Susmel, P. Li, Prediction methods of fatigue critical point for notched components under multiaxial fatigue loading. Fatigue & Fracture of Engineering Materials & Structures. 2019 Dec;42(12):2782-93.

APPENDIX A

ACTS OF IMPLEMENTATION OF THE RESULTS OF THE DISSERTATION WORK

ЗАТВЕРДЖУЮ
Проректор з наукової роботи
Національного аерокосмічного
університету ім. М. Є. Жуковського
«Харківський авіаційний інститут»
доктор технічних наук,
старший науковий співробітник
Володимир ПАВЛІКОВ
«___» ______________ 202 5 р.

АКТ

впровадження результатів дисертаційної роботи
здобувача наукового ступеня доктора філософії
Сунь Іфан
«Scientific grounds to provide lifetime of regional passenger airplane wing structural members»
в навчальний процес Національного аерокосмічного університету ім. М. Є. Жуковського «Харківський авіаційний інститут»

Комісія у складі:
- завідуючого кафедри №103, к.т.н., доцента Сергія ТРУБАЄВА;
- доцента кафедри №103, к.т.н., доцента Андрія ГУМЕННОГО;
- професора кафедри №103, д.т.н, професора Олександра ГРЕБЕНІКОВА.

встановила, що наукові положення дисертаційної роботи «Scientific grounds to provide lifetime of regional passenger airplane wing structural members», які Сунь Іфан розробив особисто, використовуються в навчальному процесі при навчанні за дисциплінами «Моделювання об'єктів авіаційної техніки за допомогою системи SIEMENS NX», «Інтегроване проектування літаків та вертольотів».

Результати дисертаційної роботи Сунь Іфан використовуються в навчальному процесі, в практичних заняттях, дипломному і курсовому проектуванні студентів які навчаються за спеціальностями 134 «Авіаційна та ракетно техніка», навчальними програмами «Літаки і вертольоти», «Проектування, випробування та сертифікація об'єктів АРКТ», Інтегроване проектування літаків та вертольотів», «Наукові принципи проектування і виробництва об'єктів авіаційної та ракетно-космічної техніки».

к.т.н., доцент, зав. кафедри №103	____________	Сергій ТРУБАЄВ
к.т.н., доцент, проректор з НПР	____________	Андрій ГУМЕННИЙ
д.т.н., професор, проф. кафедри №103	____________	Олександр ГРЕБЕНІКОВ

APPENDIX B
LIST OF PUBLICATIONS OF THE APPLICANT BY DISSERTATION SUBJECT

Scientific works in which the main scientific results of the dissertation are published:

1. А. Г. Гребеніков, А. М. Гуменний, С. В. Трубаєв, В. А. Гребеніков, Сунь Іфан. Методи забезпечення ресурсних характеристик типових конструктивних елементів літакових конструкцій // Проблеми створення та забезпечення життєвого циклу авіаційної техніки : матеріали Міжнар. наук.-техн. конф., Харків, 28–29 квіт. 2020 р. Харків, 2020. С. 11. **The collection is included in the international bibliometric and scientometric databases Index Copernicus, WorldCat, Ulrich's Periodicals Directory and Google Scholar.** Personal contribution of the acquirer: collect relevant information on aircraft life performance assurance methods.

2. Yifan Sun. ANALYSIS OF THE STRESS-STRAIN STATE OF COMPONENTS IN THE FITTING JOINT OF OUTER WING SECTION AND CENTER SECTION OF REGIONAL AIRCRAFT / Yifan Sun. A. A. Vendin // Open Information and Computer Integrated Technologies : National Aerospace University «Kharkiv Aviation Institute» , – Kharkiv, 2021 – Vol. 91. – P. 97 – 112. DOI: https://doi.org/10.32620/oikit.2021.91.07. **The collection is included in the international bibliometric and scientometric databases Index Copernicus, WorldCat, Ulrich's Periodicals Directory and Google Scholar.** Personal contribution of the acquirer: build a 3D model and finite element analysis model of the fitting joint.

3. Sun, Y. Analysis of Force Distribution of Four Rows of Bolts in Aircraft Fitting Joint / Sun Yifang, O. G. Grebenikov, Chenghu Li // International Journal of Aerospace Engineering. – 2021. – Vol. 2011, – P. 11. https://doi.org/10.1155/2021/9962645. **The collection is included in the**

international bibliometric and scientometric databases Scopus (Q3) and Google Scholar. Personal contribution of the acquirer: analyze the stress-strain state of the fitting joint by using the finite element software ANSYS.

4. Yifang Sun, O. G. Grebenikov, Chenghu Li. The effect of extrusion arc groove on the fatigue life of wing panel with functional holes: experiment and simulation // Engineering Failure Analysis. 2022 Nov 1; 141:106643. **The collection is included in the international bibliometric and scientometric databases Scopus (Q1) and Google Scholar.** Personal contribution of the acquirer: analyze the optimal depth and angle of the extruded arc groove by finite element software ANSYS.

5. Sun, Y. Method of design calculating of the strength of the transverse joint of the panels of outer wing section and the center wing section of the regional aircraft / Sun Yifang, V. E. Vasilevskiy, O. O. Vendin, O. G Grebenikov // Open Information and Computer Integrated Technologies – Kharkiv: Nat. Aerospace Univ. "KhAI". – 2023. – Vol. 97. – P. 142 – 157. https://doi.org/10.32620/oikit.2023.97.09. **The collection is included in the international bibliometric and scientometric databases Index Copernicus, WorldCat, Ulrich's Periodicals Directory and Google Scholar.** Personal contribution of the acquirer: analyze the optimal depth and angle of the extruded arc groove by finite element software ANSYS.

6. Yifang Sun. Influence of radial tension of bolts on the characteristics of vat of models of connections of elements of aircraft structures / Yifang Sun // Open Information and Computer Integrated Technologies – Kharkiv: Nat. Aerospace Univ. "KhAI". – 2023. – Vol. 98. – P. 36 – 45. DOI: https://doi.org/10.32620/oikit.2023.98.03. **The collection is included in the international bibliometric and scientometric databases Index Copernicus, WorldCat, Ulrich's Periodicals Directory and Google Scholar.** Personal contribution of the acquirer: propose an effective solution to the design, quality and static strength calculation of the joint in the modeling stage. The method and its

application are introduced by taking the preliminary analysis and design calculation of the flange connection design of the mid-wing of a regional aircraft as an example.

7. Sun Yifang. The effect of cold extruded annular grooves on the fatigue life of wing panels with functional holes / Sun Yifang, O. G. Grebenikov, O. O. Vendin // Open Information and Computer Integrated Technologies – Kharkiv: Nat. Aerospace Univ. "KhAI". – 2023. – Vol. 99. – P. 22 – 31. DOI: https://doi.org/10.32620/oikit.2023.99.02. **The collection is included in the international bibliometric and scientometric databases Index Copernicus, WorldCat, Ulrich's Periodicals Directory and Google Scholar.** Personal contribution of the acquirer: conducted experiments to confirm that extruded annular grooves can extend the fatigue life of perforated wing panels.

8. Li Chenghu, Sun Yifang, Duan Chunxu, Li Renfu. Study on Properties of Z-pin-reinforced and Rivet-reinforced Composite T-joint: Experiment and Simulation// Applied Composite Materials, 2021, 28: 395-408. **The collection is included in the international bibliometric and scientometric databases Scopus (Q2) and Google Scholar.** Personal contribution of the acquirer: carried out model building and simulation, and participated in validation experiments.

APPENDIX C

FATIGUE TEST REPORT

SGS

通标标准技术服务（青岛）有限公司

检测报告

QDF24-0001680-01

发布日期：2024-01-19

客户名称： 孙一方

客户地址： 武汉市江汉区江汉北路江都仕嘉 A 座 2307 室

样品 1 及编号：

样品 1	编号 1		编号 2	
	I-1	I-0-1, I-0-2, I-0-3	II-1	II-0-1, II-0-2, II-0-3
	I-2	I-20-1, I-20-2, I-20-3	II-2	II-20-1, II-20-2, II-20-3
	I-3	I-40-1, I-40-2, I-40-3	II-3	II-40-1, II-40-2, II-40-3
	I-4	I-60-1, I-60-2, I-60-3	II-4	II-60-1, II-60-2, II-60-3
	I-5	I-80-1, I-80-2, I-80-3	II-5	II-80-1, II-80-2, II-80-3
	I-6	I-100-1, I-100-2, I-100-3	II-6	II-100-1, II-100-2, II -100-3

样品 2、3、4 及编号：

样品 2、3、4	编号 3	
	III-1	III-60-1, III-60-2, III-60-3
	IV-1	IV-60-1, IV-60-2, IV-60-3
	V-1	V-60-1, V-60-2, V-60-3

****

以上样品及信息由客户提供及确认，SGS 不承担证实客户提供信息的准确性，适当性和完整性责任。

样品接收日期： 2024-01-10

检测周期： 2024-01-10 – 2024-01-18

检测方法与结果： 根据客户要求测试试件疲劳寿命，正弦波加载，试验条件及结果请参见下一页。

SGS 授权签字人

检测报告

QDF24-0001680-01 发布日期：2024-01-19

检测条件 1 与结果 1：

工况	试件编号	工作频率（Hz）	加载力（kN）	疲劳寿命		
				1	2	3
I-1	I-0-1, I-0-2, I-0-3	20	25.85	5490	7408	21526
I-2	I-20-1, I-20-2, I-20-3	20	25.85	19378	32771	27026
I-3	I-40-1, I-40-2, I-40-3	20	25.85	137795	105450	70923
I-4	I-60-1, I-60-2, I-60-3	20	25.85	379797	337384	415450
I-5	I-80-1, I-80-2, I-80-3	20	25.85	189778	178839	144559
I-6	I-100-1, I-100-2, I-100-3	20	25.85	176103	150050	115800

检测条件 2 与结果 2：

工况	试件编号	工作频率（Hz）	加载力（kN）	疲劳寿命		
				1	2	3
II-1	II-0-1, II-0-2, II-0-3	20	34.48	6086	5233	7800
II-2	II-20-1, II-20-2, II-20-3	20	34.48	10545	11200	12020
II-3	II-40-1, II-40-2, II-40-3	20	34.48	11912	15506	13033
II-4	II-60-1, II-60-2, II-60-3	20	34.48	12388	17578	14996
II-5	II-80-1, II-80-2, II-80-3	20	34.48	7408	12300	11053
II-6	II-100-1, II-100-2, II -100-3	20	34.48	7063	10360	9043

检测条件 3 与结果 3：

工况	试件编号	工作频率（Hz）	加载力（kN）	疲劳寿命		
				1	2	3
III-1	III-60-1, III-60-2, III-60-3	20	56.43	13542	18042	21355
IV-1	IV-60-1, IV-60-2, IV-60-3	20	56.43	38428	40456	42332
V-1	V-60-1, V-60-2, V-60-3	20	56.43	47256	51620	55860

备注：

1. 疲劳寿命为加载循环次数。

注意事项：

除非另有说明，本检测结果仅与被检测物品有关。

结束